Universidade de Lisboa

Faculdade de Medicina de Lisboa

Genetic Profiling of Pediatric Brain Gliomas

Laura Passos Morgado Franco Frazão

Orientadores:

Doutora Maria Lúcia Primo Nobre de Oliveira Roque

Professor Doutor José Guilherme de Brito Cortez Pimentel

Dissertação especialmente elaborada para obtenção do grau de Mestre em Neurociências

2016

Universidade de Lisboa

Faculdade de Medicina de Lisboa

Genetic Profiling of Pediatric Brain Gliomas

Laura Passos Morgado Franco Frazão

Orientadores:

Doutora Maria Lúcia Primo Nobre de Oliveira Roque

Professor Doutor José Guilherme de Brito Cortez Pimentel

Dissertação especialmente elaborada para obtenção do grau de Mestre em Neurociências

2016

A impressão desta dissertação foi aprovada pelo Conselho Cientifico da Faculdade de Medicina de Lisboa em reunião de 22 de Março de 2016

Agradecimentos

À Doutora Lúcia Roque, pela oportunidade, pelo conhecimento transmitido, pela disponibilidade e pela paciência.

Ao Professor Doutor José Pimentel pela disponibilidade e interesse no trabalho. Também pela classificação histológica dos tumores e pela cedência dos mesmos, sem os quais este trabalho não seria possível.

À Doutora Carmo Martins, pela disponibilidade constante, pelo apoio e pelo que me ensinou. Ao Dr. Vasco e à Joaquina pelo acompanhamento e ajuda no laboratório.

À Doutora Ana Rita Silvestre pela ajuda na obtenção dos tumores e pelo interesse que sempre demonstrou sobre o trabalho.

À Doutora Manuela Mafra pela classificação histológica de alguns tumores. Ao Dr. Duarte Salgado e à Dra. Sofia Nunes por terem cedido os dados clínicos dos pacientes, pela disponibilidade e interesse no trabalho. Ao Dr. José Miguens, Dra. Cláudia Faria, Dr. Amets Sagarribay e Dr. Mário Matos por de forma indirecta terem participado neste trabalho, cedendo amostras de tumores e dados clínicos dos pacientes.

Aos meus pais, irmãos, família, amigos e ao Sebastião pelo apoio, ajuda e compreensão.

Muito Obrigada.

Laura Frazão.

Abstract

The genetic alterations in pediatric gliomas can be used as diagnostic and prognostic markers and are the basis for the development of new target therapies that, ideally, would be associated with less mortality and morbidity.

The aim of this study was to determine the genetic profile of pediatric gliomas and to do the translation of the genetic data for the clinical and laboratorial practice. Thus, the frequency of alterations in *BRAF*, *CDKN2A*, *MYB*, *MYBL1*, *FGFR1*, *H3F3A*, *H3F3B* and *HIST1H3I* genes were analyzed in 109 pediatric gliomas using Fluorescent In Situ Hybridization (FISH) and Sequencing using Sanger methodology.

In the present project we found that the *BRAF/KIAA1549* rearrangement was associated with cerebelar pilocytic astrocytomas and was exclusive of low-grade gliomas, being useful as a diagnostic marker. The *BRAFV600E* mutation was associated with a better patients' overall survival and the deletion of the *CDKN2A* gene was associated with tumor recurrences. So, these two genetic alterations may be used as prognostic markers in pediatric gliomas. A cell line was established from a high-grade glioma that harbor the *BRAFV600E* mutation. The identification of *MYB, MYBL1* and *FGFR1* rearrangements by *FISH* did not seem to be useful as diagnostic or prognostic markers. *K27M* and *G34R/V* mutations were identified in the *H3F3A* gene and were shown to be exclusive of high-grade gliomas and to vary with the tumor location and patients´ age.

In sum, it was determined, for the first time, the genetic profile of pediatric gliomas in the Portuguese population and it was demonstrated that it is useful to the tumor characterization, with prognostic and diagnostic information. In this context, the establishment of cell lines from tumors with specific genetic alterations, such as the BRAFV600E mutation, may be the basis for susceptibility trials to new drugs and for a better understanding of the disease.

Key-words: pediatric gliomas; *BRAF* gene; *MYB, MYBL1* and *FGFR1* genes; *CDKN2A* gene; histone genes

Resumo

As alterações genéticas presentes em gliomas pediátricos constituem importantes marcadores de diagnóstico e prognóstico e são base para o desenvolvimento de novas formas terapêuticas, que se espera, impliquem menor mortalidade e morbilidade.

Neste trabalho avaliámos a frequência de alterações nos genes *BRAF, CDKN2A, MYB, MYBL1, FGFR1*, *H3F3A, H3F3B* e *HIST1H3I* com o objetivo de determinar o perfil genético dos gliomas pediátricos que foram referidos ao IPOLFG, e fazer a translação dos dados genéticos para a prática clínica e laboratorial. Assim, 109 tumores foram analisados por "Fluorescent I*n Situ Hybridization* (FISH)" e por sequenciação pelo método de Sanger.

Foi observado que o rearranjo *BRAF/KIAA1549* estava associado a astrocitomas pilocíticos com localização cerebelar e era exclusivo dos gliomas de baixo grau, sendo útil como marcador de diagnóstico nestes tumores. A mutação *BRAFV600E* estava associada a uma maior sobrevivência dos pacientes e a deleção do gene *CDKN2A* com a ocorrência de recidivas. Assim, parece que estas duas alterações genéticas podem ser usadas como marcadores de prognóstico em gliomas pediátricos. Foi estabelecida uma linha de cultura a partir de um glioma de alto grau com a mutação *BRAFV600E*. A identificação, por FISH, de rearranjos nos genes *MYB, MYBL1* e *FGFR1*, não pareceu ser útil a nível de diagnóstico ou prognóstico. Nos genes das histonas, as mutações *K27M* e *G34R/V* eram exclusivas dos gliomas de alto grau e só foram observadas no gene *H3F3A*. Estas mutações estavam associadas à localização do tumor e idade do paciente.

Em suma, foi caracterizado, pela primeira vez, o perfil genético de gliomas pediátricos na população portuguesa e foi demonstrada a sua utilidade para a caracterização tumoral, com informação diagnóstica e prognóstica. Neste contexto, o estabelecimento de linhas tumorais com alterações genéticas, como a mutação *BRAFV600E*, pode servir de base para ensaios de susceptibilidade a novos fármacos e para um melhor conhecimento da doença.

Palavras-chave: gliomas pediátricos; *BRAF*; *MYB, MYBL1* e *FGFR1*; *CDKN2A*; genes das histonas

Resumo Alargado

Os tumores primários do Sistema Nervoso Central (SNC) são a seguir às leucemias, os tumores pediátricos mais frequentes e constituem a principal causa de morte, por cancro, em crianças e adolescentes com menos de 20 anos de idade. Estes tumores estão também associados a uma elevada taxa de morbilidade provocada pelos tratamentos (cirurgia, radioterapia e quimioterapia) a que estas crianças são habitualmente sujeitas [1].

Os gliomas são o tipo histológico mais comum dos tumores pediátricos do SNC e têm a sua origem no tecido neuroepitelial e nas células da glia. De acordo com a última classificação da Organização Mundial de Saúde, de 2007, estes tumores são subdivididos em quatro subgrupos histológicos principais: (I) Tumores astrocíticos; (II) Tumores oligodendrogliais; (III) Tumores neuronais e neurogliais; (IV) Ependimomas. Este último subgrupo é geralmente excluído desta classificação, sendo considerado uma doença distinta. Posteriormente, os gliomas são classificados de acordo com a sua malignidade em 4 graus (I-IV), sendo o grau I o menos e o grau IV o mais agressivo [2]. No entanto, devido à sua grande heterogeneidade, a classificação histológica e biológica dos gliomas pediátricos, não é na maior parte das vezes fácil, pelo que o risco de sobre-tratamento, com todos os efeitos secundários daí decorrentes, é grande. Esta situação começou a alterar-se em 2012 com o surgimento de trabalhos de sequenciação massiva dos vários tipos de gliomas, que permitiram classificar tumores histologicamente idênticos em sub-grupos genéticos e epigenéticos distintos [1].

Assim, um conjunto de alterações genéticas começou a ser identificado como característico dos gliomas pediátricos. Por exemplo, no contexto dos gliomas de baixo grau, foi verificado que o rearranjo do gene *BRAF*, que resulta na formação do gene de fusão *BRAF/KIAA1549* era exclusivo deste tipo de gliomas e característico de astrocitomas pilociticos; que a mutação *BRAFV600E* embora comum, não era exclusiva destes gliomas; e que a existência de rearranjos nos genes *MYB, MYBL1* e *FGFR1* poderia estar relacionada com os gliomas pediátricos difusos (gliomas de baixo grau com comportamento infiltrativo) [3–6].

Todas estas alterações genéticas identificadas em gliomas de baixo grau levam a uma activação da via de sinalização *MAPK/ERK*. Assim, levantou-se a hipótese de os gliomas pediátricos de baixo grau serem uma "doença de uma única via de sinalização" [7]. Visto que a activação da via *MAPK/ERK* pode resultar tanto em proliferação, sobrevivência e tumorigénese, como em diferenciação e senescência celular, foi possível perceber o porquê dos gliomas de baixo grau raramente se tornarem tumores de alto grau. Neste contexto, foi demonstrado que a deleção do gene *CDKN2A* em gliomas pediátricos com alterações no gene *BRAF* estava

associada a tumores mais agressivos, provavelmente por refletir uma falha ou em escape da senescência celular induzida [5,8,9].

Por outro lado, as mutações *K27M* e *G34R/V* nas histonas *H3.3* e *H3.1* são exclusivas dos gliomas pediátricos de alto grau. Enquanto a mutação *K27M* na histona *H3.1* parece ser exclusiva de "diffuse intrinsic pontine gliomas" (tumor agressivo com localização no tronco cerebral) e glioblastomas não localizados no tronco cerebral; a mutação *K27M* na histona *H3.3* é específica de tumores com localização na linha média e de pacientes mais jovens, e as mutações *G34R/V* da mesma histona só foram observadas em tumores de pacientes mais velhos e localizados no córtex cerebral. A mutação *K27M* na histona *H3.3* está também associada a um pior prognóstico, relativamente à mutação *G34R/V* [10–13].

O objectivo deste trabalho é determinar, retrospectivamente, o perfil genético dos gliomas pediátricos referidos ao IPOLFG e fazer a translação dos dados genéticos para a prática laboratorial. Para isso, foi investigada, numa série de 109 gliomas pediátricos, a frequência de alterações nos genes *BRAF, MYB, MYBL1, FGFR1, CDKN2A, H3F3A, H3F3B* e *HIST1H3I*. Para além de terem sido relacionadas com a classificação histológica e a localização do tumor, a idade e género do paciente, estas alterações genéticas foram, também, identificadas em linhas celulares estabelecidas a partir de tumores. Assim, a parte experimental deste trabalho foi dividida em três fases principais: a primeira consistiu numa análise por "Fluorescent I*n Situ Hybridization* (FISH)", a segunda na sequenciação pelo método de Sanger, e a terceira em cultura celular. Enquanto a técnica FISH foi utilizada para identificar o rearranjo *BRAF/KIAA1549*, os rearranjos dos *genes MYB, MYBL1* e *FGFR1*, e a deleção do gene *CDKN2A*; a sequenciação pelo método de Sanger foi utilizada para identificar mutações nos genes *BRAF, H3F3A, H3F3B* e *HIST1H3I.* As amostras dos gliomas foram recebidas em material fresco ou embebidas em parafina.

Dos 109 gliomas estudados, 67 eram de grau I, 13 de grau II, 14 de grau III, 8 de grau IV e 7 com classificação histológica não especificada. Na série de gliomas pediátricos analisados, como descrito na literatura, a presença do rearranjo *BRAF/KIAA1549* era exclusiva dos gliomas baixo grau e estava relacionada com a histologia de astrocitoma pilocítco (p-value <0.0001) e com tumores localizados no cerebelo (*p-value* <0.0001). Estes resultados sugerem que a identificação deste rearranjo genético na prática laboratorial tem utilidade como marcador de diagnóstico em gliomas pediátricos de baixo grau. A ocorrência da mutação *BRAFV600E* era independente do tipo histológico e localização do tumor bem como da idade ou género do paciente. No entanto, estava associada a uma maior sobrevivência dos pacientes (*p-value*=0.0443). Apesar de serem necessários mais estudos em séries maiores de gliomas

pediátricos, os nossos resultados sugerem que utilização desta mutação como marcador de prognóstico pode ser útil. Além disto, durante este trabalho foi estabelecida uma linha de cultura a partir de um glioma de alto grau com a mutação *BRAFV600E* que poderá servir de base para ensaios de susceptibilidade a novos fármacos e para um melhor entendimento da doença a nível molecular.

Quanto à deleção do gene *CDKN2A* foi verificado que a sua incidência aumentava com o grau dos tumores: 10% nos gliomas de grau I, 30% nos de grau II e III, e 42.9% nos de grau IV. Além disso, todos os gliomas de baixo grau apresentavam uma deleção heterozigótica deste gene e só em três gliomas de alto grau foram identificadas deleções homozigóticas do gene *CDKN2A*. Esta alteração genética mostrou estar relacionada com a ocorrência de recidivas (*p-value=0.0149*), sugerindo a sua utilização como marcador de prognóstico em gliomas pediátricos.

A identificação, por FISH, de rearranjos nos genes *MYB, MYBL1* e *FGFR1*, não pareceu ser útil a nível de diagnóstico ou prognóstico visto que na série de gliomas estudados só foi identificado um rearranjo do gene *MYB* num glioma com classificação histológica não especificada, um rearranjo do gene *MYBL1*, não descrito anteriormente, num astrocitoma pilocítico e nenhum rearranjo do gene *FGFR1*.

As mutações *K27M* e *G34R/V* só foram identificadas no gene *H3F3A* e, como descrito na literatura, estavam relacionadas com a localização do tumor e idade dos pacientes. Foi também possível verificar que estas mutações não são exclusivas dos astrocitomas pediátricos de alto grau, estando presentes noutros gliomas de alto grau como tumores oligoastrocíticos e oligodendrogliais. Isto levanta a hipótese de a classificação usada hoje em dia para a estratificação dos glioblastomas poder ser estendida para outros subtipos histológicos de gliomas de alto grau.

Assim, com este trabalho, foi possível verificar que o perfil genético de gliomas pediátricos pode ser útil para melhorar a classificação tumoral, tanto com informação diagnóstica como prognóstica, e para melhorar o conhecimento da doença, o que idealmente, contribuirá para o desenvolvimento de terapias mais eficazes.

Table of Contents

List of Figures

List of Tables and Supplementary Tables

List of Abbreviations, symbols and conventions

BRAF – B-Raf proto-oncogene, serine/threonine kinase

CDK – cyclin-dependent kinase

CDKN2A – Cyclin-Dependent Kinase Inhibitor 2A

CLCN6 – Choride channel, voltage-sensitive 6

CNS – Central Nervous System

C-terminal/terminus – Carboxyl-terminal

Cy3 – Cyanine 3

DAPI – 4’ 6-diamidino-2-phenylindole

DNA – Deoxyribonucleic acid

dNTPs – Deoxynucleotides

ddNTPs – modified deoxynucleotides that lack a 3’-OH group

EDTA – Ethylene Diamine Tetra Acetic acid

EGFR – Epidermal Growth Factor Receptor

ERK – Extracellular signal regulated kinase

ESR1 – Estrogen receptor 1

EZH2 – Enhancer of Zeste 2 Polycomb Repressive Complex 2 Subunit

E2F – E2 transcription factor

FAM131B – Family with sequence similarity 131 member B

FBS – Fetal Bovine Serum

FGFR1 – fibroblast growth factor receptor 1

FISH – Fluorescent In Situ Hybridization

g - gram

GNAI1 – Guanine nucleotide binding protein (G protein), alpha inhibiting activity polypeptide 1

G1 phase – Gap 1 phase of the cell cycle

HIST1H3B – Histone cluster 1, H3b

HIST1H3I – Histone cluster 1, H3i

H3F3A – H3 histone, family 3A

H3F3B – H3 histone, family 3B

IDH1 – Isocitrate Dehydrogenase 1

IDH2 – Isocitrate Dehydrogenase 2

IPOLFG – Instituto Português de Oncologia de Lisboa Francisco Gentil

IQ – Intelligence Quotient

KIAA1549 – KIAA1549 gene

KV – kilovolts

l – liter

MACF1 – Microtubule-Actin Crosslinking Factor 1

MAML2 – Mastermind like transcriptional coactivator 2

MAPK – Mitogen-activated protein kinases

MEK – Mitogen-activated protein kinase

min – minutes

MRKN1 – an E3 ubiquitin ligase

MYB – v-myb avian myeloblastosis viral oncogene homolog

MYBL1 – v-myb avian myeloblastosis viral oncogene homolog-like 1

MYBL2 – v-myb avian myeloblastosis viral oncogene homolog-like 2

NF1 – Neurofibromin 1

ng - nanogram

NOS – Not Otherwise Specified gliomas

N-terminal – Amino-terminal

PBS – Phosphate-buffered saline

PCDHGA1 – Protocadherin Gamma subfamily A, 1

PCR – Polymerase Chain Reaction

PDGFRA – Platelet Derived Growth Factor Receptor Alpha

PHGG – Pediatric High Grade Gliomas

PI3K – Phosphoinositide 3-Kinase

PLGG – Pediatric Low Grade Gliomas

PXA-like - pleomorphic xanthoastrocytomas-like

QKI – QKI, KH domain containing, RNA binding

Ras - Rat sarcoma viral oncogene homolog

Rb1 – Retinoblastoma 1

RNF130 – Ring finger protein 130

rpm – rotations per minute

RTK – Receptor Tyrosine Kinase

SDS – Sodium dodecyl sulfate

SETD2 – SET Domain Containing 2

S phase – Synthesis phase of cell cycle

SRGAP3 – SLIT-ROBO Rho GTPase activating protein 3

SSC – Saline Sodium Citrate Buffer

TACC1 – Transforming, Acidic Coiled-Coil containing protein 1

TACC2 – Transforming, Acidic Coiled-Coil containing protein 2

TE – Tris-EDTA buffer

TKD – Tyrosine Kinase Domain

TNB – Tris-NaCl-Blocking Buffer

TP53 – Tumor Protein p53

WHO – World Health Organization

WT – Wild-type

°C – Celsius degrees

µ – micro-

I - Introduction:

1 - Pediatric Tumors of the Central Nervous System (CNS):

Tumors of the CNS account for 20-25% of all pediatric cancer diagnoses in the developed world [14,15], being the most prevalent group of cancers in children, after leukemia [15]. Although uncommon, pediatric brain tumors represent the leading cause of cancer-related mortality in children and adolescents aged 20 years and under [1,15–17]; and the third leading cause of cancer-related death in young adults aged 20 to 39 years [1]. In addition to their relatively high mortality, CNS tumors are associated with extensive morbidities such as pituitary dysfunction, growth hormone deficiency, epilepsy, vision loss, impaired motor skills, memory dysfunction, attention and behavioral disorders and reduced IQ. So, about 90% of survivors are left with long term cognitive and psycho-social deficits [15].

Diagnosis of pediatric CNS tumors is traditionally based on histological grading. CNS tumors are classified according to World Health Organization (WHO) criteria based on cell morphology and location of the tumor. According to the last classification, from 2007, the main tumor classes are the following: neuroepithelial, cranial and paraspinal nerve, meningeal, lymphoma and hematopoietic, germ cell, sellar region and metastatic. Tumors are further segregated into distinct histological grades, from WHO grade I to WHO grade IV, on the basis of defined cytological and histological features, including cellularity, mitotic activity, nuclear atypia, microvascular proliferation and necrosis. The WHO grading scheme functions as a malignancy scale (grade I being the least and grade IV the most aggressive), as represented in Figure I.1 [2].

Gliomas are the most common histological type of primary CNS tumors in children [1]; they are a heterogeneous group of tumors that have neuroepithelial tissue origin and originate from glial cells (astrocytes, oligodendrocytes and ependymal cells) [18]. So, there are four major histologic classes of gliomas: (I) Astrocytic tumors; (II) Oligodendroglial tumors; (III) Neuronal and Mixed Neuroglial tumors, (IV) Ependymomas [1,19,20], often excluded from the glioma classification and regarded as a distinct disease [14] (see Figure I.1).

Pediatric Low-grade Gliomas (PLGGs) account for nearly half of all pediatric CNS tumors [7,21], comprising a diverse group of WHO Grade I and II tumors [7] that are generally categorized as nondiffuse or diffuse based on their extent of brain infiltration. Nondiffuse tumors, such as pilocytic astrocytomas, exhibit minimal infiltration, are predominantly benign and are often cured by surgery alone. In contrast, diffuse tumors such as diffuse astrocytomas, oligoastrocytomas and oligodendrogliomas, are associated with less favorable clinical outcomes,

including recurrence after initial resection, by virtue of their extensive infiltration and invasion into the brain [16] (Figure I.1).

A

	WHO Grades			
	I	II	III	IV
Astrocytic tumors				
Subependymal giant cell astrocytoma	■			
Pilocytic astrocytoma	■			
Pilomyxoid astrocytoma		■		
Diffuse astrocytoma		■		
Pleomorphic xantoastrocytoma		■		
Anaplastic astrocytoma			■	
Glioblastoma				■
Giant cell glioblastoma				■
Gliosarcoma				■
Oligoastrocytic gliomas				
Oligoastrocytoma		■		
Anaplastic Oligoastrocytoma			■	
Oligodendroglial tumors				
Oligodendroglioma		■		
Anaplastic oligodendroglioma			■	

	WHO Grades			
	I	II	III	IV
Neuronal and mixed neuronal-glial tumors				
Gangliocytoma	■			
Ganglioglioma	■			
Anaplastic ganglioglioma			■	
Desmoplastic infantile astrocytoma and ganglioglioma	■			
Dysembryoplastic neuroepithelial tumor	■			
Central neurocytoma		■		
Extraventricular neurocytoma		■		
Cerebellar liponeurocytoma		■		
Paraganglioma of the spinal cord	■			
Papillary glioneuronal tumor	■			
Rosette-forming glioneuronal tumor of the fourth ventricle	■			

B

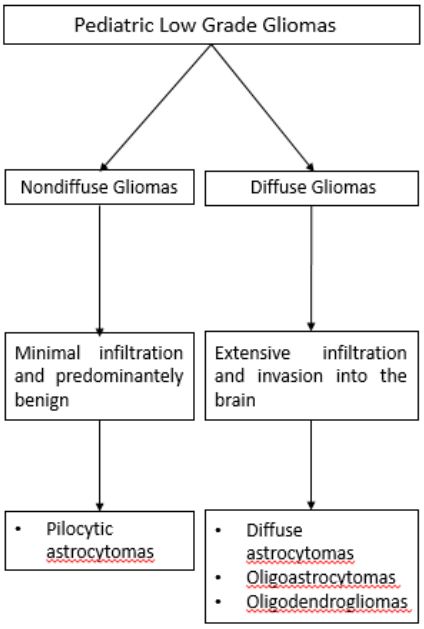

Figure I.1 – Classification of gliomas. (A) WHO Grading of Gliomas, adapted from Louis, et al (2007)[2]. (B) Schematic representation of pediatric low-grade gliomas in diffuse and nondiffuse gliomas [16]

Pediatric High-grade Gliomas (PHGG) comprise WHO Grade III and WHO Grade IV gliomas and remain one of very few incurable pediatric cancers, with a long-term survival rate of less than 10% [19]. The most common histological subtypes are glioblastoma anaplastic astrocytoma and anaplastic oligodendroglioma [19] and they account for 15-20% of pediatric brain tumors [7].

Due to the great heterogeneity and histologic overlap, some tumors cannot be categorized and are often referred to as Not Otherwise Specified gliomas (NOS). In low-grade gliomas, this entity represents nearly one-third of all PLGGs [16].

2 - Tumorigenesis

Cancer is a genetic disease that involves dynamic changes in the genome. So, despite the existence of distinct types of human cancer, the development of genomic instability and epigenetic modifications are essential for normal cells to acquire a variety of characteristics (such as self-sufficiency in growth signals, insensitivity to growth-inhibitory signals, evasion of programed cell death and immune destruction, limitless replicative potential, sustained

angiogenesis, tissue invasion and metastasis, and changes in cellular metabolism) that will rule their transformation into malignant cells [22,23].

For example, in the context of the development of genomic instability, the activating mutations or genetic rearrangements, affecting the structure of the *B-Raf* protein and resulting in a constitutive activation of mitogen-activated protein kinase (*MAPK*) pathway, are tightly related with the growth factor independence in tumor cells, contributing to uncontrolled cell proliferation. Another example is related with the insensitivity to growth-inhibitory signals in cancer cells that are tightly related with somatic, loss of function mutations or genetic rearrangements involving tumor suppressor genes (such as *RB1* and *TP53* genes). The loss of function of *TP53* gene is also associated with evasion to apoptosis [23].

In the context of epigenetic modifications, the repression of some genes through promoter methylation and the de-repression of others through demethylation, may also contribute importantly to tumor progression, not only in the cancer cells but also in the altered cells of the tumor-associated stroma [22,23]. Moreover, hypomethylation (demethylation of normally methylated sequences) has been associated with an extensive chromosomal instability which may favors tumor progression [22].

Like cancer, in general, gliomas develop as a result of genetic alterations that accumulate with tumor progression. Given the existent data that show that genetic alterations in gliomas vary according to the age of the patient, location, histology and tumor grade [1], it is becoming clear that information derived from cytogenetics and molecular genetics will play an increasingly more important role in tumor classification, particularly with respect to providing more precise diagnostic and prognostic information about particular tumors. So, incorporating these findings as companion diagnostics to routine pathology seems to be essential for better stratifying tumors and for the development of targeted treatments [3]. However, molecular diagnostics have only recently begun to be incorporated into the initial evaluation of CNS tumors [20].

3 - Pediatric Low-grade Gliomas (PLGGs)

PLGGs have been defined by MAPK/ERK pathway activation through a number of well-defined genetic aberrations [3,7], supporting the concept that PLGG is a "single pathway disease" (see Figure I.2) [1,5].

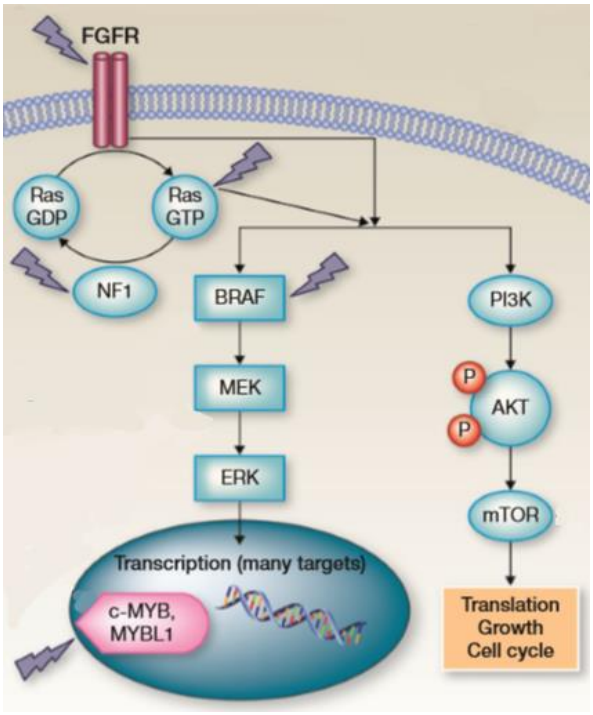

Figure I.2 – Overview of the major known mutations in PLGG. In this figure the strikes indicate the genes known to be altered in PLGGs: *BRAF, MYB* (*c-MYB*), *MYBL1*, *FGFR1* and *NF1*. The majority of the known genetic alterations in PLGGs lead to *MAPK/ERK* pathway activation. In some cases, the *PI3K* pathway is also activated. Adapted from Raabe, et al (2013). © 2013 American Association for Cancer

3.1 – *BRAF*-driven gliomas

About 95% of Grade I gliomas are characterized by defects in *BRAF* proto-oncogene, in the 7q34 region [3], that encodes the *B-Raf* protein, an intracellular serine-threonine kinase member of the *Raf* kinase family that regulates the *MAPK* pathway signaling [1,5]. This pathway normally begins with the activation of a transmembrane receptor tyrosine kinase, which binds, phosphorylates and activates *Ras*, which in turn activates a *Raf* kinase, in turn activating *MEK1/2*, leading to activation of the *ERK1/2* transcription complex (see Figure I.2) [5].

Under normal circumstances, *B-Raf N-terminal* regulatory domain inhibits its *C-terminal* kinase domain. When *Ras* activates *B-Raf*, it binds to the *N-terminal* domain of *B-Raf*, the inhibition is released, and *MEK* is phosphorylated by the *Raf* kinases [5]. Thus, activating mutations or genetic rearrangements, affecting the *N-terminal* regulatory domain of *B-Raf* may result in a constitutive activation of MAPK pathway, involved in tumorigenesis [5].

In PLGGs, the most common genetic alteration involving the *BRAF* gene is a tandem duplication and rearrangement between *BRAF* and a gene centromeric to *BRAF, KIAA1549* [5,19], as demonstrated in Figure I.3. There are five known variants of this genetic rearrangement. The most frequent is the one that occurs between exon 16 of *KIAA1549* and exon 9 of *BRAF* [24]. The mechanism leading to *BRAF/KIAA1549* rearrangement is unclear. However, recent studies suggest that the process of microhomology-mediated break-induced replication may be involved in the generation of these structural rearrangements [1]. The end result of this genetic rearrangement is a fusion protein in which the *N-terminus* of the protein encoded by *KIAA1549* gene is fused with the *C-terminus* of the protein encoded by *BRAF* gene, preserving the *BRAF* kinase domain [25]. Consequently, it leads to the expression of the *B-Raf* protein that lacks its *N-terminal auto-inhibitory domain* and is constitutively active, resulting in the activation of the *MAPK/ERK* pathway [1,3,21].

The normal function of the *KIAA1549* gene is not known. However its participation in the fusion is apparently not critical because there are other alternative *BRAF* fusion partners such as *FAM131B, SRGAP3, MACF1, RNF130, CLCN6, MRKN1* and *GNAI1* genes that also result in an equally potent *BRAF* activation through loss of the *N-terminal auto-regulatory domain* [5,7,26].

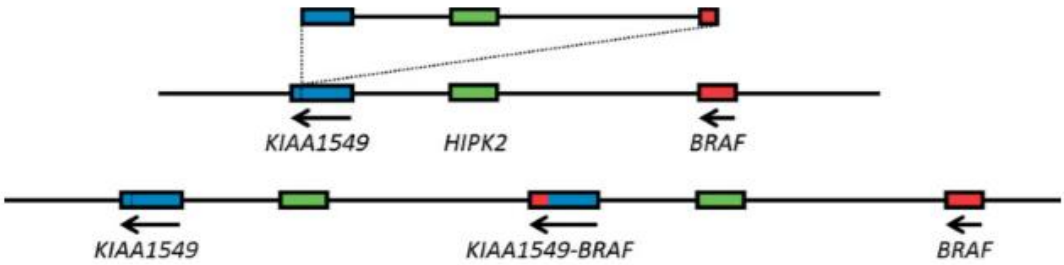

Figure I.3 – Schematic representation of *BRAF/KIAA1549* rearrangement. The *BRAF/KIAA1549* rearrangement is a result of a tandem duplication and fusion between *BRAF* and *KIAA1549* genes. Adapted from Forshew, et al (2009)[24].

The *BRAF/KIAA1549* rearrangement has been tightly correlated with pilocytic astrocytoma morphology [5,6]. However, Horbinski et al (2013)[5] and Gierke, et al (2015)[21] have observed that the frequency of this genetic rearrangement lessens with age, from approximately 80% in the first decade of life to 50% in the second decade, and less than 10% of pilocytic astrocytomas in patients over 40 years. In children (first two decades of life), the *BRAF/KIAA1549* rearrangement is nearly ubiquitous in posterior fossa pilocytic astrocytomas[7]. Cerebellar astrocytomas are the most frequent posterior fossa tumors in children and nearly

80% of cerebellar pilocytic astrocytomas have this *BRAF/KIAA1549* rearrangement, compared to 50%–55% of non-cerebellar pilocytic astrocytomas [5]. However, the *BRAF/KIAA1549* fusion is also described in diffuse low-grade gliomas [7], though with lower incidences (15%). In PHGG the rearrangement is rarely seen [5], suggesting that this genetic alteration is exclusive of PLGG. The *BRAF/KIAA1549* rearrangement also appears to be a relatively favorable prognostic marker [9].

Besides the *BRAF/KIAA1549* rearrangement, several other different genetic alterations that transform the *B-Raf* kinase into a constitutively activated form have been reported to occur in PLGGs [19,21]. One of these alterations is the *BRAFV600E* mutation, a somatic mutation causing substitution of the amino acid valine by glutamic acid, at codon 600 [5,7]. Such somatic activating *BRAF* mutations are observed in up to 7% of human cancers and occur most frequently in malignant melanomas (60%) and papillary thyroid carcinomas (40-50%) [4,5,21].

Under normal circumstances, when *B-Raf* is activated by *Ras* (see Figure I.2), T599 and S602 amino acids, within the *B-Raf* activation segment, require phosphorylation to achieve maximal kinase activity. It was shown that, in human diseases, amino acids can be mutated to acidic residues to mimic phosphorylation and consequently activate kinases. Thus, it is thought that *BRAFV600E* mutation mimics the phosphorylation of the activating amino acids *T599* and *S602*, thereby leading to constitutive activation of the protein *B-Raf* which activates the *MAPK* pathway in a Ras-independent manner [4,27]**.**

This activating point mutation is highly prevalent in WHO Grade II pleomorphic xanthoastrocytomas [3,4] and in anaplastic pleomorphic xanthoastrocytomas [4]. The *BRAFV600E* mutation was also described to occur in 33% of the gagliogliomas, in 23% of the diffuse astrocytomas [3] and, in 10% of the glioblastomas [28]. As *BRAF* mutation rarely occur in conjunction with a *BRAF/KIAA1549* rearrangement in the same tumor [5], its incidence in pilocytic astrocytomas is low, around 6-9% [3,4].

The majority of *BRAF*-driven gliomas are low-grade and tend to stay that way [5]. This may be explained because the activation of the *MAPK/ERK* pathway can result in proliferation, survival and tumorigenesis but it can also trigger cell differentiation and senescence [5] (see Figure I.4). Raabe, et al (2011)[8] demonstrated this *MAPK/ERK* pathway duality in a pilocytic astrocytoma model with constitutive *BRAF* activation: initially the expression of the *BRAFV600E* mutation strongly promoted colony formation, without leading to significantly increased proliferation, but subsequently, oncogene-induced senescence limited proliferation.

Moreover, it was shown by Horbinski, et al (2012)[9] that the *CDKN2A* gene deletion in BRAF-driven gliomas had an adverse impact in the tumors' outcomes. The *CDKN2A* gene (cyclin-

dependent kinase inhibitor *2A*) located in the 9p21 region, coded a tumor suppressor protein – p16. The p16 protein acts as a negative regulator of the proliferation of normal cells, controlling the progression through *G1* into the *S phase* of the cell cycle. It interacts with the cyclin-dependent kinases *CDK4* and *CDK6*, inhibiting theirs ability to interact with *cyclins D* and, consequently, to phosphorylate the retinoblastoma protein (encoded by the *RB1* gene). This results in the non-release of *E2F* transcription factor that activates genes involved in the *G1-S* transition [22] (see Figure I.4). Thus, the worst outcomes associated with *CDKN2A* gene deletion can be explained because it was shown that *CDKN2A* deletion in *BRAF*-driven tumors could reflect a failure to induce senescence or an escape from the induced tumor senescence [8].

This *CDKN2A* gene deletion was also reported in several PHGGs with *MAPK/ERK* pathway activation [11,29]. However, in PHGGs this pathway activation is usually accompanied by impairment of the *p53/Rb* cell cycle pathway, which could explain why these tumors undergo progression rather than senescence [9].

Mistry, et al (2015)[30] demonstrated that *BRAFV600E* mutations and *CDKN2A* deletions constituted a clinically distinct subtype of pediatric secondary high-grade gliomas that arise from a primary PLGG, suggesting that these two genetic alteration may play a role in the malignant transformation of PLGGs.

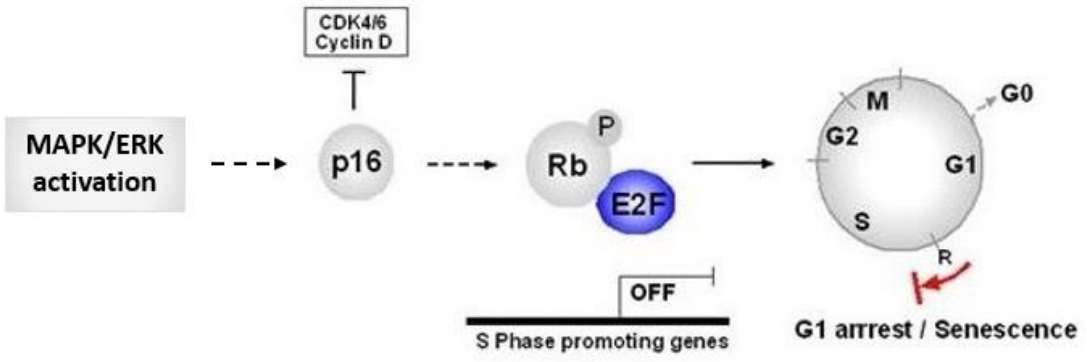

Figure I.4 – The role of *CDKN2A* gene in *BRAF*-driven gliomas: The activation of the MAPK/ERK pathway leads to the expression of the tumor suppressor gene *CDKN2A*. The p16 protein (coded by *CDKN2A* gene) blocks the hyperphosphorylation of Rb (retinoblastoma protein) by inhibitory binding to the kinase CDK4/6. This keeps E2F transcription to bind to Rb, resulting in a permanent cell cycle stop in G1 phase (senescence). Adapted from Braig, 2007[48] (available in: http://edoc.hu-berlin.de/dissertationen/braig-melanie-2007-10-25/HTML/chapter1.html)

Another mechanism that activates the *MAPK/ERK pathway* in PLGGs are alterations, such as mutations or deletion, of the *NF1* gene (at 17q11.2), as represented in Figure I.2. The *NF1* gene is a tumor suppressor gene that encodes the Neurofibromin 1 protein. In normal

circumstances, this protein acts as a negative regulator of *Ras* in the *MAPK/ERK* pathway, preventing cell overgrowth. Alterations in *NF1* gene are related with Neurofibromatosis type 1, which is a hereditary tumor syndrome associated with the appearance of neurofibromas, gliomas and malignant peripheral nerve sheath tumors. In PLGGs, the NF1-related tumors account for less than 15% of the cases [3,31].

3.2 – Grade II Gliomas

Zhang, et al (2013)[3] reported, in their series of pediatric gliomas, that 56% of grade II gliomas were characterized by mutually exclusive gene rearrangements inducing gain of function of the *MYB*, *MYBL1* and *FGFR1* genes.

3.2.1 – *MYB* and *MYBL1* genes

The *myb* gene family consists of three members, named *A-myb* (8q22), *B-myb* (20q13) and *c-myb* (6q22), which encode nuclear proteins that function as transcriptional transactivators (*MYBL1, MYBL2* and *MYB*, respectively). Although these three genes share an extensive homology, their expression and biological functions are different [14,32]**.** While *MYB* and *MYBL1* genes expression is restricted to specific cell types and stages of development, *MYBL2* gene is expressed in all proliferating cells [32]. So, the *MYB* gene is highly expressed in proliferation epithelial, endothelial and hematopoietic cells and the *MYBL1* gene expression is restricted to the developing mammary gland, spermatogenic tissue, central nervous system, T and B cells [33,34].

The overexpression of *MYB* gene had been reported to be associated with leukemias, lymphomas, pancreatic, colon and breast tumors and the disruption of *MYBL1* expression leads to defects in the tissues where it is expressed that may be involved in tumorigenesis [33,34].

In their series of pediatric gliomas, Tatevossian, et al (2010)[14] and Zhang, et al (2013)[3] verified that *MYB* abnormalities at a genomic level, such as, *MYB* amplification or *MYB* rearrangements involving fusion with several different genes (*ESR1, MAML2, PCDHGA1* and *QKI*), were exclusive of diffuse gliomas, being present in 13%-22% of the cases. Moreover, Ramkissoon, et al (2013) [16] demonstrated in their series of diffuse PLGGs that 28% of the diffuse astrocytomas presented a partial duplication (of the first 9 exons) of *MYBL1* gene that resulted in the expression of a truncated *MYBL1* protein, without its *C-terminal* negative regulatory domain. However, Zhang et al (2013)[3] only described *MYBL1* rearrangements in 4.3% of the diffuse astrocytomas (one case) of their series of PLGGs.

3.2.2 – *FGFR1* gene

The *FGFR* (Fibroblast Growth Factor Receptors) family consists of four genes encoding closely related transmembrane tyrosine kinase receptors, named *FGFR1* to *FGFR4*. The *FGFR1* gene (8p11) encodes the Fibroblast Growth Factor Receptor 1. The *FGFR* proteins contain in their full-length form a hydrophobic leader sequence, three immunoglobulin-like (Ig I, II, and III) domains, an acidic box, a transmembrane domain and, a divided tyrosine kinase domain (TKD) (Haugsten, Wiedlocha, Olsnes, & Wesche, 2010; Turner & Grose, 2010).

FGFR1 overexpression has been identified in breast and prostate cancer, being associated with tumor progression and poorer prognostic due to cell division, motility, and formation of new blood vessels.

FGFR1 rearrangements and mutations were identified in pediatric gliomas [3,35]. According with Zhang, et al (2013) [3], the most frequent *FGFR1* rearrangement in PLGGs consists in an intragenic duplication of the entire *FGFR1* region encoding the TKD, resulting in two full-length TKDs that lead to *FGFR1* autophosporylation (Figure I.5). This rearrangement seemed to be exclusive of cerebral diffuse gliomas, being present in 24% of the cases. Zhang, et al (2013) [3] also described other *FGFR1* rearrangement in PLGGs, that involved fusion with *TACC1* and *TACC2* genes, in 2% and 0.7% of the cases, respectively. In their series of pediatric gliomas, Jones et al (2013) [35] and Zhang, et al (2013) [3] also reported three *FGFR1* missense mutations (*N554K, V559M, N546K* and *K656E*) occurring in 5% of pilocytic astrocytomas, in 6% of glioblastomas harboring the *K27M* mutations and in one oligoastrocytoma.

In pediatric gliomas, all of the reported alterations in the *FGFR1* gene lead to a substantial activation of both *MAPK/ERK* and *PI3K* pathways [3,35].

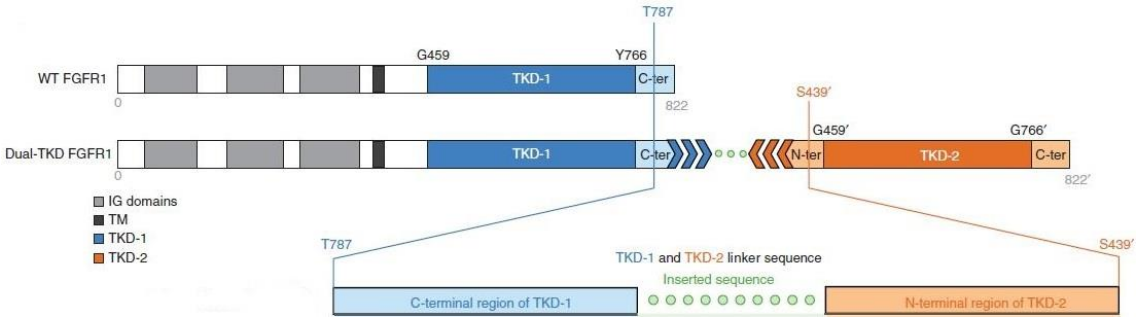

Figure I.5 - *FGFR1* rearrangement: TKD duplication. In this figure the wild-type FGFR1 proteins (WT FGFR1) are compared with the most frequent FGFR1 rearrangement in PLGG. This rearrangement consists in a TKD duplication that results in two full-length TKDs (TKD1 and TKD2) that are separated by a linker sequence. This rearrangement leads to FGFR1 autophosphorylation, resulting in the activation of MAPK/ERK and PI3K pathways. Adapted from Zhang, et al (2013)[3].

4 – Pediatric High-grade Gliomas (PHGG)

Gerges, et al (2013)[1] and Yuen and Knoepfler (2013)[36] showed that the most common and exclusive alterations of PHGGs, occurring in 60-80% of cases, were *K27M* and *G34R/V* mutations in *H3.1* and *H3.3* histones.

The histones *H3.1* and *H3.3* belong to the histone *H3* family. Histone *H3* is one of the five main histones involved in the chromatin structure of the eukaryotic cells [36,37]. However, the two variants have distinct functions: while the *H3.3* variant is enriched for posttranslational modifications associated with active transcription, in the *H3.1* variant, marks associated with gene silencing are the most common [37]. Moreover, while the histone *H3.3* is encoded by two different genes: *H3F3A* (1q41) and *H3F3B* (17q15) and is expressed in a replication-independent way [37,38], the histone H3.1 is encoded by several genes (being *HIST1H3B* gene one of them) and is only expressed during the S phase of the cell cycle [37].

In human gliomas, the *K27M* mutation (a lysine substitution for a methionine at codon 27) was reported to occur in *H3F3A* and *HIST1H3B* genes, but *G34R/V* mutations (a glycine substitution for an arginine or a valine, at codon 34) were only found in the *H3F3A* gene. These mutations lead to alterations of the *N-terminal* tail of the histone proteins, a region enriched in posttranslational modifications [12,36]. The roles of *K27M* and *G34R/V* mutations in tumorigenesis are independent of each other and occur through different mechanisms (Figure I.6) [36].

The *K27M* mutation (in *H3.3* and *H3.1)* is a gain-of-function mutation that leads to a global downregulation of the repressive histone mark *H3K27me3* and, consequently, to an increased acetylation of *K27* (*K27ac* is a histone mark mutually exclusive to *K27me3* and associated with active transcription) [18,36,38]. It is thought that the *H3K27M* mutant histone binds aberrantly to *EZH2* (the catalytic subunit of polycomb repressive complex 2 that spreads the *H3K27me3* mark throughout the genome) and inhibits it enzymatic activity [18,36]. In this way, reduced *H3K27me3* levels and consequent loss of polycomb repressive complex 2 activity could be altering specific transcriptional processes within the cell (as gene activation and abnormal gene expression) and thus become a driver of gliomagenesis in *K27M*-mutant PHGG [1,18,36] (see Figure I.6).

The *G34R* and the *G34V* mutations (in *H3.3*) interfere with the activating histone mark *H3K36me3*, leading to an alteration on *K36* methylation that is associated with abnormal gene expression [1,18]. As *SETD2* is the only known methyltransferase that catalyzes *H3K36me3* in humans, it is thought that the *H3.3G34R/V* mutant histone inhibits its function, leading to a consequent decrease in *H3K36me3* levels [12].

Schwartzentruber, et al (2012)[10] and Sturm, et al (2012)[11] observed in their series of pediatric glioblastomas that the *K27M* and the *G34R/V* mutations were heterozygously expressed and mutually exclusive in tumors. Moreover, Sturm et al (2012)[11] also demonstrated, in the same series of pediatric glioblastomas, that the gene expression patterns of the *K27M* mutant tumors closely match with the mid- to late-fetal stages of striatum and thalamus development and that the *G34R/V* mutant signature appears to be most strongly expressed in early embryonic regions and early- to mid-fetal stages of neocortex and striatum development, possibly indicating different cellular origins and/or time of tumor initiation for these two subgroups. In fact, these histone mutations were shown to have different distributions according to the brain region and patients' age: while *H3.1 K27M* mutation appears to be restricted to diffuse infantile pontine gliomas and non-brainstem pediatric glioblastomas in a younger range of patients (median age of 4.75 years) [12,13]; *H3.3 K27M* mutations are specific of tumors with midline locations (thalamus, pons and spinal cord) of patients with a median age of 10.5 years and; *H3.3 G34R/V* mutations were only observed in the cerebral cortex of older children and adolescents (median age of 18 years) [10,11] (Figure I.6). The comparison of the patients' overall survival also showed that the patients with gliomas harboring the *K27M* mutation had a shorter survival time and consequently a worse prognostic, relatively to the patients with *G34R/V*-mutant gliomas [11] (Figure I.6).

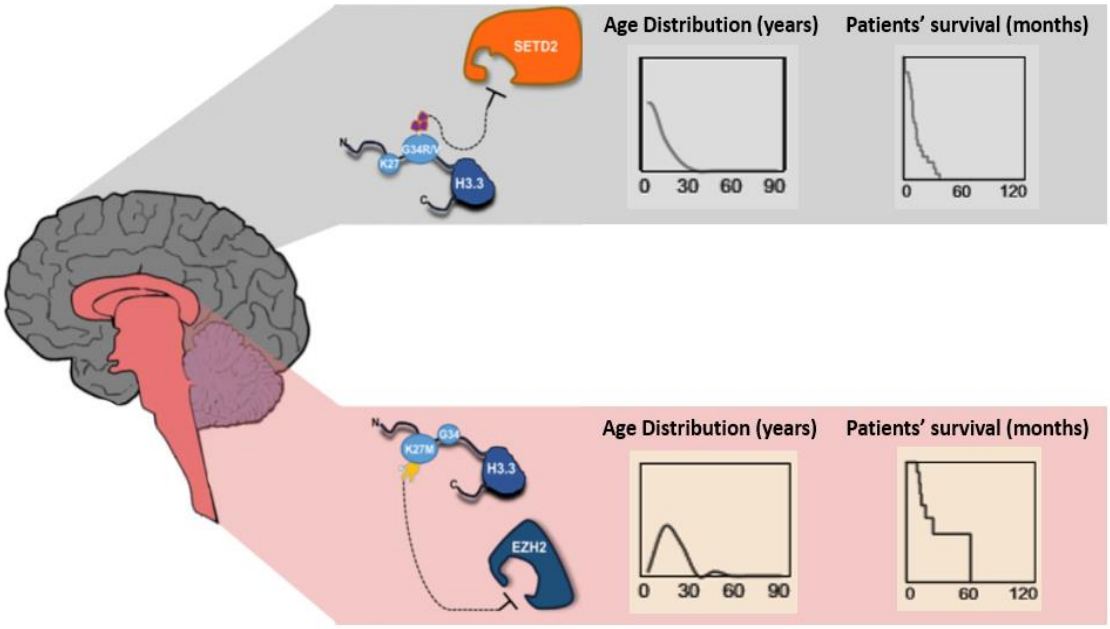

Figure I.6 - Distribution and Characteristics of *H3.3*-Mutated Gliomas. *G34R/V* mutations (gray, top) in *H3F3A* gene are located, primarily, in the cerebral hemispheres of older children and adolescents (median age 18 years) and appear to affect *K36me3* levels, possibly through inhibition of the methyltransferase *SETD2*. *K27M* mutations (pink, down) in the *H3F3A* gene are found, primarily in midline locations (spinal cord, thalamus, pons and brainstem) of child patients (median age 10.5 years) and seem to attenuate the *EZH2* methyltransferase function, decreasing global *K27me3* levels. Moreover, the *K27M* mutation is associated with a shorter overall survival time when compared to the G34R/V mutations. Adapted from Yuen & Knoepfler (2013)[36] and Schwartzentruber, et al (2012)[10].

Other genetic alterations have been identified in pediatric and adult glioblastomas, such as alterations in *PDGFRA, EGFR, IDH1* and *IDH2* genes. Thus, seven biologic subgroups of pediatric and adult glioblastomas were identified based on specific molecular-genetic alterations and key clinical parameters, which are the following: K27 (characterized by the *K27M* mutation), G34 (characterized by the *G34R/V* mutations), PXA-like (characterized by the *BRAFV600E* mutation and CDKN2A homozygous deletion), RTK-I (enriched for *PDGFRA* amplification and *CDKN2A* gene deletion), RTK-II (associated with *EGFR* gene amplification and *CDKN2A* gene deletion) Mesenchymal (characterized by low incidence of copy-number changes and no characteristic point mutation) and IDH (associated with mutations in *IDH1* and *IDH2* genes). While the K27, the G34 and the PXA-like subgroups are exclusive of the pediatric population, the RTK-II subgroup was only identified in adult patients and the RTK-I, the Mesenchymal and the IDH subgroups were identified in both adult and pediatric populations. Moreover, the patients' overall survival seems to be longer in PXA-like, IDH1 and G34 subgroups when compared with K27, RTK-I, RTK-II and Mesenchymal subgroups. All glioblastomas subgroups, except the K27, are associated with hemispheric locations [11,18,28,29].

II - Objectives:

The aims of the current study were fundamentally two:

1) To establish the genetic profiling by investigating the frequency of alterations in the *BRAF, MYB, MYBL1, FGFR1, CDKN2A, H3F3A, H3F3B* and *HIST1H3I* genes in pediatric gliomas; to correlate them with clinical features, such as: patients' gender, age at time of surgery, outcome and tumors' location and histological classification and to discuss our findings in order to better stratify tumors and treatments

2) To analyze the aforementioned genetic alterations in cell lines established from pediatric brain tumors at the laboratory, aiming that these cell lines offer findings that may pave the way into the development of more efficient therapies for pediatric gliomas.

III - Materials and Methods:

The present work can be divided into three major experimental stages: the first is a fluorescent in situ hybridization (FISH) analysis (in fresh and paraffin embedded material), the second is sequencing using Sanger methodology (in fresh and paraffin embedded material), and the third, cell culture (from fresh material).

While FISH analysis was used to identify the *BRAF/KIAA1549* rearrangement and fusion, *MYB, MYBL1* and *FGFR1* rearrangements and *CDKN2A* deletion; sequencing (using Sanger methodology) was used to identify single point mutations in *BRAF, H3F3A, H3F3B* and *HIST1H3I* genes. Cell culture was used to establish cell lines from tumors (see Figure III.1).

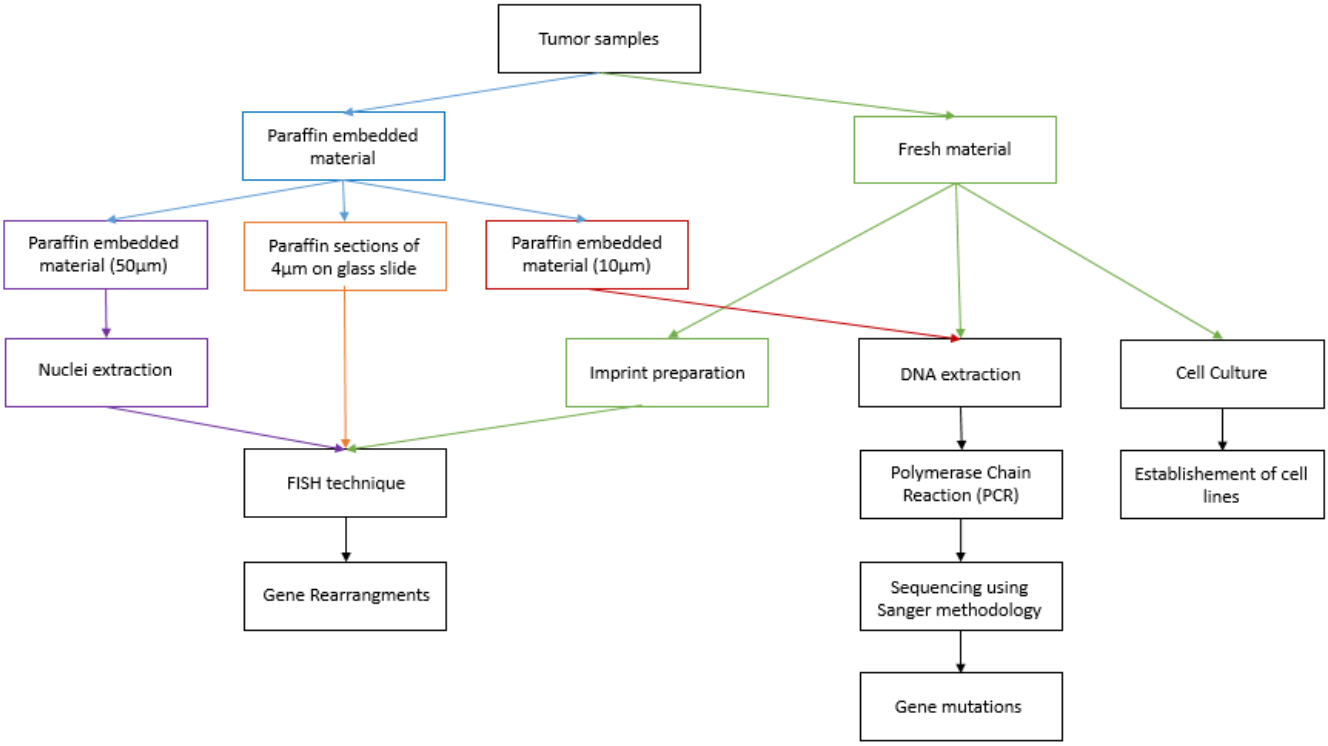

Figure III.1 – Schematic representation of the experimental work. Tumor samples were received as fresh material or embedded in paraffin, normally 10 cuts of 10µm and 3 cuts of 50µm or as 4µm cut on a glass slide. The experimental work was divided into three stages: (1) FISH (in fresh and paraffin embedded material) to analyze gene rearrangements; (2) Sequencing using Sanger methodology to analyze gene mutations; and (3) Cell culture (from fresh material) to establish cell lines from tumors.

1 – Biological Material – Patients Samples

In the context of this thesis, samples were studied from pediatric gliomas referred to the IPOFG from 1992 to 2015. Tumor samples were received as fresh material or embedded in paraffin, normally 10 cuts of 10µm and 3 cuts of 50µm or as 4µm cut on a glass slide.

In total, 109 pediatric gliomas were studied for genetic alterations: 67 (61.5%) grade I gliomas, 13 (11.5%) grade II gliomas, 14 (12.8%) grade III gliomas, 8 (7.3%) grade IV gliomas and 7 (6.4%) not otherwise specified (NOS) gliomas (Figure III.2). The following variables were collected: patient's gender, patient's age at the time of tumor surgery or biopsy, tumor location and histological classification.

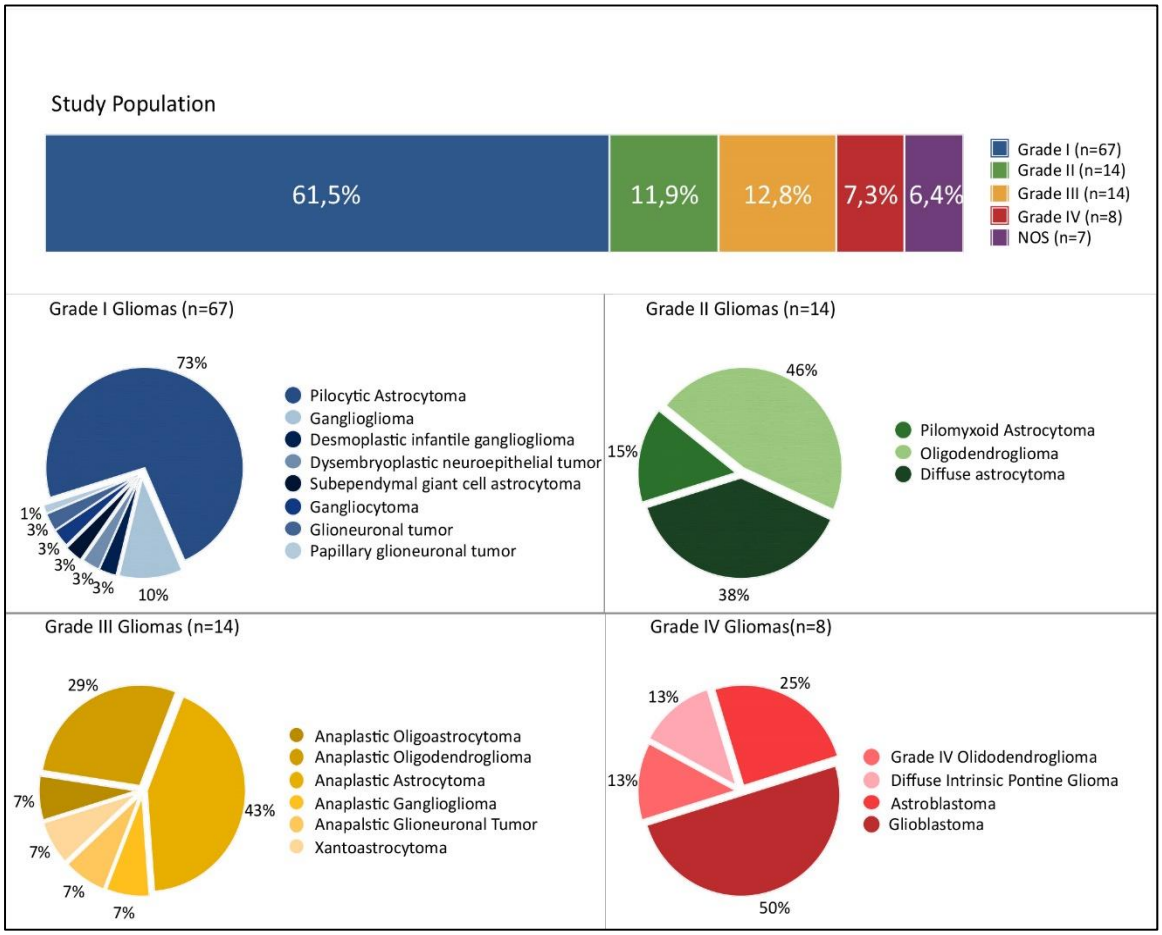

Figure III.2 – Representation of the study population. The graphic "Study Population" (on top) represents all the studied gliomas (in the context of this work) by WHO Grades. In this graphic, NOS (in purple) represents the group of the Not-Otherwise Specified Gliomas. Each one of the remaining four graphics (Grade I Gliomas, Grade II Gliomas, Grade III Gliomas and Grade IV Gliomas) represents the histological subgroups within each WHO grade. The number of gliomas studied is represented between brackets in each graphic.

Due to the lack of biological material or quality of the results, not all genes were analyzed in all samples.

Although posterior fossa gliomas normally include brainstem and cerebellum gliomas, for research purposes a subdivision in three groups was done based on the location of the glioma: cerebellum, brainstem and, when no further information was obtained, posterior fossa.

2 – Fluorescent In Situ Hybridization (FISH)

FISH is a cytogenetic technique in which a specific short strand of DNA labeled with a fluorescent dye (DNA probe) is used to detect genetic abnormalities in a target DNA sequence. Thus, FISH is based on the inherent organization of DNA into two antiparallel complementary strands: after denaturation of target DNA, single-stranded DNA probes are allowed to form hybrid double-stranded complexes with their complementary genomic sequence. FISH probes can be directly labelled with the incorporation of a fluorophore or indirectly labelled with the incorporation of a non-fluorescent hapten or molecule that uses an enzymatic or immunological detection system [39]. The principles of FISH are represented in Figure III.3.

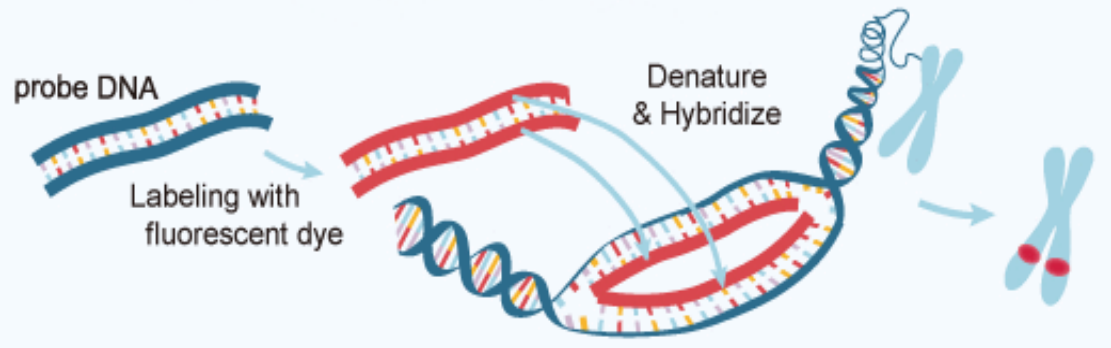

Figure III.3 – The Principles of FISH. In FISH technique, a DNA probe (blue) is directly or indirectly labelled with a fluorescent dye (red). The labelled probe and the target DNA are then denatured and hybridized which allows the detection of the probe signal by a fluorescent microscope. Available in: http://www.abnova.com /support/resources.asp?switchfunctionid=%7BB4285500-DB85-435D-BE02-2BF420D5C70D%7D

One of the most important considerations in FISH analysis is the choice of probe. There are three main types of probes, each with a different range of applications: whole-chromosome painting probes (mainly used in the identification of both numerical and structural chromosome aberrations in metaphase spreads), repetitive sequence or enumeration probes (mainly used as centromeric-specific probes to detect aneuploidies), and locus-specific probes (which are usually genomic clones used to detect structural rearrangements) [40,41].

FISH enables a multicolor detection of simultaneously hybridized probes. So, beyond single signal probes, dual-color probes are broadly used as dual fusion (translocation) probes, break apart ("split-apart" rearrangement) probes, and deletion detection probes. In a dual fusion probe, each gene involved in a translocation is labelled in a different color (normally, red and green) and a juxtaposition of the genes (due to the translocation) results in a fusion signal (yellow). A break apart probe consists of sequences flanking the target gene causing the 5' and 3' portions of the gene, to be labeled in different colors (normally, red and green). Thus, a separation of the different colored signals, is observed when a translocation or a rearrangement occurs. In a deletion detection probe a locus-specific probe is used in conjunction with an enumeration probe [40,41].

In the present work, the FISH technique was performed in interphase nuclei with DNA probes indirectly labelled. These probes are labelled with biotine or digoxigenin that are then detected with specific antibodies: streptavidin combined with cyanine 3 (Cy3) fluorophore (*Jackson ImmunoResearch Laboratories*) and anti-digoxigenin-fluorescein (*Roche*), respectively. Cy3 is detected in the red spectrum, while fluorescein is observed in the green spectrum, thereby being detectable under a fluorescence microscope through a red and a green filter, respectively (Table III.1).

The *BRAF/KIAA1549* rearrangement was studied by FISH with a dual fusion probe in which the *BRAF* gene was labeled in red and the *KIAA1549* gene was labelled in green (see table III.1), as well as with an enumeration probe directed against the centromeric region of chromosome 7. Break apart probes were used to study *MYB, MYBL1*, and *FGFR1* genes and to study the *CDKN2A* gene; furthermore, a locus-specific probe for the gene and an enumeration probe for chromosome 9 were used (see table III.1).

2.1 – DNA Probes Preparation

To label the DNA probes a commercial kit was used: the BioPrime® DNA Labeling System. The principle of this technique is to incorporate the biotin (or digoxigenin) into nucleic acid probes, which will be detected by anti-biotin or anti-digoxigenin antibodies, respectively. So, random primers (octamers) are annealed to the denatured DNA template and extended by Klenow fragment (large fragment of DNA polymerase I) in the presence of biotin or digoxigenin, to produce sensitive biotinylated or digoxigenin labeled-DNA probes for use. With this kit, a DNA synthesis occurs, resulting in a 10-40 fold amplification of the probe. To separate unincorporated nucleotides from the labelled probes, an ethanol precipitation was used. The probes were then dissolved in TE (DNA Hydration Solution, *Citogene*) and stored at -20°C. Labelled DNA was

precipitated in the presence of Human Cot-1 DNA® or UltraPure™ Salmon Sperm DNA Solution (for centromeric probes), as both block non-specific hybridization. A FISH protocol was used for metaphases from a normal human donor peripheral blood to confirm labelled probes specificity.

Table III.1 – Probes used for FISH and their characteristics. Descriptive table of the probes used in FISH analysis. Each column represents a probe characteristic: name, type, localization and application, and the label used.

Gene	Name	Type	Chromosomic Localization and Application	Label
BRAF	RP4-592P3	Dual Fusion	7q34. To detect the BRAF/KIAA1549 fusion	Biotine (red)
	RP4-726N20	Dual Fusion	7q34. To detect the BRAF/KIAA1549 fusion	Biotine (red)
KIAA1549	RP11-148L5	Dual Fusion	7q34. To detect the BRAF/KIAA1549 fusion	Digoxigenin (green)
MYB	RP11-63K22	Break Apart	6q23.3 (5' gene portion). To detect gene rearrangements	Biotine (red)
	RP11-170P19	Break Apart	6q23.3 (3' gene portion). To detect gene rearrangements	Digoxigenin (green)
MYBL1	RP11-117K19	Break Apart	8q13.1 (5' gene portion). To detect gene rearrangements	Biotine (red)
	RP11-110J18	Break Apart	8q13.1 (3' gene portion). To detect gene rearrangements	Digoxigenin (green)
FGFR1	RP11-118H9	Break Apart	8p11.23 (5' gene portion). To detect gene rearrangements	Digoxigenin (green)
	RP11-246A12	Break Apart	8p11.23 (3' gene portion). To detect gene rearrangements	Biotine (red)
CDKN2A	RP11-149I2	Single signal	9p21.3. To detect gene deletions	Digoxigenin (green)
Centromere of chromosome 7 (CEP 7)	pZ7.5	Enumeration	Centromeric region of CEP 7. To detect chromosome deletions	Biotine (red)
Centromere of chromosome 9 (CEP 9)	pMR9A	Enumeration	Centromeric region of CEP 9. To detect chromosome deletions	Biotine (red)

2.2 - The FISH Methodology:

FISH techniques were performed in our series of cases as represented in Figure III.4.

2.2.1 - Nuclei Extraction from paraffin embedded material:

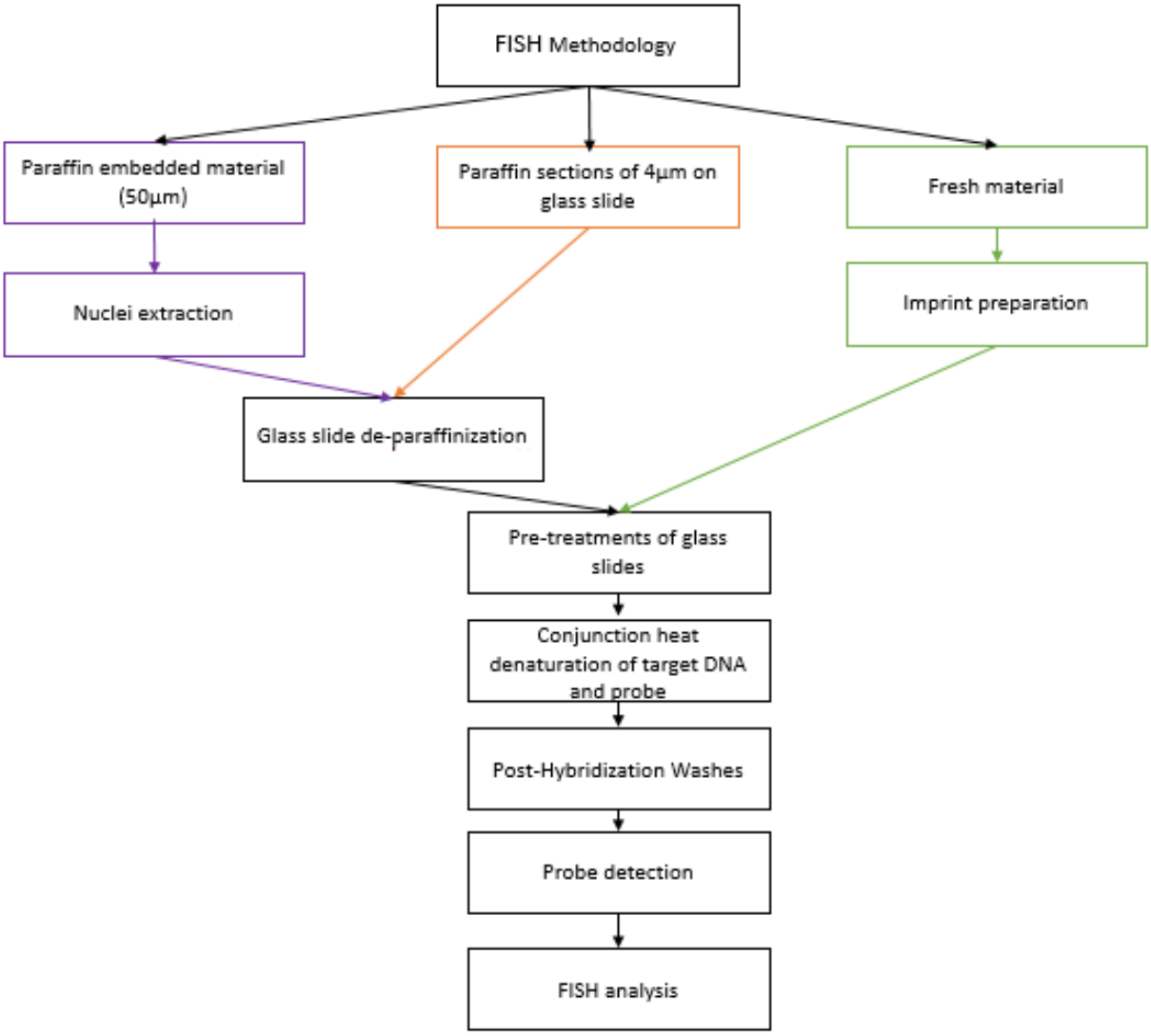

Figure III.4 – Schematic representation of the FISH methodology. The FISH technique was performed in fresh tumor material, paraffin embedded tumor material (cuts of 50µm and sections of 4µm on glass slide). First it was necessary to obtain nuclei from paraffin embedded material (nuclei extraction) and from fresh material (imprint). Paraffin sections of 4µm on glass slide were ready to use. A glass slide de-paraffinization was done in the paraffin embedded material. Five steps were then performed: Pre-treatment of glass slides, heat denaturation of target DNA and probe, Post-hybridization washes, Probe detection, and FISH analysis.

Nuclei extraction was done in paraffin embedded material (cuts of 50µm). This procedure consisted in a tissue de-paraffination, in which paraffin was dissolved at room temperature with three 10 min changes of xylene. Then, to digest the cytoplasm and set the nuclei free, paraffin sections were treated with protease (P8038-100MG, *Sigma-Aldrich*; 100µl protease/1ml Carlsberg solution) for 1 hour at 37°C. This enzymatic digestion was accompanied by a mechanical digestion and was stopped with ice cold (4°C) PBS. Free nuclei were then

submitted to a fixation process which consisted in the destruction of non-nuclear material by nuclei resuspension in a freshly prepared fixative (three parts methanol and one part glacial acetic acid). The resulting fixed nuclei suspension was spread on a glass slide (Appendix 1).

2.2.2 – Imprint preparation from fresh material

An imprint consists in touching the tumor fragment gently on a glass slide. After a 30min drying period at room temperature, glass slides were submitted to a hypotonic solution (NaCl 0.2%), which caused cellular membrane rupture and cellular lysis. Then, nuclei were submitted to a fixation process, to destroy non-nuclear material, by using a freshly prepared fixative (three parts methanol and one part glacial acetic acid).

2.2.3 – Glass slide de-paraffinization

This procedure was only done to glass slides from paraffin embedded material (10µm) and paraffin sections (4µm) in glass slide. It is an incubation in xylene and 100% ethanol for 30min each.

2.2.4 – Pre-treatments of glass slides

Pre-treatments of glass slides consisted in cell permeabilization with the purpose of making the target DNA (from the tumor) accessible for probe binding. This was accomplished with 2xSSC washes at different temperatures (5min at 37˚C, 30min at 75˚C, 3min at 37˚C) for imprints and nuclei from embedded paraffin material; with Juice (citrate buffer, 1x at 90°C for 17 min) for 4µm paraffin sections; and with enzymatic reactions, which digest the proteins that surround the nucleus: Proteinase K (P6556-100MG, *Sigma-Aldrich*) for nuclei from embedded paraffin material (10min) and Pepsin (P7000-100G, *Sigma-Aldrich*) for imprints and sections in glass slide (5-10min and 45min, respectively). Enzymatic reactions were stopped with ice cold (4˚C) PBS. At room temperature, glass slides were washed in PBS for 5 min and incubated in a Buffer Solution (5ml $MgCl_2$ with 95ml PBS). Subsequently they were submitted to a Fixation Solution (5ml $MgCl_2$, 3,7ml of Formaldehyde and 91.3ml of PBS). Finally, glass slides were dehydrated and air dried. (Appendix 1).

2.2.5 – Conjunction heat denaturation of target DNA and probe

The specific probe, diluted in hybridization solution, was added to the nuclei area in the glass slides and co-denatured with sample DNA: 5min at 90°C for nuclei from paraffin embedded material, 5min at 75°C for imprints, and 15min at 85°C for 4µm sections in glass slide. After denaturation, glass slides were stored for 16h at 37°C in a moist chamber for hybridization.

2.2.6 – Post-Hybridization Washes

Post-hybridization washes remove residual probe and unspecific bindings that interfere with the hybridization signal and are performed by first immerging glass slides for 15min, in a 50% of formamide solution at 42-43˚C and, then, in a 2xSSC solution with Tween 20 at 42-43˚C.

2.2.7 – Probe detection

The probes used in the present work were indirectly labelled. So, after post-hybridization washes, two incubation steps were performed: in the first incubation, TNB (Blocking Reagent, *Roche*) was used (10min at room temperature) to bind to nonspecific sequences and decrease background; the second incubation (30min at 37°C) was done with specific antibodies: Streptavidin conjugated with Cy3 fluorophore (*Jackson ImmunoResearch Laboratories*) and anti-digoxigenin-fluorecein (*Roche*), for biotine and digoxigenin labeled probes (respectively). To avoid unspecific bindings, antibodies were diluted in TNB in a proportion of 1:300 for streptavidin conjugated with Cy3 fluorophore and 1:100 for anti-digoxigenin-fluorecein. To remove residual antibodies, glass slides were washed twice in TNB buffer, with agitation. After being dehydrated, glass slides were air dried and mounted in VECTASHIELD® Mounting Medium with DAPI (4',6-diamidino-2-phenylindole). DAPI is a nuclear counterstain, it is observed in the blue spectrum, thereby being detectable under a fluorescence microscope through a blue/cyan filter. Glass slides were stored in the dark at 4°C.

2.2.8 – FISH analysis

FISH analysis was performed under a fluorescence microscope linked to a CytoVision® software (Applied Imaging, UK). FISH analysis was performed by counting at least 100 cells per slide with intact, non-overlapping nuclei taken from different randomly chosen fields of view. The counted scores were expressed as percentage value, using a minimum cutoff level of 10% to define significant cell clone.

3 – Sequencing using Sanger Methodology:

DNA sequencing allows nucleotide sequence determination. This technique is based on Sanger's methodology, where there is a selective incorporation of chain-terminating dideoxynucleotides (ddNTPs: modified dNTPs that lack a 3'-OH group, required for the formation of a phosphodiester bond between two nucleotides, causing DNA polymerase to cease extension of DNA when a modified ddNTP is incorporated) by DNA polymerase during in vitro DNA replication. Each ddNTP is labelled with a different color fluorophore to differentiate the four nitrogenous bases (adenine, guanine, cytosine and thymine) [41].

In the context of this work, sequencing using Sanger methodology was used to identify single point mutations in four specific genes: *BRAF, H3F3A, H3F3B* and *HIST1H3I* genes. DNA for gene analysis was extracted by different procedures according to the material used (as described in sections 3.1, 3.2, and 3.3). Target genes amplification was achieved through polymerase chain reaction (PCR), as described in section 3.5.

3.1 – DNA extraction from paraffin embedded material

The protocol used was adapted from Imyanitov, et al (2001), BioTechniques[42]. This procedure briefly consisted in a tissue de-paraffinization, where 10µm sections of paraffin embedded material were incubated in xylene and ethanol for 30min each. To permeabilize nuclei Proteinase K (P6556-100MG, *Sigma-Aldrich*) was used. The extracted DNA was diluted in chelating resin Chelex (Instagene matrix BIO-RAD) and precipitated with sodium acetate (3M NaAc, pH 5.2) and 100% ethanol. For mutation analysis DNA was dissolved in TE (DNA Hydration Solution, *Citogene*).

3.2 – DNA extraction from fresh material

The first step was a mechanical digestion of the tumor fragment. Then, a chemical disintegration was done with Buffer Lysis, SDS 10% and Proteinase K (P6556, *Sigma-Aldrich*), for 2-3 hours at 56°C. These three reagents provoke cellular lysis, lipids dissolution and proteins digestion. Acid nucleic extraction from the tumor fragment was done through the phenol-chloroform method. These two reagents denature proteins, rendering them solubilized in the phenolic phase. The latter is efficiently separated from the aqueous phase, where the DNA is. DNA precipitation was done with sodium acetate (3M NaAc, pH 5.2) and 100% ethanol. It was then dissolved in TE (DNA Hydration Solution, *Citogene*).

3.3 – DNA extraction from cell culture

The protocol used was adapted from the Citogene® DNA cell and tissue kit. The obtained DNA was precipitated with isopropanol and then dissolved in TE (DNA Hydration Solution, *Citogene*).

3.4 – DNA quantification

Quantification of DNA re-suspended in TE (DNA Hydration Solution, *Citogene*) was done using NanoDrop 2000 (*Thermo Scientific*) spectrophotometer. For gene analysis, DNA was diluted to 80ng/µl.

3.5 – Polymerase Chain Reaction (PCR)

PCR is an enzymatic technique that allows *in vitro* amplification of DNA fragments. This process involves three main steps that are repeated in various cycles, normally between 30-40 cycles: target DNA denaturation (at 95°C), annealing (primers bind to their complementary sequences) and enlongation (polymerase synthesizes a new DNA chain in the presence of magnesium ions – Mg^{2+} – and deoxynucleotides – dNTP's). Primers used in the PCR reactions are those described in Table III.2. All PCR reactions were done in a termocycler *Veriti* (*Applied Biosystems*), using the programs in Figure III.5.

Table III.2 – Primers used for each gene PCR reaction. Representation of the primers used in PCR for the genes analyzed: *BRAF*, *H3F3A*, *H3F3B* and *HIST1H3I*

Gene	Foward Primer	Reverse Primer
BRAF	5' tcataatgcttgctctgatagga 3'	5' ccggtttttaaattagtcacct 3'
H3F3A	5' tttcctgttatccatcttttgtt 3'	5' tgaagattacgtctacccaaaatc 3'
H3F3B	5' cgcagcctgagtcattagggg 3'	5' atctccctcaccaacctctg 3'
HIST1H3I	5' cgtttcttgacccaaaacaga 3'	5' gagctctggaagcgcagat 3'

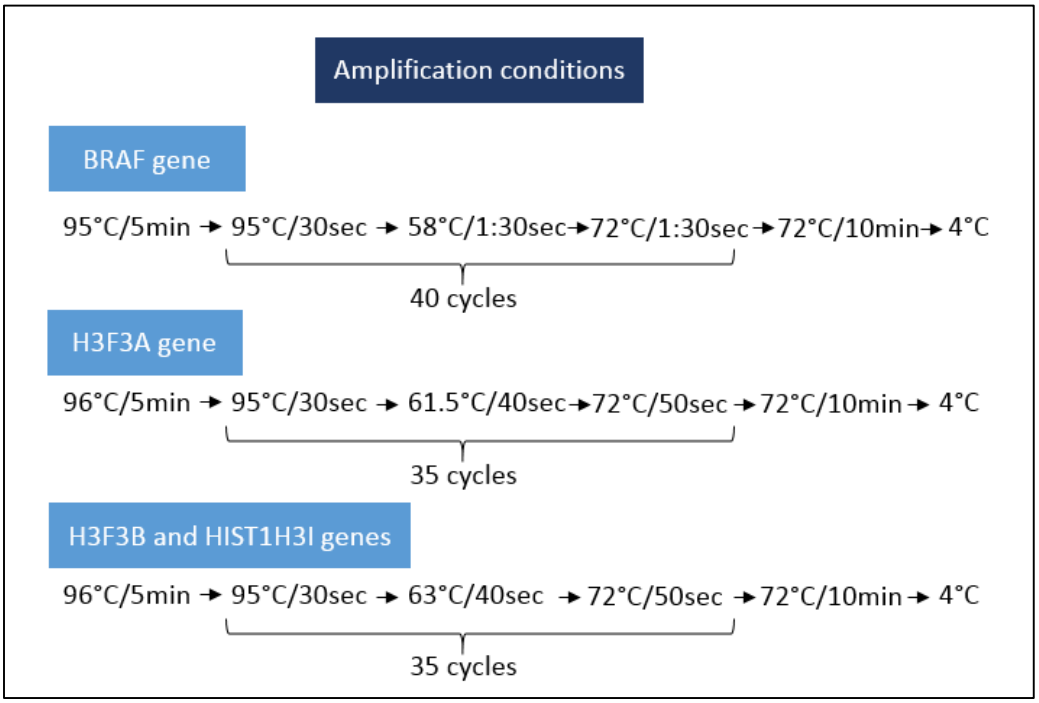

Figure III.5 - Programs used for PCR amplification *of BRAF, H3F3A, H3F3B* and *HIST1H3I* genes. The DNA denaturation step was performed at 95°C. The temperature used for the annealing step was different for each gene: 58°C, 61.5°C and 63°C for *BRAF, H3F3A, H3F3B* and *HIST1H3I* genes (respectively). For the enlongation step the temperature used was 72°C for all genes. The time of each step is represented in seconds (sec) and minutes (min). The number of cycles were 40 for *BRAF* gene and 35 for *H3F3A, H3F3B* and *HIST1H3I* genes. The reactions stopped at 4°C.

The PCR reaction efficiency was controlled through an agarose gel 2% (p/v) horizontal electrophorese. Each PCR product was enzymatic purified, using Exonuclease I (20U/µl *Thermo Scientific*) and a Thermosensitive Alkaline Phosphatase (FastAP: 1U/µl *Thermo Scientific*). After purification, PCR products were amplified by PCR with ddNTP labelled with different color fluorophores, using the conditions described in Figure III.6. These second PCR products were then purified and precipitated with a reactional mixture with EDTA (125mM) that chelates Mg^{2+} ions, and sodium acetate (3M, pH 4.6) that neutralizes nucleic acids charges.

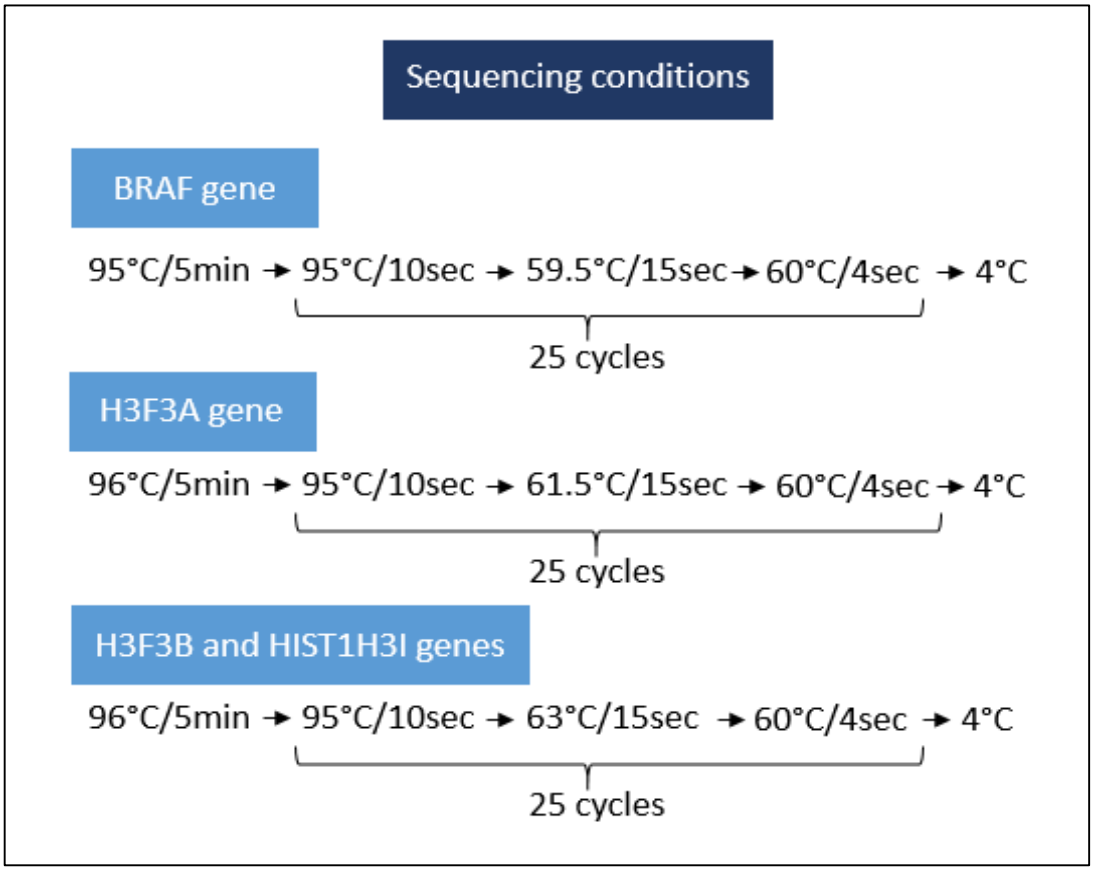

Figure III.6 – Programs used for sequencing reactions of *BRAF, H3F3A, H3F3B* and *HIST1H3I* genes. The DNA denaturation step was performed at 95°C. The temperature used for the hybridization step was different for each gene: 59.5°C, 61.5°C and 63°C for *BRAF, H3F3A, H3F3B* and *HIST1H3I* genes (respectively). For the extension step the temperature used was 60°C for all genes. The time of each step is represented in seconds (sec) and minutes (min). The number of cycles were 25 for all genes. The reactions stopped at 4°C.

3.6 – Sequencing

To sequence samples, an automatic sequencer, ABI Prism™ 3130 Genetic Analyser (*Applied Biosystems)*, was used, where capillary electrophorese occurred at 50°C and 15KV. Electrophoretograms were compared with the reference DNA sequence for the gene being studied to identify the presence or absence of mutations. Reference DNA sequences were obtained from *Ensembl* data base, available from: http://www.ensembl.org/index.html.

4 – Establishment of cell lines from tumors

Cell lines were established from tumor fragments at the laboratory. All the procedures were done in a laminar flow hood to guarantee sterile conditions.

First, the tumor fragment was mechanically disintegrated. The disintegrated tumor fragment was incubated at 37°C, in a moist 5% CO_2 environment, with collagenase the necessary time to achieve a complete dissociation of the tumor cells without plasmatic membrane destruction. The dissociation level was analyzed through an inverted microscope. The disintegrated material was then washed with RPMI 17% and centrifuged twice, at 2400rpm for 2min, in order to remove death cells and cellular debris. Tumor cells were then diluted in CNS tumors medium with 10% fetal bovine serum (FBS) and transferred to a culture flask (T25cm^2). At the end, there should have been, approximately, $1x10^5$ cells (1ml) per flask.

Cell cultures were maintained in a moist 5% CO_2 environment to preserve the neutral and stable pH. Culture mediums were renewed three times per week to avoid lack of nutrients and growth factors.

When cell cultures were confluent (70-80%), they were subcultured with trypsin in order to achieve cellular propagation. A cell line was considered to be established when it had the potential to be subcultured indefinitely under appropriate conditions (such as culture medium and space).

5 – Statistical Analyses

Statistical Analyses were carried out using *GraphPad Prism 5* software (San Diego, USA). The two-tailed Fisher's exact test was used to determine the correlations between the presence or absence of genetic alterations and patients' gender, tumors' WHO grade, histology and location. The unpaired two tailed Student's t-test was used to study the presence or absence of genetic alterations with patient's age. Survival curves were compared using the Log-Rank (Mantel-Cox) test. Differences were considered statistical significant at p-value < 0.05.

IV – Results:

In the present work, 109 pediatric gliomas were analyzed. The figure below (Figure VI.1) represents the summary of the obtained results.

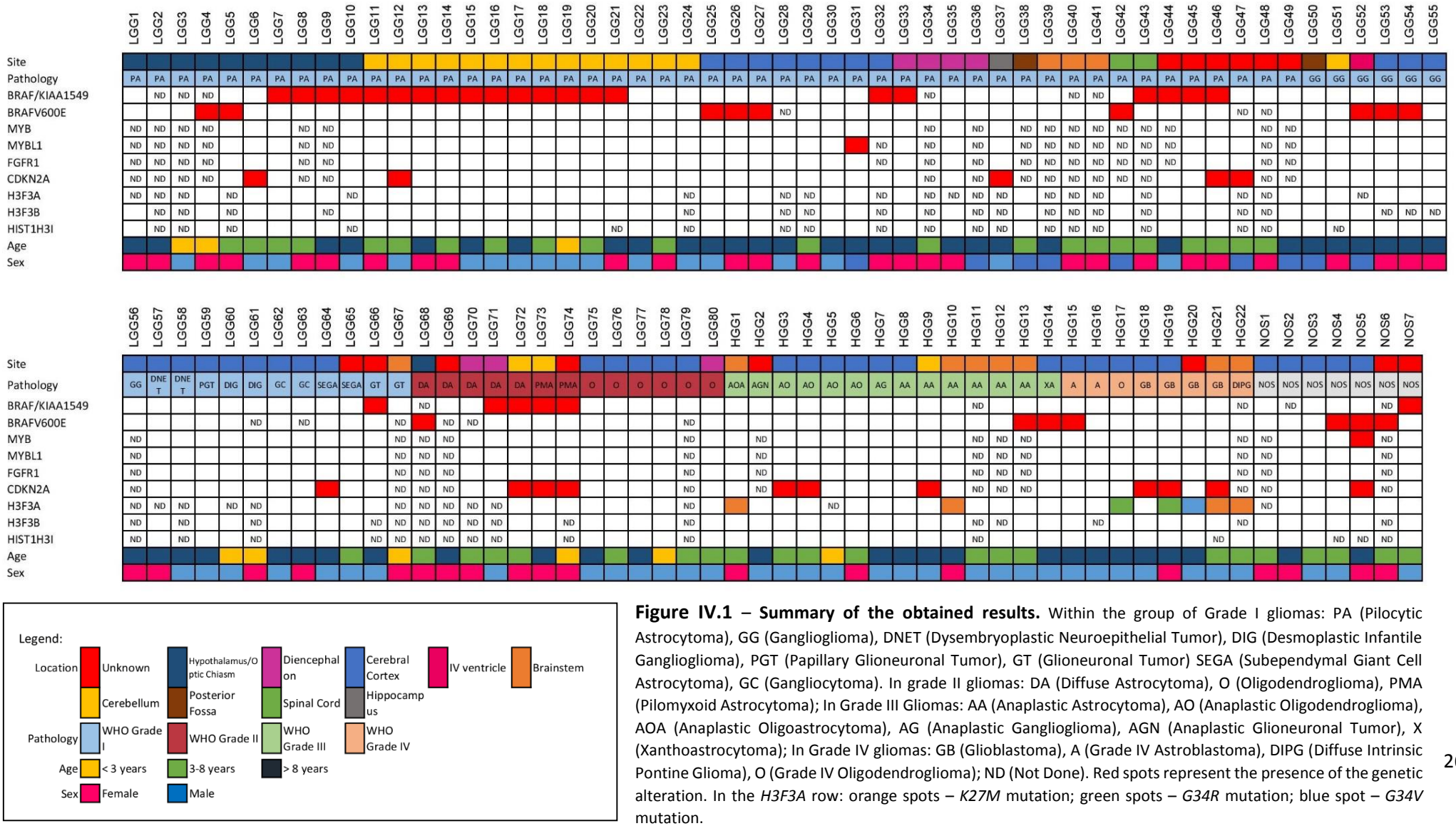

Figure IV.1 – **Summary of the obtained results.** Within the group of Grade I gliomas: PA (Pilocytic Astrocytoma), GG (Ganglioglioma), DNET (Dysembryoplastic Neuroepithelial Tumor), DIG (Desmoplastic Infantile Ganglioglioma), PGT (Papillary Glioneuronal Tumor), GT (Glioneuronal Tumor) SEGA (Subependymal Giant Cell Astrocytoma), GC (Gangliocytoma). In grade II gliomas: DA (Diffuse Astrocytoma), O (Oligodendroglioma), PMA (Pilomyxoid Astrocytoma); In Grade III Gliomas: AA (Anaplastic Astrocytoma), AO (Anaplastic Oligodendroglioma), AOA (Anaplastic Oligoastrocytoma), AG (Anaplastic Ganglioglioma), AGN (Anaplastic Glioneuronal Tumor), X (Xanthoastrocytoma); In Grade IV gliomas: GB (Glioblastoma), A (Grade IV Astroblastoma), DIPG (Diffuse Intrinsic Pontine Glioma), O (Grade IV Oligodendroglioma); ND (Not Done). Red spots represent the presence of the genetic alteration. In the *H3F3A* row: orange spots – *K27M* mutation; green spots – *G34R* mutation; blue spot – *G34V* mutation.

1 – *BRAF/KIAA1549* rearrangement

For the *BRAF/KIAA1549* rearrangement, 97 pediatric gliomas were analyzed: 60 Grade I, 12 Grade II, 13 Grade III, 7 Grade IV and 5 NOS. Of these, 27 cases were positive for the *BRAF/KIAA1549* rearrangement: 22 Grade I Gliomas (21 pilocytic astrocytomas and 1 glioneuronal tumor), 4 Grade II Gliomas (2 diffuse astrocytomas and 2 pilomyxoid astrocytomas), and 1 NOS. None of the PHGG analyzed was positive (Table IV.1).

Table IV.1 – Cases studied for *BRAF/KIAA1549* rearrangement. The gliomas studied for *BRAF/KIAA1549* rearrangement are represented in the table above. Each row corresponds to the tumors' histological classification. Each column presents the number of cases and the respective percentage in brackets.

BRAF/KIAA1549	Positive (dup/fus)	Negative
Grade I Gliomas	22 (37%)	38 (63%)
Pilocytic Astrocytomas	21 (48.8%)	22 (51.2%)
Gangliogliomas	0 (0%)	6 (100%)
Desmoplastic Infantile Gangliogliomas	0 (0%)	2 (100%)
Gangliocytomas	0 (0%)	2 (100%)
Subependymal Giant Cell Astrocytomas	0 (0%)	2 (100%)
Dysembryoplastic Neuroepithelial Tumors	0 (0%)	2 (100%)
Papillary Glioneuronal Tumor	0 (0%)	1 (100%)
Glioneuronal Tumor	1 (50%)	1 (50%)
Grade II Gliomas	4 (33.3%)	8 (66.7%)
Diffuse Astrocytoma	2 (50%)	2 (50%)
Oligodendroglioma	0 (0%)	6 (100%)
Pilomyxoid Astrocytoma	2 (100%)	0 (0%)

BRAF/KIAA1549	Positive (dup/fus)	Negative
Grade III Gliomas	0 (0%)	13 (100%)
Anaplasic Oligoastrocytoma	0 (0%)	1 (100%)
Anaplastic Oligodendroglioma	0 (0%)	4 (100%)
Anaplastic Astrocytoma	0 (0%)	5 (100%)
Anaplastic Ganglioglioma	0 (0%)	1 (100%)
Anaplastic Glioneuronal Tumor	0 (0%)	1 (100%)
Xanthoastrocytoma	0 (0%)	1 (100%)
Grade IV Gliomas	0 (0%)	7 (100%)
Glioblastoma	0 (0%)	4 (100%)
Astroblastoma	0 (0%)	2 (100%)
Diffuse Instrinsic Pontine Glioma	0 (0%)	0 (0%)
Grade IV Oligodendroglioma	0 (0%)	1 (100%)
Not otherwise specified Gliomas	1 (20%)	4 (80%)

By using a two-tailed Fisher's test, the *BRAF/KIAA1549* rearrangement was significantly correlated with grade I gliomas (*p-value*=0.0189). Of the grade I gliomas positive for *BRAF/KIAA1549* rearrangement, all except one (a glioneuronal tumor), were pilocytic astrocytomas. This allowed us to conclude that this rearrangement was significantly correlated with the histology of pilocytic astrocytoma (*p-value*<0.0001 when compared with all analyzed gliomas and *p-value*=0.0024 when compared with grade I gliomas).

The *BRAF/KIAA1549* rearrangement was also related with cerebellar locations (two tailed Fisher exact test: *p-value*<0.0001). Moreover, a significant statistic correlation was identified between *BRAF/KIAA1549*-negative cases and cerebral cortex localizations (*p-value*<0.0001),

suggesting that there is a lower probability of this rearrangement to occur in those locations (Figure IV.2-A).

In the cohort of pediatric gliomas under analysis, this genetic rearrangement did not show any correlation with the patient's age or gender (Figure IV.2 – B and C).

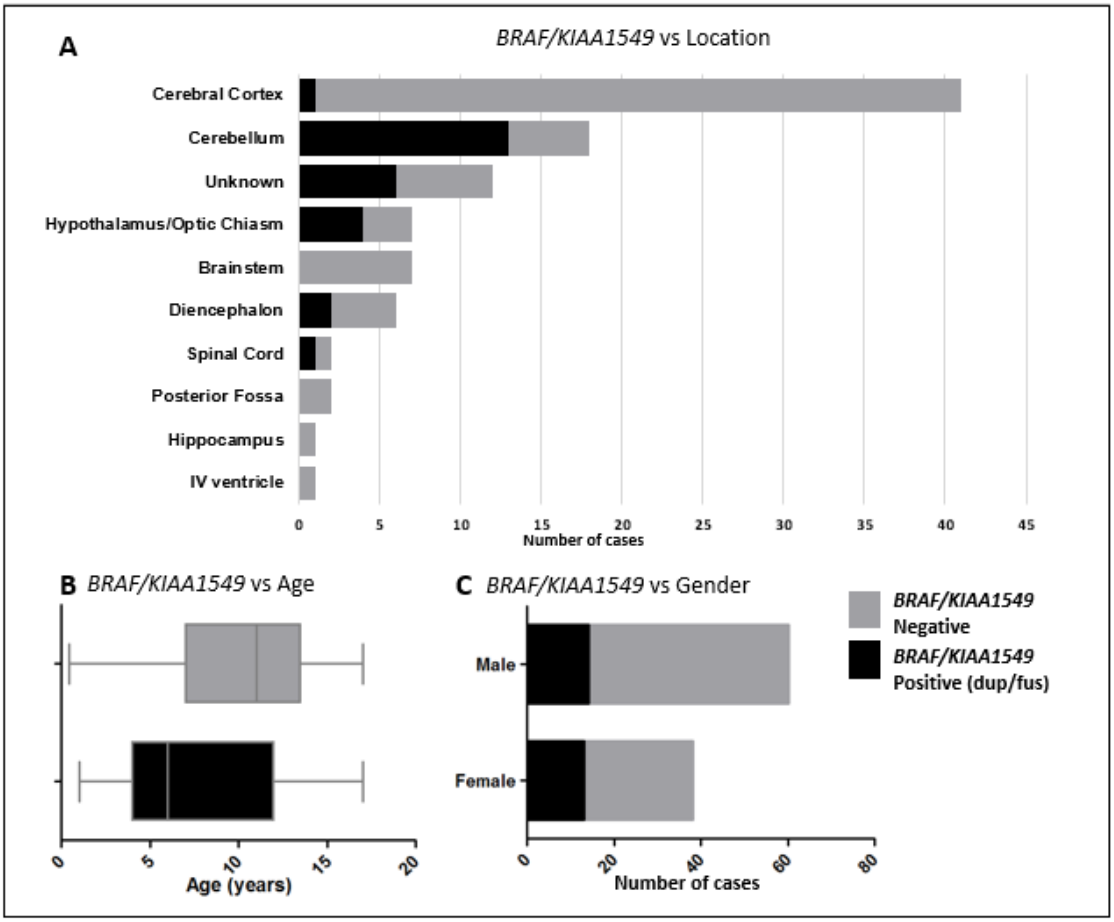

Figure IV.2 – Summary of the *BRAF/KIAA1549* results. (A) *BRAF/KIAA1549* vs Location: the presence of *BRAF/KIAA1549* rearrangement was correlated with cerebellar locations (*p-value*<0.0001) and its absence was correlated with cerebral cortex locations (*p-value*<0.0001); (B) *BRAF/KIAA1549* vs Age: *BRAF/KIAA1549* rearrangement was not correlated with patients' age (*p-value*=0.0573); (C) *BRAF/KIAA1549* vs Gender: *BRAF/KIAA1549* rearrangement was not correlated with patients' gender (*p-value*=0.3535).

2 – *BRAF V600E* mutation

In total, 100 pediatric gliomas were analyzed for the *BRAFV600E* mutation: 61 Grade I gliomas, 10 Grade II gliomas, 14 Grade III gliomas, 8 Grade IV gliomas and 7 NOS gliomas (as represented in Table IV.2). Of these, 16 cases were positive for the mutation: 9 grade I gliomas (6 pilocytic astrocytomas and 3 gangliogliomas), one diffuse astrocytoma, 2 grade III gliomas (1 anaplastic astrocytoma and 1 xanthoastrocytoma), one astroblastoma, and 3 NOS gliomas.

Table IV.2 – Cases studied for *BRAFV600E* mutation. The gliomas studied for *BRAFV600E* mutation are represented in the table above. Each row corresponds to the tumors' histological classification. Each column shows the number of cases and the respective percentage in brackets.

BRAFV600E	Positive (mutation)	Negative
Grade I Gliomas	9 (15%)	52 (85%)
Pilocytic Astrocytomas	6 (13%)	40 (87%)
Gangliogliomas	3 (43%)	4 (57%)
Desmoplastic Infantile Gangliogliomas	0 (0%)	1 (100%)
Gangliocytomas	0 (0%)	1 (100%)
Subependymal Giant Cell Astrocytomas	0 (0%)	2 (100%)
Dysembryoplastic Neuroepithelial Tumors	0 (0%)	2 (100%)
Papillary Glioneuronal Tumor	0 (0%)	1 (100%)
Glioneuronal Tumor	0 (0%)	1 (100%)
Grade II Gliomas	1 (10%)	9 (90%)
Diffuse Astrocytoma	1 (33.3%)	2 (66.7%)
Oligodendroglioma	0 (0%)	5 (100%)
Pilomyxoid Astrocytoma	0 (0%)	2 (100%)

BRAFV600E	Positive (mutation)	Negative
Grade III Gliomas	2 (14%)	12 (86%)
Anaplasic Oligoastrocytoma	0 (0%)	1 (100%)
Anaplastic Oligodendroglioma	0 (0%)	4 (100%)
Anaplastic Astrocytoma	1 (17%)	5 (83%)
Anaplastic Ganglioglioma	0 (0%)	1 (100%)
Anaplastic Glioneuronal Tumor	0 (0%)	1 (100%)
Xanthoastrocytoma	1 (100%)	0 (0%)
Grade IV Gliomas	1 (12.5%)	7 (87.5%)
Glioblastoma	0 (0%)	4 (100%)
Astroblastoma	1 (50%)	1 (50%)
Diffuse Instrinsic Pontine Glioma	0 (0%)	1 (100%)
Grade IV Oligodendroglioma	0 (0%)	1 (100%)
Not otherwise specified Gliomas	3 (43%)	4 (57%)

In our series of cases, *BRAFV600E* mutation did not show any correlation with tumor's WHO grades, histologic subtype and location (p-values>0.05) or with patients' age (*p-value*=0.9253) or gender (*p-value*=0.2669) (Figure IV.3).

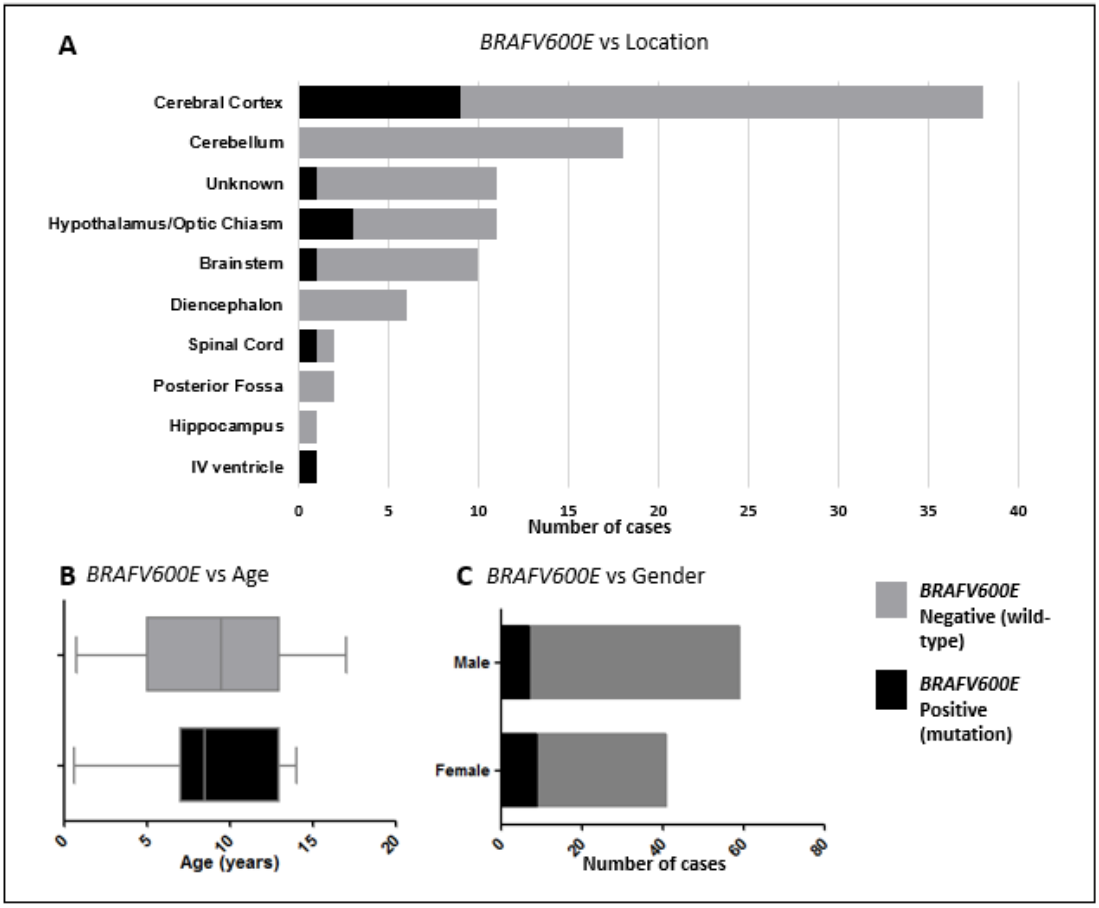

Figure IV.3 – Summary of the *BRAFV600E* results. The presence of *BRAFV600E* mutation was not correlated with (A) tumors' location, *p-values*>0.05; (B) patients' age, *p-value*=0.9253; (C) patients' gender, *p-value*=0.2669.

3 – MYB, MYBL1 and *FGFR1* rearrangement

For the *MYB* gene, 80 gliomas were analyzed: 51 Grade I gliomas, 11 Grade II Gliomas, 10 Grade III gliomas, 7 Grade IV gliomas and 5 NOS gliomas (Figure IV.4).

Only one glioma (NOS5 – Figure IV.1) was considered to be positive for the *MYB* gene rearrangement, with 25% of cells showing two red signals and one green signal, representing a deletion of the *3' gene portion* (see Figure IV.4).

For the *MYBL1* and FGFR1 genes, 79 gliomas were studied: 47 grade I gliomas, 10 grade II gliomas, 10 grade III gliomas, 7 grade IV gliomas and 5 NOS.

Only one glioma (LGG31 – Figure IV.1) was considered to be positive for the *MYBL1* gene rearrangement, with 12% of cells showing two red signals and three green signals, representing a deletion of the *5' gene portion* (see Figure IV.4). However, none of the tumors analyzed for the *FGFR1* gene was positive for that gene rearrangement.

A

	MYB		MYBL1		FGFR1	
	Positive (rearrang)	Negative	Positive (rearrang)	Negative	Positive (rearrang)	Negative
Grade I Gliomas	0 (0%)	48 (100%)	1 (2%)	46 (98%)	0 (0%)	47 (100%)
Grade II Gliomas	0 (0%)	10 (100%)	0 (0%)	10 (100%)	0 (0%)	10 (100%)
Grade III Gliomas	0 (0%)	10 (100%)	0 (0%)	10(100%)	0 (0%)	10(100%)
Grade IV Gliomas	0 (0%)	7 (100%)	0 (0%)	7 (100%)	0 (0%)	7 (100%)
Not otherwise specified Gliomas	1 (20%)	4 (80%)	0 (0%)	5 (100%)	0 (0%)	5 (100%)

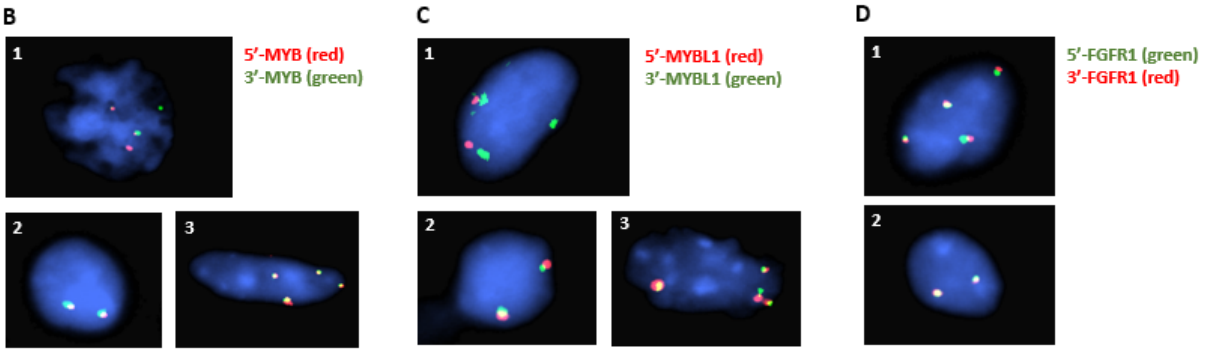

Figure IV.4 – Summary of the *MYB, MYBL1* and *FGFR1* results. (A) The gliomas studied for *MYB, MYBL1 and FGFR1* genes are represented in the table above. Each row corresponds to the tumors' WHO grade. Each column shows the number of cases and the respective percentage in brackets. (B) FISH images using probes corresponding to sequences immediately distal (red) and proximal (green) of *MYB* 1) *MYB* rearrangement; 2) Copy Neutral; 3) *MYB* gain. (C) FISH images, using probes corresponding to sequences immediately distal (green) and proximal (red) of *MYBL1*: 1) *MYBL1* rearrangement; 2) Copy Neutral; 3) *MYBL1* gain. (D) FISH images using probes corresponding to sequences immediately distal (red) and proximal (green) of *FGFR1*: 1) *FGFR1* gain; 2) Copy Neutral.

4 – *CDKN2A* deletion

For *CDKN2A* gene, 81 gliomas were analyzed: 49 Grade I gliomas, 10 Grade II gliomas, 10 Grade III gliomas, 7 Grade IV gliomas and 5 NOS gliomas (see Table IV.3). The deletion of the *CDKN2A* oncossupressor gene was identified in 15 cases: 5 grade I gliomas (4 pilocytic astrocytomas and 1 subependymal giant cell astrocytoma), 3 grade II gliomas (2 pilomyxoid astrocytomas and 1 diffuse astrocytoma), 3 grade IV gliomas (2 astroblastomas and 1 glioblastoma), and 1 NOS glioma.

Table IV.3 – Cases studied for *CDKN2A* gene deletion. The gliomas studied for *CDKN2A* deletion are represented in this table. Each row corresponds to the tumors' histological classification. Each column shows the number of cases and the respective percentage in brackets.

CDKN2A	Positive (deletion)	Negative
Grade I Gliomas	5 (10%)	44 (90%)
Pilocytic Astrocytomas	4 (12%)	29 (88%)
Gangliogliomas	0 (%)	6 (100%)
Desmoplastic Infantile Gangliogliomas	0 (0%)	2 (100%)
Gangliocytomas	0 (0%)	2 (100%)
Subependymal Giant Cell Astrocytomas	1 (50%)	1 (50%)
Dysembryoplastic Neuroepithelial Tumors	0 (0%)	2 (100%)
Papillary Glioneuronal Tumor	0 (0%)	1 (100%)
Glioneuronal Tumor	0 (0%)	1 (100%)
Grade II Gliomas	3 (30%)	7 (70%)
Diffuse Astrocytoma	1 (33.3%)	2 (66.7%)
Oligodendroglioma	0 (0%)	5 (100%)
Pilomyxoid Astrocytoma	2 (100%)	0 (0%)

CDKN2A	Positive (deletion)	Negative
Grade III Gliomas	3 (30%)	7 (70%)
Anaplasic Oligoastrocytoma	0 (0%)	1 (100%)
Anaplastic Oligodendroglioma	2 (50%)	2 (50%)
Anaplastic Astrocytoma	1 (33.3%)	2(66.7%)
Anaplastic Ganglioglioma	0 (0%)	1 (100%)
Anaplastic Glioneuronal Tumor	0 (0%)	0 (0%)
Xanthoastrocytoma	0 (0%)	1 (100%)
Grade IV Gliomas	3 (42.9%)	4 (57.1%)
Glioblastoma	3 (75%)	1 (25%)
Astroblastoma	0 (0%)	2 (100%)
Diffuse Instrinsic Pontine Glioma	0 (0%)	0 (0%)
Grade IV Oligodendroglioma	0 (0%)	1 (100%)
Not otherwise specified Gliomas	1 (20%)	4 (80%)

Results showed that the incidence of *CDKN2A* deletion tended to increase with the tumors' WHO grade: 10% in grade I gliomas, 30% in grade II and III gliomas and 42.9% in grade IV gliomas. However, the two-tailed Fisher's test used, only allowed for identification of a statistical significant correlation between grade I gliomas and the absence of this genetic deletion (*p-value*= 0.0219).

Although *CDKN2A* deletion did not correlates with tumor location (*p-values*>0.05), patients' age (*p-value*=0.5985) or gender (*p-value*=1) (Figure IV.5), it correlated with the histology of glioblastomas (Table IV.3). However, this correlation was only observed when glioblastomas were compared with all gliomas (*p-value*=0.0189). When glioblastomas were compared with grade IV gliomas this correlation was not significant (*p-value*=0.1429), which may be explain by the small sample size (7 cases).

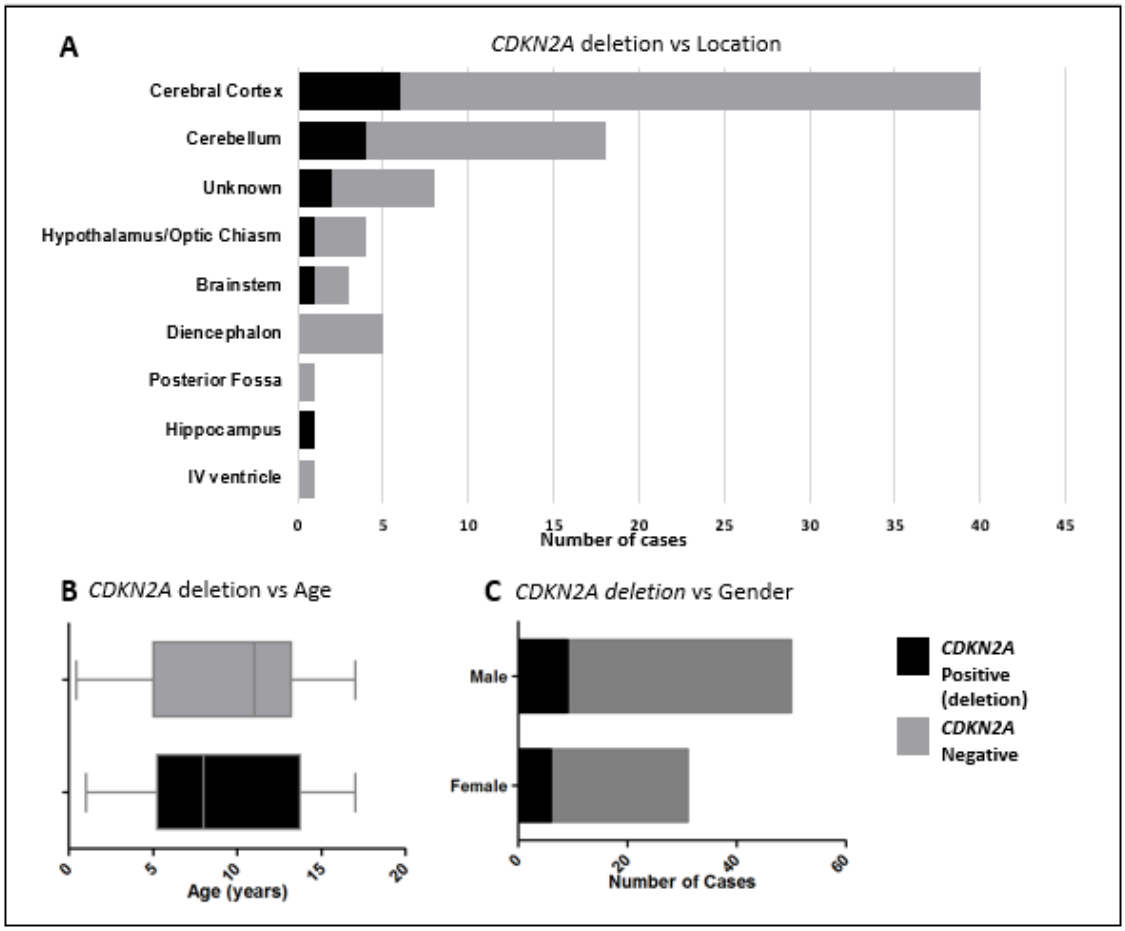

Figure IV.5 – Summary of the *CDKN2A* results. The *CDKN2A* gene deletion was not correlated with (A) tumors' location (*p-values*>0.05); (B) patients' age, *p-value*=0.5985; (C) patients' gender, *p-value*=1.

All *CDKN2A* deletions in PLGG were heterozygous and also presented a chromosome 9 centromeric region deletion. This suggested that a complete loss of chromosome 9 or at least of the 9p arm occurred in these cases, rather than a specific gene deletion. In PHGG, 3 cases had a homozygous *CDKN2A* deletion without loss of chromosome 9 suggesting that in these cases a specific deletion of *CDKN2A* region occurred (Appendix 2).

5 – Histone genes mutations

Exon 1 was studied in the three histone genes (*H3F3A*, *H3F3B* and *HIST1H3I*) to search for mutations at codons 27, 34 and 36. The *K27M* mutation was identified in 4 cases. At codon 34, the *G34R* mutation was identified in 2 cases and the *G34V* mutation in 1 case. These mutations were only observed in the *H3F3A* gene and in PHGG. No alterations were seen at codon 36 in the three genes studied. The obtained results are depicted in Figure IV.6.

A	H3F3A				H3F3B		HIST1H3I	
	Positive (mutation)			Negative (wild-type)	Positive (mutation)	Negative (wild-type)	Positive (mutation)	Negative (wild-type)
	K27M	G34R	G34V					
Grade I Gliomas	0 (0%)	0 (0%)	0 (0%)	41 (100%)	0 (0%)	42 (100%)	0 (0%)	43 (100%)
Grade II Gliomas	0 (0%)	0 (0%)	0 (0%)	8 (100%)	0 (0%)	7 (100%)	0 (0%)	7 (100%)
Grade III Gliomas	2 (15.4%)	0 (0%)	0 (0%)	11 (84.6%)	0 (0%)	12 (100%)	0 (0%)	13 (100%)
Grade IV Gliomas	2 (25%)	2 (25%)	1 (12.5%)	3 (37.5%)	0 (0%)	6 (100%)	0 (0%)	7 (100%)
Not otherwise specified Gliomas	0 (0%)	0 (0%)	0 (0%)	6 (100%)	0 (0%)	6 (100%)	0 (0%)	4 (100%)

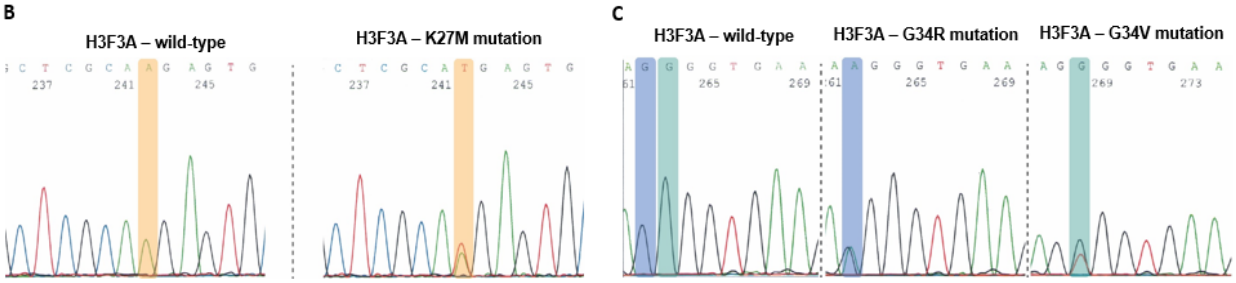

Figure IV.6 – Summary of the histone genes results. (A) The gliomas studied for *H3F3A, H3F3B and HIST1H3I* genes are represented in the table above. Each row corresponds to the tumors' WHO grade. Each column shows the number of cases and the respective percentage in brackets. (B) Comparison of Sanger sequencing chromatograms of *wild-type H3F3A* gene *and H3F3A-K27M* mutation: substitution of an adenine for a thymine that results in the substitution of amino acid lysine for the amino acid methionine, at codon 27. (C) Comparison of Sanger sequencing chromatograms of *wild-type H3F3A* gene *and H3F3A-G34R and H3F3A-G34V* mutations: in *G34R* there is a substitution of a guanine for an adenine, resulting in a glycine substitution for an arginine; in *G34V* the substitution is between a guanine and a thymine, resulting in the amino acid valine instead of glycine.

All *H3F3A-K27M* mutations (n=4) were identified in tumors located in the brainstem, while all *H3F3A-G34R* mutations (n=2) occurred in tumors located in the cerebral cortex (Figure IV.1). By using a Student t test, one could observe that *H3F3A* mutations were correlated with patients' age (*p-value*=0.0088): *K27M* mutations occurred in younger children (mean=7.5 years) and *G34R/V* mutations occurred in older children (mean=13 years), as represented in Figure IV.7. The presence of H3F3A mutations was not correlated with patients' gender, *p-value*=0.0877 (Figure IV.7).

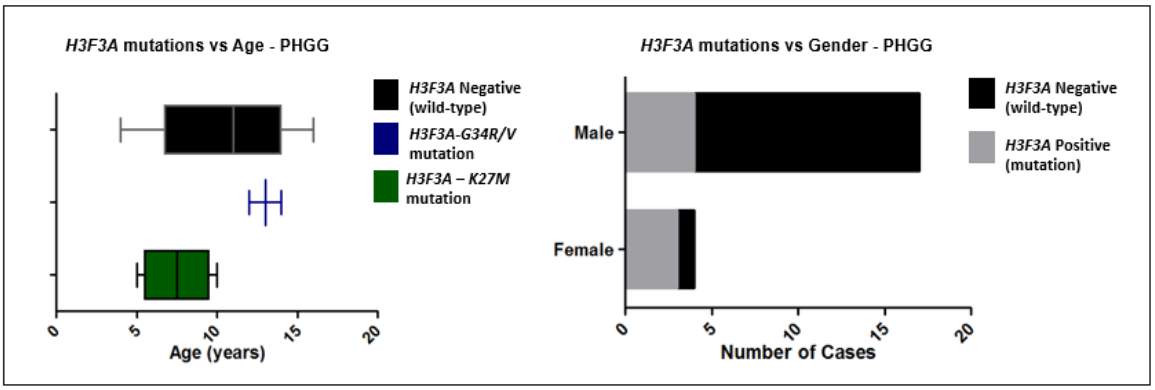

Figure IV.7 – Summary of the *H3F3A* results in PHGG. The graphic on the left shows that, in PHGG, the *H3F3A-G34R/V* mutant tumors tended to appear in older children, while *H3F3A-K27M* mutant tumors tended to appear in younger children (*p-value*=0.0088). The graphic of the right shows that, in PHGG, the *H3F3A* mutations were not correlated with the patients' gender (*p-value*=0.0877).

6 – Tumor recurrences

Of the 109 gliomas studied, 14 were primary tumors that recurred and 9 gliomas were recurrences (secondary tumors). However, only in 8 cases both the primary and the recurrence were evaluated, as represented in Figure IV.8.

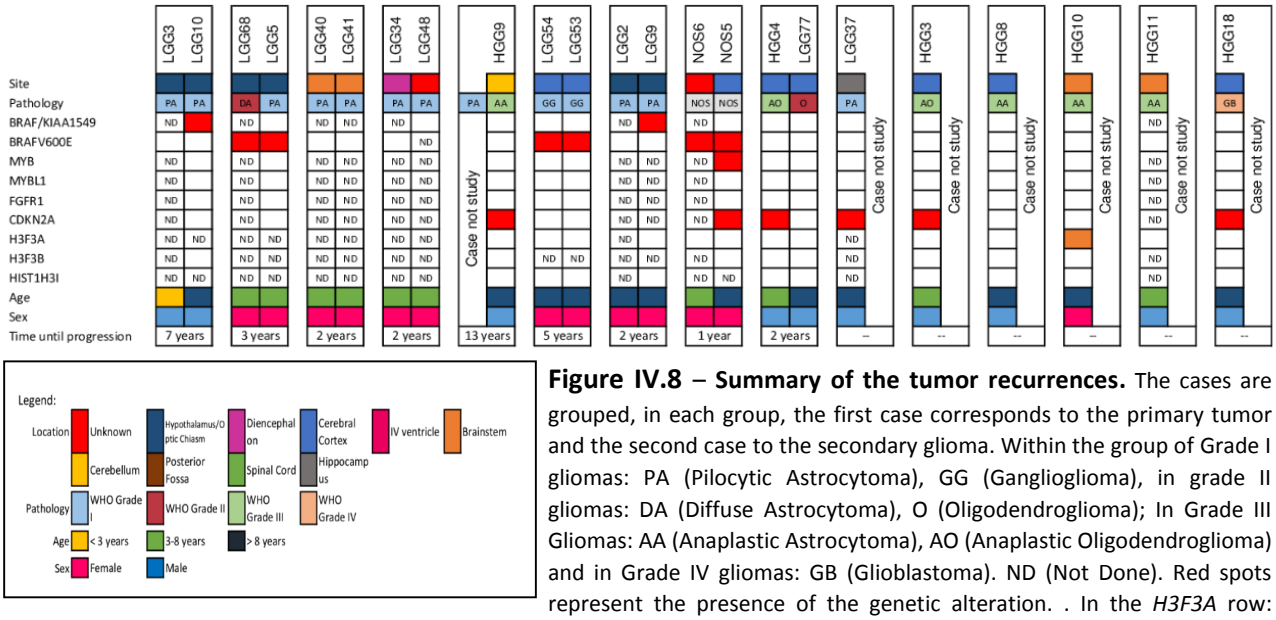

Figure IV.8 – Summary of the tumor recurrences. The cases are grouped, in each group, the first case corresponds to the primary tumor and the second case to the secondary glioma. Within the group of Grade I gliomas: PA (Pilocytic Astrocytoma), GG (Ganglioglioma), in grade II gliomas: DA (Diffuse Astrocytoma), O (Oligodendroglioma); In Grade III Gliomas: AA (Anaplastic Astrocytoma), AO (Anaplastic Oligodendroglioma) and in Grade IV gliomas: GB (Glioblastoma). ND (Not Done). Red spots represent the presence of the genetic alteration. . In the *H3F3A* row: orange spots – *K27M* mutation; green spots – *G34R* mutation; blue spot – *G34V* mutation.

The 14 primary tumors that recurred were compared with the remaining study population (excluding the secondary tumors) and the only statistically significant correlation found was between recurrence and loss of the *CDKN2A* gene (*p-value*=0.0149). The same procedure was done for secondary tumors, but no correlations were found between these and the studied variables (Figure IV.9).

A

	Primary Tumors		Primary Tumors - Recurrences		Secondary Tumors - Recurrences	
	Positive (dup/fus; mut, rearr; del)	Negative	Positive (dup/fus; mut, rearr; del)	Negative	Positive (dup/fus; mut, rearr; del)	Negative
BRAF/KIAA	25(30.5%)	57 (69.5)	0 (0%)	7 (100%)	2 (25%)	6 (75%)
BRAFV600E	10 (13%)	68 (87%)	3 (21%)	11 (79%)	3 (37.5%)	5 (62.5%)
MYB	0 (0%)	67 (100%)	0 (0%)	7 (100%)	1 (16.7%)	5 (83.3%)
MYBL1	1 (1.5%)	65 (98.5%)	0 (0%)	7 (100%)	0 (0%)	6 (100%)
FGFR1	0 (0%)	66 (100%)	0 (0%)	7 (100%)	0 (0%)	6 (100%)
CDKN2A	9 (13.2%)	59 (86.8%)	4 (57%)	3 (43%)	2 (33.3%)	4 (66,7%)
H3F3A	6 (9.5%)	57 (90.5%)	1 (12.5)	7 (87.5)	0 (0%)	5 (100%)
H3F3B	0 (0%)	66 (100%)	0 (0%)	5 (100%)	0 (0%)	4 (100%)
HIST1H3I	0 (0%)	65 (100%)	0 (0%)	6 (100%)	0 (0%)	4 (100%)

B

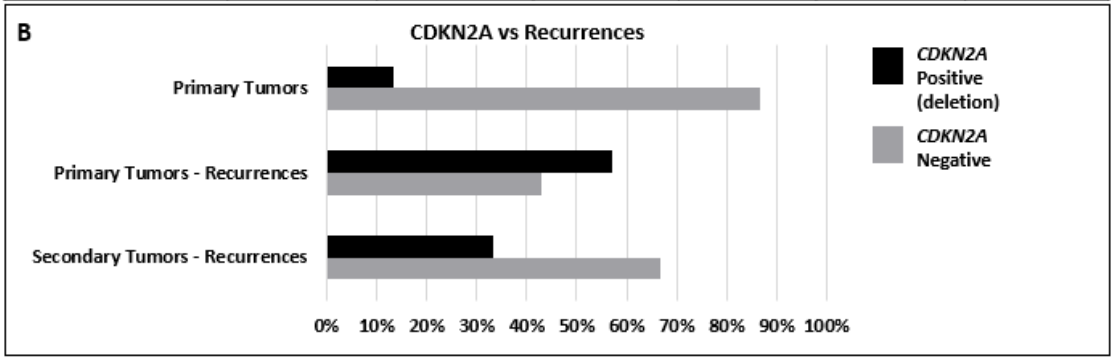

Figure IV.9 – Summary of the tumor recurrences results. (A) The primary tumors that did not recur, the primary tumors that recurred and the secondary tumors, are represented in the table above. Each row corresponds to the studied genes. Each column shows the number of cases and the respective percentage in brackets (B) The *CDKN2A* gene deletion was related with the primary tumors that recurred (*p-value*=0.0149).

7 – Cell Line

A cell line was established from a high-grade tumor (HGG14 – Figure IV.1) from a 14 year-old male child. The case was classified as a WHO grade III xanthoastrocytoma and was located in the cerebral cortex. Among the panel of genes evaluated in this study the only genetic alteration identified in this case was a *BRAFV600E* mutation.

8 – Survival Curves

Survival curves were drawn for the different genetic alterations by using the Kaplan-Meier test. No statistical significant differences in patients' survival curves were observed for *BRAF/KIAA1549* rearrangement (*p-value*= 0.5224), *CDKN2A* deletion (*p-value*= 0.2286) or between the *K27M* and the *G34R/V H3F3A* mutations (*p-value*= 0.4795). However, the presence of the *BRAF* mutation seemed to be associated (*p-value*=0.0443) to a better overall survival rate, when compared with its absence (see Figure IV.10). Moreover, the *K27M* mutation in histone *H3F3A* was associated with a worse overall survival curve, when compared with patients with *H3F3A wild-type* gliomas, *p-value*= 0.0255 (see Figure IV.11).

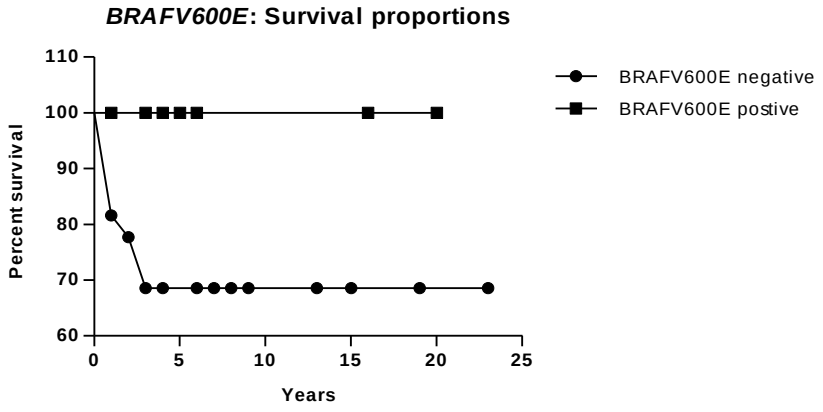

Figure IV.10 – *BRAFV600E*: Survival proportions. There is a statistical significant difference between the two survival curves (tumors not harboring the *BRAF* mutation and tumors with the mutation), with a *p-value*= 0.0443.

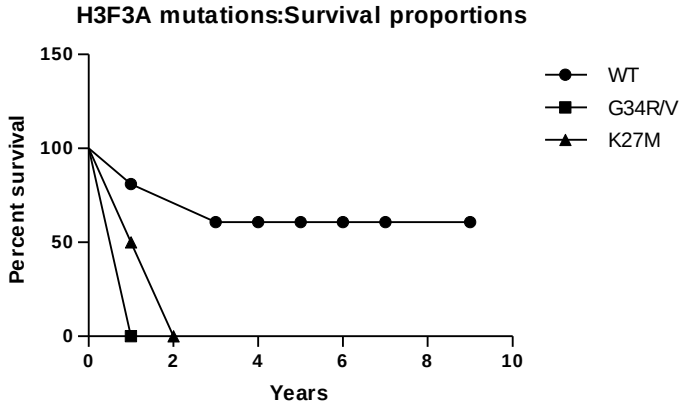

Figure IV.11 – *H3F3A* mutations: Survival Proportions. This graphic represents three survival curves: one for *wild-type H3F3A* gliomas, one for *K27M*-mutant gliomas and another for *G34R/V*-mutant tumors. The only statistically significant difference found between these curves was between the wild-type and the *K27M* curves (*p-value*= 0.0255)

V – Discussion:

1 – Study Population

As was to be expected from previous similar studies [1,3,43], in the glioma cohort analyzed, the most frequent were pilocytic astrocytomas (44.9%) and the less common were oligoastrocytic tumors (0.9%).

However, the incidences of glioblastomas and diffuse astrocytomas, in the analyzed cohort of gliomas, 3.7% and 4.6%, respectively, were lower than the ones described in previous literature: 6.3% and 11.1%, respectively. Furthermore, the incidences of anaplastic astrocytomas and oligodendrogliomas – 5.5% for both, in the study population – were higher than expected – 3.6% and 2.5%, respectively [43]**.** This difference between the incidences of each tumor histological subtype may be explained due to disparities in pediatric CNS tumors incidence among different countries [44].

In the present work, 109 pediatric gliomas were analyzed. This represents a robust population of a rare tumor entity and it was the first time that the genetic profile of pediatric gliomas was determine in the Portuguese population.

2 – *BRAF* gene alterations

The *BRAF/KIAA1549* rearrangement has been described as a driver genetic event in pilocytic astrocytomas, rarely detected in other gliomas and extremely rare in PHGG [5,6]. Our results corroborate this finding: the majority of the cases positive for the *BRAF/KIAA1549* rearrangement were pilocytic astrocytomas (77.8%) and none were PHGGs. Although *BRAF/KIAA1549* rearrangement was tightly correlated with pilocytic astrocytoma morphology in the studied cohort of gliomas (*p-value*<0.0001), it was not exclusive of this histological subtype. The *BRAF/KIAA1549* rearrangement was further identified in other PLGGs, such as: glioneuronal tumors, diffuse astrocytomas and pilomyxoid astrocytomas. The frequencies of the *BRAF/KIAA1549* rearrangement in these histologic subtypes (50%, 50% and 100%, respectively) were higher than expected [5,7]. These results may be explained by the small sample size for each histological subgroup. Moreover and in accordance with Horbinski (2013)[5], results also show that the presence of the *BRAF/KIAA1549* rearrangement correlates with cerebellar tumors locations (p-value<0.0001) and its absence correlates with cerebral cortex tumors locations (p-value<0.0001).

In the studied glioma cohort, the *BRAFV600E* mutation did not show any statistical significant correlation with the tumors' WHO grades, histologic subtypes, patients' age or

gender. Our data is in line with the results of Schindler, et al (2011) [4] and Zhang, et al (2013) [3] since the *BRAFV600E* mutation, in our study, was identified in 43% of the gangliogliomas, in 33% of the diffuse astrocytomas and in 13% of the pilocytic astrocytomas. Although Korshunov, et al (2015) [28] had shown that *BRAFV600E* mutation was present in 10% of the glioblastomas, in our cohort of gliomas no glioblastoma showed this mutation. These results may be connected to the fact that only 4 glioblastomas were analyzed. Moreover, our data also show that the *BRAFV600E*-positive gliomas have a statistical significant (*p-value*=0.0443) longer overall survival when compared with the gliomas that did not harbor this mutation. A correlation between *BRAFV600E*-postive gliomas and a better prognosis had already been described by Korshunov, et al (2015)[28] and Mistry, et al (2015)[30] in different contexts: in PHGGs and in secondary gliomas, respectively.

Accordingly to Horbinski (2013)[5] the *BRAF* mutation and the *BRAF/KIAA1549* rearrangement rarely occur in conjunction in the same tumor. Our results corroborate this finding and also show that these two genetic alterations were related with different tumor locations: the *BRAF/KIAA1549* rearrangement was more common in the cerebellum while the *BRAFV600E* mutation was more common in the cerebral cortex. This is an interesting finding because, as it was demonstrated by Horbinski (2013)[5], although both *BRAF* alterations have the same effect of turning the *B-raf* on, leading to *MAPK/ERK* pathway activation, the tumors that harbor either the mutation or the rearrangement have different biologic and clinical behaviors [5]. These differences have great implications for the patients' treatment because *BRAFV600E*-positive tumors are sensible to *RAF* inhibitors, such as vemurafenib, whereas tumors harboring the *BRAF/KIAA1549* rearrangement are resistant to it but associated with a favorable response to *MEK* inhibitors, such as selumetinib and trametinib [7,20,25]. This implies that, in this context, it is important to establish cell cultures from tumors harboring *BRAF* alterations not only to understand the influence of a specific genetic alteration in the tumor behavior at a cellular and molecular level, but also to understand how the tumor cells will respond to a specific blockage in the context of their other accumulated genetic alterations. In the current work a cell line could be established from a tumor harboring the *BRAFV600E* mutation with the purpose to be used for future studies.

3 – *MYB, MYBL1* and *FGFR1* rearrangements

Although Tatevossian, et al (2010)[14] showed that an increased nuclear expression of *MYB* was present in diffuse gliomas, pilocytic astrocytomas and PHGG, *MYB* abnormalities at a genomic level, such as genetic rearrangements or amplifications, were only identified in diffuse gliomas [3,14]. In contrast to these results, in the studied glioma cohort, only one case (NOS5 –

Figure IV.1), not classified as a diffuse glioma was considered to be positive for the *MYB* rearrangement. This case showed a *3' gene portion* deletion that had been described as one of the two known mechanisms responsible for *MYB* upregulation in gliomas [14].

The *MYBL1* rearrangement described by Ramkissoon, et al (2013)[16] and Zhang, et al (2013)[3], consisting in a partial duplication of *MYBL1* gene giving rise to a truncated protein, was not identified in our series of gliomas. However, in the studied cohort of gliomas, a different *MYBL1* rearrangement, involving a 5' gene portion deletion, was identified in one pilocytic astrocytoma. There is no data in literature showing *MYBL1* rearrangements involving 5' gene portion deletion in gliomas. Thus, further studies are needed to verify if the rearrangement identified in this cohort of gliomas could lead to oncogenesis.

Disparities between the results of this study and the data described in literature may be explained due to the small size of the diffuse gliomas sample (only 18 diffuse gliomas were analyzed) and also to the fact that only few studies in the literature access the genetic alterations of *MYB* and *MYBL1* genes in pediatric gliomas [3,14,16]. Thus, further studies are needed to better understand the mechanisms leading to *MYB* upregulation.

Zhang, et al (2013)[3] showed, through whole-genome sequencing, that, although relatively infrequent across the entire cohort of low-grade gliomas (7.4%), the *FGFR1* duplication involving the tyrosine kinase domain was present in 24% of grade II diffuse cerebral gliomas. In the studied cohort of gliomas no *FGFR1* rearrangements were seen by FISH. Although rare in the context of pediatric grade II gliomas, other *FGFR1* gene alterations may be linked to oncogenesis, as missense mutations and *FGFR1* fusions with *TACC* genes [3]. Jones, et al (2013)[35] identified the presence of *FGFR1* mutations in 5% of pilocytic astrocytomas. These *FGFR1* mutated-cases were *BRAF/KIAA1549* negative and had extra-cerebellar locations, mostly in midline locations. In the same work, these mutations were also identified in glioblastomas harboring *H3F3A* gene *K27M* mutation. However, the *FGFR1* mutations described by Zhang, et al (2013)[3] – *N554K* and *V559M* – were different from *FGFR1* mutations described by Jones, et al (2013)[35] – *N546K* and *K656E*. Thus, it is important to investigate thoroughly the relation between the *FGFR1* mutations and tumors located in midline. As the *FGFR1* gene has an important role in neural stem cell self-renewal and in midline glial cells development, this spatial clustering may reflect differential sensitivity of distinct neuronal precursors to an activating stimuli. Moreover it is important to understand how second hits (timing and type) and/or differentiation stage of the cell of origin contribute to determine a pilocytic astrocytoma or a glioblastoma formation [35].

4 - *CDKN2A* gene deletion

Several studies in pediatric gliomas have identified an association between a homozygous deletion of the *CDKN2A* gene with a worst clinical outcome in *BRAF*-driven gliomas, related with a failure to induce senescence or an escape from *BRAF*-induced tumor senescence [8,9,30].

Our results allowed us to conclude that a homozygous or a heterozygous *CDKN2A* gene deletions are associated with tumor recurrences, independently of the tumors' WHO Grade, histologic classification, location or other genetic alterations. Although the existence of tumor recurrences may be reflected in worst outcomes, no statistically significant differences were observed between the survival curves from tumors with and without *CDKN2A* gene deletion, suggesting that the *CDKN2A* gene deletion may not independently affect patients' survival. Moreover, and in contrast with Horbinski, et al (2012)[9] who identified homozygous deletions of *CDKN2A* gene in low and high-grade pediatric gliomas, in our series of tumors, homozygous deletions of the *CDKN2A* gene were only observed in 3 cases, all high-grade gliomas. Nevertheless, Steilen-Gimbel, et al (1999)[45] hypothesized that the *CDKN2A* gene may already show a gene-dosage effect with a reduced proliferation-repressing function when it was heterozygously deleted.

5- Histone genes mutations

In human gliomas, all reported *H3.3* mutations (*K27M* and *G34R/V*) have been identified in the *H3F3A* gene [12,36]. In fact, the two genes (*H3F3A* and *H3F3B*) that encode the *H3.3* histone were analyzed in this glioma cohort and genetic alterations were only found in the *H3F3A* gene. Following on Schwartzentruber, et al (2012)[10] and Sturm, et al (2012)[11], the results show that mutations in the *H3F3A* gene were related with tumor location and patients' age: the *K27M* mutations occurred in brainstem gliomas and in younger patients (median and mean=7.5 years, range 5-10 years) and the *G34R/V* mutations in tumors located in the cerebral cortex and in older patients (median and mean=13 years; range 12-14 years). However, in the context of survival curves, a difference between these two groups in our series was not clearly identified, which may be ascribed to lack of information about some patients outcomes and to the small number of cases showing *H3F3A* mutations (n=7). Nevertheless, our results could demonstrate that the *H3F3A-K27M* mutation was associated with a shorter overall survival when compared to wild-type *H3F3A* cases.

In contrast with the results presented by Kraushaar, et al (2013)[37] and Wu, et al (2012)[13], in our cohort of gliomas alterations in the *H3.1* histone were not identified. However, in the

current work, only the *HIST1H3I* gene was analyzed and the genetic alterations in the *H3.1* histone have been reported to occur in the *HIST1H3B* gene [13]. However, these alterations in the *HIST1H3B* gene have been only described in diffuse intrinsic pontine gliomas and in non-brainstem pediatric glioblastomas, in low frequencies, 18% and 3%, respectively [13]. In the analyzed population, these subtypes of gliomas were rare: 1 diffuse intrinsic pontine glioma and 2 non-brainstem glioblastomas.

The majority of studies about histone genes alterations in gliomas were performed using high-grade astrocytomas, mainly glioblastomas [1,11,13]. The described incidence for the *H3F3A-K27M* and *H3F3A-G34R/V* mutations in pediatric high-grade astrocytomas is 60-80% [1]. However, in our glioma cohort, only 40% of the pediatric high-grade astrocytomas were *H3F3A-K27M* or *H3F3A-G34R/V* positive. Moreover, Schwartzentruber, et al (2012)[10] and Gielen, et al (2013)[38], showed that in pediatric population the *H3F3A* mutations occurred exclusively in high-grade astrocytomas. In contrast with these findings, we identified a *H3F3A-K27M* mutation in one anaplastic oligoastrocytoma (HGG1 – Figure IV.1 and Appendix 2) and a *H3F3A-G34R* mutation in one oligodendroglioma (HGG17 – Figure IV.1 and Appendix 2). Although further studies using larger cohorts of non-astrocytic high-grade gliomas are needed, the results suggest that these two subgroups of pediatric glioblastomas (*K27M* and *G34R/V*) can be extended to other histologic subtypes of pediatric high-grade gliomas. The same may be also true for the other four biologic subgroups described for pediatric glioblastomas (RTK-I, Mesenchymal, IDH and PXA-like). However, to stratify the studied PHGGs in these subgroups, it would be necessary to study genetic alterations in other genes, such as *PDGFRA, EGFR, TP53, NF1, IDH1* and *IDH2*.

6 – Recurrences

Mistry, et al (2015)[30] demonstrated a clinically distinct subtype of pediatric secondary high-grade gliomas that arises from primary low-grade gliomas, defined by *BRAFV600E* mutations and *CDKN2A* gene deletions. They show that these two genetic alterations are commonly identified in low- and secondary high-grade gliomas and occur concomitantly in 75% of the transformed low-grade gliomas. We could not confirm these observations. In our series, most of the secondary gliomas that arose from low-grade gliomas were also low-grade tumors. Moreover, in the study population, the *BRAFV600E* mutation and the *CDKN2A* gene deletion were only seen simultaneously in one case that did not recur. These results were not totally unexpected because Broniscer (2015)[46] has pointed out some fragilities in the results presented by Mistry, et al (2015)[30] in connection to a sampling error due to the inclusion of patients whose tumors were not histologically confirmed to be either low or high-grade gliomas as long as there was clinical and radiologic evidence to support that diagnosis. This had led to the identification

of some tumors as low-grade gliomas that experienced malignant transformation within 1 year or less after diagnosis, having been shown previously that the minimal latency for malignant transformation was 1.6 years [47]. This argument may partly be extended to the present case, since there may be some weaknesses in not having analyzed all *BRAFV600E* positive gliomas for the *CDKN2A* gene deletion (and vice-versa) or, due to lack of quality or quantity of material, not having analyzed all primary and secondary tumors for all genetic alterations.

Interestingly, in the three pairs of primary and secondary gliomas positive for the *BRAFV600E* mutation, this genetic alteration remained present in the secondary tumor, but in the only pair of primary and secondary gliomas positive for *CDKN2A* gene deletion, the secondary tumor did not show a deletion of the *CDKN2A* gene. Thus, further studies are important to understand how the therapeutic regimens, directed at the primary tumor, affect the genetic characteristics of secondary tumors.

VI - Conclusion:

The objective of the study was to determine the genetic profile of pediatric gliomas. Results suggest that the *BRAF/KIAA1549* rearrangement can be used as a diagnostic marker in association with the tumor histologic classification for low-grade gliomas, and *BRAFV600E* mutation (associated with a longer overall survival) and *CDKN2A* gene deletion (associated with tumor's recurrences) as prognostic makers. Identification of *MYB, MYBL1* and *FGFR1* rearrangements by *FISH* did not seem to be useful as diagnostic or prognostic markers. Mutations in the *H3F3A* gene at codons 27 and 34 of exon 1 were shown to play an important role in the stratification, not only of pediatric glioblastomas but also of the other histologic subtypes of PHGGs. The same was not seen for *H3F3B* and *HIST1H3I* genes.

A cell line from a high-grade glioma harboring the *BRAFV600E* mutation, was established, which, may be used in future studies to test new therapeutic approaches.

In sum, the genetic profile of pediatric gliomas in the Portuguese population was determined for the first time, and this study contributed to the characterization of pediatric gliomas, giving new insights for future studies. Since FISH and Sanger's sequencing can be performed in most clinical laboratories, the study supports that these techniques can be added to the current battery of tests used in pediatric gliomas, for the identification of genetic alterations with diagnostic and prognostic value.

VII – Future Perspectives:

Future studies are needed to verify if the *BRAFV600E* mutation can be used as an independent favorable prognostic factor in pediatric gliomas. It is also important to understand the mechanisms that lead to *MYB* upregulation in pediatric pilocytic astrocytomas, diffuse astrocytomas and high-grade gliomas. Further studies that use a sequencing methodology are needed to understand if the *FGFR1* duplication involving the tyrosine kinase domain can be used as a diagnostic marker for diffuse gliomas and to understand if the different *FGFR1* described mutations (*N554K, V559M, N546K and K656E*) may be used as diagnostic and/or prognostic markers.

More studies with larger cohorts of recurrent primary and secondary pediatric gliomas are needed to better understand tumor transformation and specific genetic alterations over time, such as *CDKN2A* gene deletion and *BRAFV600E* mutation. It is also very relevant for future studies to investigate how a specific therapeutic regimen affects the potential secondary tumors.

In future clinical trials, a genetic stratification of the patients should be done to avoid bias of the results. The established cell line may be used for the development of target therapies and to understand their effects in the context of the accumulated genetic alterations that characterize a tumor.

VIII – Bibliography

1. Gerges, N., Fontebasso, A. M., Albrecht, S., Faury, D. & Jabado, N. 2013. Pediatric High-Grade Astrocytomas: A Distinct Neuro-Oncological Paradigm, *Genome Medicine* 5 (7) :66.

2. Louis, D. N., Ohgaki, H., Wiestler, O.D., Cavenee, W.K., Burger, P.C., Jouvet, A., Scheithauer, B.W. and Kleihues, P. 2007. *The 2007 WHO classification of tumours of the central nervous system*. *Acta Neuropathologica* 114 (2), 97-109.

3. Zhang, J., Wu, G., Miler, C.P., Tatevossian, R., Dalton, J.D., Tang, B., Orisme,W. *et al.* 2013. Whole-genome sequencing identifies genetic alterations in pediatric low-grade gliomas. *Nat. Genet.* 45 (6), 602–12.

4. Schindler, G., Capper, D., Meyer, J., Janzarik, W., Omran, H., Herold-Mende, C., Schmieder, K., et al. 2011 Analysis of BRAF V600E mutation in 1,320 nervous system tumors reveals high mutation frequencies in pleomorphic xanthoastrocytoma, ganglioglioma and extra-cerebellar pilocytic astrocytoma. *Acta Neuropathol.* 121 (3), 397–405.

5. Horbinski, C. 2013. To BRAF or Not to BRAF: Is That Even a Question Anymore? *J Neuropathol Exp Neurol.* 72 (1)**,** 2–7.

6. Antonelli, M, Badiali, M., Moi, L., Buttarelli, F.R., Baldi, C., Massimo, M., Sanson, M. and Giangaspero, F. 2015. KIAA1549-BRAF Fusion Gene in Pediatric Brain Tumors of Various Histogenesis. *Pediatr. Blood Cancer* 62**,** 724–727

7. Hoffman, L. M., Salloum, R. & Fouladi, M. 2015. Molecular Biology of Pediatric Brain Tumors and Impact on Novel Therapies. *Curr. Neurol. Neurosci. Rep.* 15 (4), :10.

8. Raabe, E. H, Lim, K.S., Kim, J.M., Meeker, A. Mao, X-G., Nikkhah, G., Maciaczyk, J., et al.2011. BRAF activation induces transformation and then senescence in human neural stem cells: a pilocytic astrocytoma model. *Clin. Cancer Res.* 17 (11), 3590–3599.

9. Horbinski, C., Nikiforova, M. N., Hagenkord, J. M., Hamilton, R. L. & Pollack, I. F. 2012. Interplay among BRAF, CDKN2A, p53, and MIB1 in pediatric low-grade gliomas. *Neuro. Oncol.* 14 (6), 777–789.

10. Schwartzentruber, J., Korshunov, A., Liu, X-Y., Jones, D. T. W., Pfaff, E., Jacob, K., Sturm, D., *et al.* 2012. Driver mutations in histone H3.3 and chromatin remodelling genes in paediatric glioblastoma. *Nature* 484 (7392)**,** 130–130.

11. Sturm, D., Witt, H., Hovestadt, V., Khuong-Quang, D. A., Jones, D.T.W., Konermann, C., Pfaff, E., *et al.* 2012. Hotspot Mutations in H3F3A and IDH1 Define Distinct Epigenetic and Biological Subgroups of Glioblastoma. *Cancer Cell* 22 (4), 425–437.

12. Fontebasso, A. M, Schwartzentruber, J., Khuong-Quang, D.A., Liu, X.Y., Sturm, D., Korshunov, A., Jones, D.T.W., *et al.* 2013. Mutations in SETD2 and genes affecting histone H3K36 methylation target hemispheric high-grade gliomas. *Acta Neuropathol.* 125 (5)**,** 659–669.

13. Wu, G., Broniscer, A., McEachron, T., Lu, C., Paugh, B. S., Becksfort, J., Qu, C., *et al.* 2012. Somatic histone H3 alterations in pediatric diffuse intrinsic pontine gliomas and non-brainstem glioblastomas. *Nat. Genet.* 44 (3), 251–253.

14. Tatevossian, R. G., Tang, B., Dalton, J., Forshew, T., Lawson, A.R., Ma, J., Neale, G., *et al.* 2010. MYB upregulation and genetic aberrations in a subset of pediatric low-grade gliomas. *Acta Neuropathol.* 120 (6), 731–743.

15. Sexton-Oates, A., MacGregor, D., Dodgshun, A. & Saffery, R. 2015. The potencial for epigenetic analysis of paediatric CNS tumours to improve diagnosis, treatment and prognosis. *Ann Oncol.* 26 (7), 1314-1324.

16. Ramkissoon, L.. A., Horowitz, P.M., Craing, J.M., Ramkissoon, S.H., & Rich, B.E. 2013. Genomic analysis of diffuse pediatric low-grade gliomas identifies recurrent oncogenic truncating rearrangements in the transcription factor MYBL1. *PNAS* 110 (20), 8188–8193.

17. Gilbert, M. R., Armstrong, T. S., Pope, W. B., van den Bent, M. & Wen, P. Y. 2014. Facing the Future of Brain Tumor Clinical Research. *Clin. Cancer Res.* 20 (22)**,** 5591–5600.

18. Sturm, D.. Bender, S., Jones, D.T.W., Lichter, P., Grill, J., Becher, O., Hawkins, C., *et al.* 2014. Paediatric and adult glioblastoma: multiform (epi)genomic culprits emerge. *Nat. Rev. Cancer* 14 (2), 92–107.

19. Gajjar, A., Pfister, S. M., Taylor, M. D. & Gilbertson, R. J. 2014. Molecular Insights into Pediatric Brain Tumors Have the Potential to Transform Therapy. *Clin. Cancer Res.* 20 (22), 5630–5640.

20. Raabe, E., Kieran, M. W. & Cohen, K. J. 2013. New strategies in pediatric gliomas: Molecular advances in pediatric low-grade gliomas as a model. 2013. *Clin. Cancer Res.* 19 (17)**,** 4553–4558.

21. Gierke, M., Sperveslage, D.S., Beschorner, R., Ebinger, M., Schuhmann, M.U. & Schittenhelm, J. 2015. Analysis of IDH1-R132 mutation, BRAF V600 mutation and KIAA1549–BRAF fusion transcript status in central nervous system tumors supports pediatric tumor classification. *J. Cancer Res. Clin. Oncol.* 142 (1), 89-100.

22. Weinberg, R. A. 2014. *The Biology of Cancer Second Edition*. New York: Garland Science, Taylor & Francis Group, LLC. 31-96, 275-390.

23. Hanahan, D. & Weinberg, R. A. Hallmarks of cancer: the next generation. 2011. *Cell.* 144 (5), 646–674.

24. Forshew, T., Tatevossian, R., Lawson, A.R.J., Ma, J., Neale, G., Ogunkolade, B.W., Jones, T.A., *et al.* 2009. Activation of the ERK/MAPK pathway: A signature genetic defect in posterior fossa pilocytic astrocytomas. *J. Pathol.* 218 (2), 172–181.

25. Sievert, A. J., Lang, S-S., Boucher, K.L., Madsen, P.J., Slaunwhite, E., Choudhari, N., Kellet, M., Storm, P.B. & Resnick, A.C. 2013. Paradoxical activation and RAF inhibitor resistance of BRAF protein kinase fusions characterizing pediatric astrocytomas. *Proc. Natl. Acad. Sci.* 110 (15), 5957–5962.

26. Cin, H., Meyer, C., Herr, R., Janzarik, W.G., Lambert, S., Jones, D.T.W., Jacob, K., *et al.* 2011. Oncogenic FAM131B-BRAF fusion resulting from 7q34 deletion comprises an alternative mechanism of MAPK pathway activation in pilocytic astrocytoma. *Acta Neuropathol.* 121 (6), 763–774.

27. Davies, H., Bignell, G., Cox, C., Stephens, P., Edkins, S., Clegg, S., Teague, J., *et al.* 2002. Mutations of the BRAF gene in human cancer. *Nature* 417 (6892), 949–954.

28. Korshunov, A., Ryzhova, M., Hovestadt, V., Bender, S., Sturm, D., Capper, D., Meyer, J., *et al.* 2015. Integrated analysis of pediatric glioblastoma reveals a subset of biologically favorable tumors with associated molecular prognostic markers. *Acta Neuropathol.* 129 (5), 669-678

29. Gajjar, A., Bowers, D.C., Karajannis, A., Leary, S., Witt, H. & Gottardo, N.G. 2015. Pediatric Brain Tumors: Innovative Genomic Information Is Transforming the Diagnostic and Clinical Landscape. *J. Clin. Oncol.* 33 (27), 2986-2998.

30. Mistry, M., Zhukova, N., Merico, D., Rakopoulos, P., Krishnarty, R., Shago, M. Starvropoulos, J., *et al.* 2015. BRAF Mutation and CDKN2A Deletion Define a Clinically Distinct Subgroup of Childhood Secondary High-Grade Glioma. *J. Clin. Oncol.* 33 (9), 1015–1022.

31. Collins, V. P., Jones, D. T. W. & Giannini, C. 2015. Pilocytic astrocytoma: pathology, molecular mechanisms and markers. *Acta Neuropathol.* 129 (6), 775–788.

32. Martinez, I. & DiMaio, D. 2011. B-Myb, cancer, senescence, and MicroRNAs. *Cancer Res.* 71 (16), 5370–5373.

33. Ramsay, R. G. & Gonda, T. J. 2008. MYB function in normal and cancer cells. *Nat. Rev. Cancer* 8 (7), 523–534.

34. Lei, W., Rushton, J. J., Davis, L. M., Liu, F. & Ness, S. A. 2004. Positive and negative determinants of target gene specificity Myb transcription factors. *J. Biol. Chem.* 279 (28), 29519–29527.

35. Jones, D. T. W., Hutter, B., Jager, N., Korshunov, A., Kool, M., Warnatz, H-J, Zichner, T., *et al.* 2013. Recurrent somatic alterations of FGFR1 and NTRK2 in pilocytic astrocytoma. *Nat. Genet.* 45 (8), 927–932.

36. Yuen, B. T. K. & Knoepfler, P. S. 2013. Histone H3.3 Mutations: A Variant Path to Cancer. *Cancer Cell* 24 (5), 567–574.

37. Kraushaar, D. C., Jin, W., Maunakea, A., Abraham, B., Há, M. & Zhao, K. 2013. Genome-wide incorporation dynamics reveal distinct categories of turnover for the histone variant H3.3. *Genome Biol.* 14 (10), 121-136.

38. Gielen, G. H., Gessi, M., Hammes, J., Kramm, C.M., Waha, A. & Pietsch, T. 2013. H3F3A K27M mutation in pediatric CNS tumors: A marker for diffuse high-grade astrocytomas. *Am. J. Clin. Pathol.* 139 (3), 345–349.

39. Gisselsson, D. Cytogenetic Methods. 2009. *IN Cancer Cytogenetics Third Edition*. New Jersey: Wiley-Blackwell, 9-16.

40. Bishop, R. 2010. Applications of fluorescence in situ hybridization (FISH) in detecting genetic aberrations of medical significance. *Biosci. Horizons* 3 (1)**,** 85–95.

41. Dolan, M. 2014 Coventional and Molecular Cytogenetics in Cancer; Pasic, M., Hojilla, C. and Yousef, G.M. 2014 Polymerase Chain Reaction; McPherson, J.D. 2014. Clinical Application of DNA Sequencing: Sanger and Next-Generation Platforms. *IN Molecular Testing in Cancer*. New York: Springer, 15-25; 39-54; 81-85.

42. Imyanitov, E., Grigoriev, M., Gorodinskaya, V., Kuligina, ES, Pozharisski, KM, Togo, A.V., Hanson, K.P. 2001. Partial restoration of degraded DNA from archival paraffin-embedded tissues. *Biotechniques* 31 (5), 1000–1002.

43. Wesseling, P., van den Bent, M. & Perry, A. 2015. Oligodendroglioma: pathology, molecular mechanisms and markers. *Acta Neuropathol.* 129 (6), 809–827.

44. Papathoma, P., Thomopoulos, T.P., Karalexi, M.A., Ryzhov, A., Zborovskaya, A., Dimitrova, N., Zivkovic, S., *et al.* 2015. Childhood central nervous system tumours: Incidence and time trends in 13 Southern and Eastern European cancer registries. *Eur. J. Cancer* 51 (11), 1444–1455.

45. Steilen-Gimbel, H., Steudel, W-I, Feiden, W., Moringlane, J-R., Henn, W. and Zhang, K.D. 1999. Genetic Heterogeneity in Human Astrocytomas : Spatial Distribution of CDKN2A and TP53 Deletions in Biopsies. *Cancer Genet. Cytogenet.* 4608 (99), 115–119.

46. Broniscer, A. 2015. Malignant Transformation of Low-Grade Gliomas in Children: Lessons Learned From Rare Medical Events. *J. Clin. Oncol.* 33 (9), 978-979.

47. Broniscer, A., Baker, S., West, A., Fraser, M.M., Proko, E., Kocak, M., Dalton, J., *et al.* 2007. Clinical and Molecular Characteristics of Malignant Transformation of Low-Grade Glioma in Children. *J. Clin. Oncol.* 25 (6), 682–689.

48. Braig, M. 2007. Thesis: Role of the Histone methyltransferase Suv39h1 in cellular senescence and Ras-induced lymphomagenesis. (University of Berlin, 2007). Page 10.

Appendices:

Appendix 1 – Solutions prepared for the experimental work

PBS 10x:

- 80g of NaCl
- 2g of KCl
- 14.4g of Na_2HPO_4
- 2.4g of KH_2PO_4
- 800ml of Distilled water
- Adjust the pH to 7.3-7.4
- Adjust final volume to 1l with distilled water

Autoclave the solution and store at room temperature.

SSC 20x:

- 175.3g of NaCl
- 88.2g of $C_6H_5Na_3O_7.H_2O$
- 800ml of Distilled water
- Adjust the pH to 5.2 or 7
- Adjust final volume to 1l, with distilled water

Autoclave the solution and store at room temperature.

TN 10x:

- 157.6g of Tris-HCl 1M
- 87.6g NaCl
- 800ml Distilled water
- Adjust the pH to 7.5
- Adjust final volume to 1l with distilled water

Autoclave the solution and store at room temperature

WB2:

- 100ml TN10x pH=7.5
- 900ml Distilled water
- Adjust the pH to 7.5
- Add 500µl of Tween 20

Store at room temperature

2x SSC/Tween 20:

- 100ml of SSC 20x pH=7
- 900ml of Distilled water
- Adjust the pH to 7.5
- Add 500µl of Tween 20

Store at room temperature

HCl 0.01N:

- 5ml of HCl
- 400ml of Distilled water
- Adjust the pH to 2
- Adjust the final volume to 500ml with Distilled water

Autoclave the solution and store at room temperature

Formamide 50%:

- 500ml of Formamide
- 100ml of SSC 20x pH=5.2
- 400ml of Distilled water
- Adjust the pH to 7

Store at 4˚C

Pepsine P7000 (20mg/ml):

In a tube of 15ml:

- 10ml Distilled water
- 200mg of pepsine

Dissolve and aliquot: 500µl per tube

Proteinase K (20mg/ml):

To a final volume of 10ml:

- 200mg of Proteinase K
- 10ml of Distilled water
- Filter the solution with a 0.22µm pore filter

Aliquot and store at -20˚C

Protease:

- 100mg of protease
- 10ml of Carlsberg solution

Dissolve and aliquot: 1000µl per tube

$MgCl_2$:

- 38.094g of $MgCl_2$
- 400ml of Distilled water

Exothermic reaction

- Let the solution cool down
- Filter the solution with a filter paper and with a 0.22µm pore filter

Store at 4˚C

TNB:

In a 15nml tube:

- 10ml of WB2
- 0.5g of Blocking Reagent
- Dissolve using a rotator (for 30min)
- Centrifuge: 20min. 14000rpm
- Transfer the supernatant to 2ml and 1.5ml tubes

Store at -20˚C

Lysis Buffer (10mM TrisHCl. 400mM NaCl. 2mM EDTA):

- 5ml of Tris-HCl 2M pH=8
- 80ml of NaCl 5M
- 4ml of EDTA 0.5M pH=8
- Adjust final volume to 1l with distilled water
- Filter with a 0.22µm pore filter

Store at room temperature

3M NaAc pH=5.2:

Para 50ml:

- 20.4g of NaAc.$3H_2O$ (nº lab 3)
- 35ml of H_2O
- Adjust the pH to 5.2
- Adjust final volume to 50ml

Store at room temperature

Appendix 2 – Detailed representation of the results obtained

Supplementary Table 1 – Clinical features and genetic abnormalities of all 109 gliomas studied.

Number	Hospital	Age (years)	Gender	Tumor location	Histologic Subtype	BRAF		p16 deletion (FISH-9p21//CEP9)	MYB rearrangement	MYBL1 rearrangement	FGFR1 rearrangement	Histones			Follow-up	Survial (years)
						BRAFV600E	FISH-BRAF/KIAA1549//CEP7					H3F3A	H3F3B	HIST1H3I		
LGG1	HDE, IPO	11	F	Hypothalamus/Optic Chiasm	Pilocityc astrocytoma	Negative	Negative 2:2(79%) // 2(96%)						WT	WT	alive, 2015	2
LGG2	IPO	10	F	Hypothalamus/Optic Chiasm	Pilocityc astrocytoma	Negative	ND sem material								alive, 2015	2
LGG3	HSM, IPO	1,25	M	Hypothalamus/Optic Chiasm	Pilocityc astrocytoma (optoquiasmático)	Negative									alive, 2015	23
LGG4	IPO	0,6	F	Hypothalamus/Optic Chiasm	Pilocityc astrocytoma	Positive						WT	WT	WT	alive, 2015	3
LGG5	IPO	7	F	Hypothalamus/Optic Chiasm	Pilocityc astrocytoma	Positive	Negative 2:2 (70%) 3:3 (19%) // 2 (52%) 3 (28%) 4 (13%)	Negative 2 (79%) 3 (14%) // 2(68%) 3(17%) 1(12%)	Negative 2:2 (77%) 3:3 (13%)	Negative 2:2 (64%) 3:3 (21%) 4:4 (11%)	Negative 2:2 (81%) 3:3 (9%)				alive, 2015	16
LGG6	HSM	7	M	Hypothalamus/Optic Chiasm	Pilocityc astrocytoma	Negative	Negative 2:2(66%) 1:1(17%) // 2(86%) 1(11%)	Positive 2(69%) 1(17%) // 2(81%)	Negative 2:2(71%) 3:3(13%)	Negative 2:2(72%) 1:1(11%)	Negative 2:2(78%)	WT	WT	WT		
LGG7	HSM	5	M	Dienchepalom	Pilocityc astrocytoma	Negative	Positive 2:2 (52%) / 2:2:1F (38%) // 2(99%)	Negative 2(84%) // 2(75%) 3(12%) 1(12%)	Negative 2:2(83%)	Negative 2:2(85%)	Negative 2:2(82%)	WT	WT	WT		
LGG8	HDE, IPO	3	F	Hypothalamus/Optic Chiasm	Pilocityc astrocytoma	Negative	Positive 2:2(29%) / 2:2:1F(71%) // 2 (88%)					WT	WT	WT	alive, 2015	2
LGG9	IPO	12	F	Hypothalamus/Optic Chiasm	Pilocityc astrocytoma	Negative	Positive 2:2:1F(18%) 2:2(41%) 4:4(16%) // 2(76%) 3(10%) 4(14%)					WT		WT	alive, 2015	1
LGG10	HSM, IPO	17	M	Hypothalamus/Optic Chiasm	Pilocityc astrocytoma (optoquiasmático)	Negative	Positive 2:2(58%) / 4:4:2F(29%) // 2 (40%) / 4 (54%)	Negative 2:2 (45%) / 3:3 (8%) 4:4 (15%) / (3:2)+(4:2)+(5:4)+(4:3)+(5:3) =24%	Negative 2:2(55%) 3:3(10%) 4:4(13%)	Negative 2:2(57%) 3:3(24%) 4:4(6%)	Negative 2:2(71%) 3:3(20%)		WT		alive, 2015	6
LGG11	HSM	3	F	Cerebellum	Pilocityc astrocytoma	Negative	Positive 2:2(49%) / 2:2:1F(46%) // 2 (96%)	Negative 2(92%) // 2(82%)	Negative 2:2(96%)	Negative 2:2(95%)	Negative 2:2(93%)	WT	WT	WT		

Number	Hospital	Age (years)	Gender	Tumor location	Histologic Subtype	BRAF		p16 deletion (FISH-9p21//CEP9)	MYB rearrangement	MYBL1 rearrangement	FGFR1 rearrangement	Histones			Follow-up	Survial (years)
						BRAFV600E	FISH-BRAF/KIAA1549//CEP7					H3F3A	H3F3B	HIST1H3I		
LGG12	HSM	6	M	Cerebellum	Pilocityc astrocytoma	Negative	Positive 2:2 (52%) / 2:2:1F (38%) // 2(99%)	Positive 2(76%) 3(11%) 1(10%) // 2(79%) 1(14%)	Negative 2:2 (79%) 3:3(12%)	Negative 2:2(99%)	Negative 2:2(90%)	WT	WT	WT		
LGG13	HSM	16	F	Cerebellum	Pilocityc astrocytoma	Negative	Positive 2:2 (49%) / 2:2:1F (23%) // 2(98%)	Negative 2(82%) 3(12%) // 2(86%)	Negative 2:2 (80%) 3:3(11%)	Negative 2:2(88%)	Negative 2:2(87%) 3:3(10%)	WT	WT	WT		
LGG14	HSM	3	F	Cerebellum	Pilocityc astrocytoma	Negative	Positive 2:2(34%) / 2:2:1F(66%) // 2 (100%)	Negative 2(95%) // 2(92%)	Negative 2:2(91%)	Negative 2:2(94%)	Negative 2:2(93%)	WT	WT	WT		
LGG15	HSM	11	M	Cerebellum	Pilocityc astrocytoma	Negative	Positive 2:2(49%) / 2:2:1F(33%)// 2(97%)	Negative 2(85%) 3(10%) // 2(86%)	Negative 2:2(93%)	Negative 2:2(83%) 3:3(9%)	Negative 2:2(98%)	WT	WT	WT		
LGG16	HSM	4	M	Cerebellum	Pilocityc astrocytoma	Negative	Positive 2:2(37%) / 2:2:1F(56%) // 2 (94%)	Negative 2(93%) // 2(81%) 1(17%)	Negative 2:2(93%)	Negative 2:2(99%)	Negative 2:2(95%)	WT	WT	WT		
LGG17	HSM	13	M	Cerebellum	Pilocityc astrocytoma	Negative	Positive 2:2 (49%) / 2:2:1F (23%)	Negative 2(82%) 3(10%) // 2(75%) 3(15%)	Negative 2:2 (77%) 3:3(10%)	Negative 2:2(93%)	Negative 2:2(89%)	WT	WT	WT		
LGG18	HSM	5	M	Cerebellum	Pilocityc astrocytoma	Negative	Positive 2:2(40%) / 2:2:1F(56%) // 2 (100%)	Negative 2(91%) // 2(80%) 1(18%)	Negative 2:2(99%)	Negative 2:2(94%)	Negative 2:2(93%)	WT	WT	WT		
LGG19	HSM, IPO	1,5	M	Cerebellum	Pilocityc astrocytoma	Negative	Positive 2:2(44%) / 2:2:1F(53%) //2 (100%)	Negative 2(76%) 3(16%) // 2(79%) 1(17%)	Negative 2:2(87%) 1:1(9%)	Negative 2:2(91%)	Negative 2:2(77%) 1:1(12%)	WT	WT	WT	alive, 2015	1
LGG20	HSM	5	M	Cerebellum	Pilocityc astrocytoma	Negative	Positive 2:2(71%) / 2:2:1F(29%) // 2 (94%)	Negative 2(91%) // 2(89%) 1(10%)	Negative 2:2(88%)	Negative 2:2(98%)	Negative 2:2(95%)	WT	WT	WT		
LGG21	HSM	12	F	Cerebellum	Pilocityc astrocytoma	Negative	Positive 2:2(%) / 4:4:2F(84%) // 2 (14%) / 4 (84%)	Negative 2(41%) 3(14%) 4(41%) // 2(50%) 3(19%) 4(25%)	Negative 2:2(61%) 3:3(16%) 4:4(19%)	Negative 2:2(20%) 4:4(65%)	Negative 2:2(36%) 4:4(49%)	WT	WT			
LGG22	HDE	12	M	Cerebellum	Pilocityc astrocytoma	Negative	Negative 2:2(100%) // 2(98%)	Negative 2:2 (80%) 2:1 (10%)	Negative 2:2 (73%) 3:3 (11%)	Negative 2:2 (84%)	Negative 2:2 (90%)	WT	WT	WT	alive, 2015	3

Number	Hospital	Age (years)	Gender	Tumor location	Histologic Subtype	BRAF		p16 deletion (FISH-9p21//CEP9)	MYB rearrangement	MYBL1 rearrangement	FGFR1 rearrangement	Histones			Follow-up	Survial (years)
						BRAFV600E	FISH-BRAF/KIAA1549//CEP7					H3F3A	H3F3B	HIST1H3I		
LGG23	HSM	3	F	Cerebellum	Pilocityc astrocytoma	Negative	Negative 2:2 (100%) // 2 (100%)	Negative 2(86%) 1(11%) // 2(86%) 1(12%)	Negative 2:2(92%)	Negative 2:2(97%)	Negative 2:2(93%)	WT	WT	WT		
LGG24	HSM	14	M	Cerebellum	Pilocityc astrocytoma	Negative	Negative 2:2(73%) / 4:4 (22%)	Negative 2(76%) 3(12%) // 2(74%) 3(12%)	Negative 2:2(58%) 3:3(24%)	Negative 2:2(60%) 3:3(14%)	Negative 2:2(62%) 3:3(14%)					
LGG25	IPO	12	M	Cerebral Cortex	Pilocityc astrocytoma	Positive	Negative 2:2(23%) / 3:3 (61%) 1 célula Positive BRAF/KIAA1549	Negative 2(41%) 3(15%) 4(40%) // 2(47%) 3(24%) 4(17%) 1(11%)	Negative 2:2(48%) 3:3(38%)	Negative 2:2(66%) 3:3(16%)	Negative 2:2(81%)	WT	WT	WT	alive, 2015	1
LGG26	HSM, IPO	13	F	Cerebral Cortex	Pilocityc astrocytoma	Positive	Negative 2:2(96%) // 2(96%)	Negative 2(83%) // 2(77%) 3(10%) 1(10%)	Negative 2:2 (88%)	Negative 2:2 (78%) 3:3 (9%)	Negative 2:2 (78%) 3:3 (12%)	WT	WT	WT	alive, 2015	3
LGG27	HSM	13	F	Cerebral Cortex	Pilocityc astrocytoma	Positive	Negative 2:2 (87%),4: (13%) // 2 (94%), 4(24%)	Negative 2(94%) // 2(79%)	Negative 2:2(86%)	Negative 2:2(84%)	Negative 2:2(90%) 3:3(10%)	WT	WT	WT		
LGG28	HSM	16	M	Cerebral Cortex	Pilocityc astrocytoma		Negative 2:2(28%) / 4:4 (69%) // 2(35%) / 4 (60%)	Negative 2 (60%) 3 (28%) 4(9%) // 2(66%) 3(14%)	Negative 2:2(43%) 3:3(22%) 4:4(29%)	Negative 2:2(59%) 3:3(32%)	Negative 2:2(67%) 3:3(27%)					
LGG29	IPO	5	F	Cerebral Cortex	Pilocityc astrocytoma	Negative	Negative ? 2:2 (57%) 1:1 (12%) // 2(70%) 3(13%) 1(14%)	Negative 2(86%)	Negative 2:2 (73%) 3:3 (17%)	Negative 2:2 (79%) 1:1 (13%)	Negative 2:2 (71%) 3:3 (22%) NOTA: só foram contados 58 núcleos				alive, 2015	19
LGG30	HSM	13	M	Cerebral Cortex	Pilocityc astrocytoma	Negative	Negative 2:2(40%) / 3:3 (53%) // 2(47%) / 3 (44%)	Negative 2(88%) // 2(77%) 1(11%)	Negative 2:2(43%) 3:3(39%)	Negative 2:2(86%)	Negative 2:2(82%)	WT	WT	WT		
LGG31	HDE	15	M	Cerebral Cortex	Pilocityc astrocytoma	Negative	Negative 2:2(95%) // 2(96%)	Negative 2(75%) 3(14%) // 2(78%) 1(14%)	Negative 2:2(96%)	Positive 2:2(53%) 3:3(13%) 2:3(12%)	Negative 2:2(57%) 3:3(14%) 1:1(11%)	WT	WT	WT		
LGG32	HSM	15	F	Cerebral Cortex	Pilocityc astrocytoma	Negative	Positive 2:2(73%) / 2:2:1F(20%) // 2 (91%)	Negative 2(66%) 3(15%) 4(12%)	Negative 2:2(71%) 3:3(14%)							

Number	Hospital	Age (years)	Gender	Tumor location	Histologic Subtype	BRAF		p16 deletion (FISH-9p21//CEP9)	MYB rearrangement	MYBL1 rearrangement	FGFR1 rearrangement	Histones			Follow-up	Survial (years)
						BRAFV600E	FISH-BRAF/KIAA1549//CEP7					H3F3A	H3F3B	HIST1H3I		
LGG33	HSM	9	F	Dienchepalom	Pilocityc astrocytoma	Negative	Positive 2:2(47%) / 2:2:1F(52%) // 2 (98%)	Negative 2(88%) // 2(76%) 1(18%)	Negative 2:2(74%) 3:3(12%)	Negative 2:2(77%)	Negative 2:2(89%)	WT	WT	WT		
LGG34	IPO	3	F	Dienchepalom	Pilocityc astrocytoma	Negative									alive, 2015	4
LGG35	HSM, IPO	15	F	Dienchepalom	Pilocityc astrocytoma	Negative	Negative 2:2 (17%) // 2 (75%) // 2 (22%) / 4 (74%)	Negative 2(50%) 3(32%) 4(13%) // 2(57%) 3(24%) 1(13%)	Negative 2:2(15%) 4:4(80%)	Negative 2:2(10%) 4:4(83%)	Negative 2:2(26%) 4:4(68%)		WT	WT	alive, 2015	1
LGG36	HDE	13	M	Dienchepalom	Pilocityc astrocytoma	Negative	Negative 2:2(91%)//2(82%) 3(16%)									
LGG37	IPO	13	M	Hippocampus	Pilocityc astrocytoma	Negative	Negative 2:2 (88%) 4:4(10%) // 2 (93%)	Positive 2(71%) 3(10%) 1(10%) // 2(71%) 1(16%)	Negative 2:2(73%)	Negative 2:2(81%)	Negative 2:2(71%) // 1:1(16%)				alive, 2015	1
LGG38	HDE	8	M	Posterior Fossa	Pilocityc astrocytoma	Negative	Negative 2:2(69%) 3:3(21%)//2(79%) 1(13%)					WT	WT	WT		
LGG39	IPO	13	M	Brainstem	Pilocityc astrocytoma	Negative	Negative 2:2 (25%) / 3:3 (60%) // 2 (42%) / 3(52%)								alive, 2015	1
LGG40	IPO	3	F	Brainstem	Pilocityc astrocytoma	Negative									alive, 2015	15
LGG41	IPO	5	F	Brainstem	Pilocityc astrocytoma	Negative									alive, 2015	13
LGG42	HDE	7	M	Spinal Cord	Pilocityc astrocytoma	Positive	Negative 2:2(20%) 3:3(16%) 4:4(52%)					WT	WT	WT		
LGG43	HDE	9	F	Spinal Cord	Pilocityc astrocytoma	Negative	Positive 2:2(29%) / 2:2:1F(71%) // 2 (98%)								alive, 2015	3
LGG44	HDE, IPO	15	M	Unknown	Pilocityc astrocytoma	Negative	Positive 2:2(45%) / 2:2:1F(55%) // 2 (94%)	Negative 2:2(79%) (2:1)+(3:2)=13%				WT	WT	WT	alive, 2014	1

Number	Hospital	Age (years)	Gender	Tumor location	Histologic Subtype	BRAF		p16 deletion (FISH-9p21//CEP9)	MYB rearrangement	MYBL1 rearrangement	FGFR1 rearrangement	Histones			Follow-up	Survial (years)
						BRAFV600E	FISH-BRAF/KIAA1549//CEP7					H3F3A	H3F3B	HIST1H3I		
LGG45	HSM	9	F	Unknown	Pilocityc astrocytoma	Negative	Positive 2:2(62%) / 2:2:1F(30%)// 2(97%)	Negative 2(85%) 3(12%) // 2(84%) 3(10%)	Negative 2:2(94%)	Negative 2:2(87%)	Negative 2:2(69%) 3:3(15%)	WT	WT	WT		
LGG46	IPO	4	F	Unknown	Pilocityc astrocytoma	Negative	Positive BLOCO 1 - 2:2(42%) / 2:2:1F(56%) // BLOCO 2 - 2:2(31%) / 2:2:1F(66%)	Positive 2(68%) 3(10%) 1(14%) // 2(60%) 1(30%)	Negative 2:2(90%)	Negative 2:2(89%)	Negative 2:2(92%)	WT	WT	WT	alive, 2013	1
LGG47	IPO	15	M	Cerebral Cortex	Pilocityc astrocytoma		Negative 2:2(83%) // 2(72%) 2(12%) 1 (15%)	Negative 2:2(89%)	Negative 2:2(76%) 3:3(16%)	Negative 2:2(83%)	Negative 2:2(76%) 1:1(16%)				alive, 2015	1
LGG48	IPO	6	F	Unknown	Pilocityc astrocytoma		Negative 2:2 (85%) // 2 (77%) /4(11%)								alive, 2015	2
LGG49	HDE	17	M	Unknown	Pilocityc astrocytoma	Negative	Negative 2:2 (79%) // 2 (86%)					WT	WT	WT		
LGG50	HDE	14	M	Posterior Fossa	Ganglioglioma	Negative	Negative 2:2(47%) 3:3(31%) 4:4(15%)	Negative 2:2(49%) 3(26%) // 2(63%) 3(16%) 1(11%)	Negative 2:2(49%) 3:3(33%)	Negative 2:2(63%) 3:3(28%)	Negative 2:2(50%) 3:3(31%) 1:1(12%)	WT	WT	WT		
LGG51	HSM, IPO	15	F	Cerebellum	Ganglioglioma	Negative	Negative 2:2 (63%) /4:4 (30%) // 2(68%) / 4 (22%)	Negative 2(80%) 3:3(10%) // 2(73%) 3(13%)	Negative 2:2(74%) 3:3(11%)	Negative 2:2 (86%) / 4:4 (11%)	Negative 2:2 (64%) / 4:4 (31%)	WT	WT		alive, 2015	4
LGG52	HSM-515627 IPO-1112247	13	M	IV ventricle	Ganglioglioma	Positive	Negative 2:2 (40%) / 3:3 (40%) // 2 (36%) / 3 (52%)	Negative 2:2 (71%) 1/1 (10%)	Negative 2:2 (79%)	Negative 2:2 (69%) / 3:3 (14%)	Negative 2:2 (76%) / 4:4 (9%)		WT	WT	alive, 2015	5
LGG53	IPO	13	F	Cerebral Cortex	Ganglioglioma	Positive	Negative 2:2(42%) 4:4(38%)	Negative 2(48%) 3(23%) 4(17%) // 2(47%) 3(27%) 4(18%)	Negative 2:2(47%) 4:4(10%) 5:5(36%)	Negative 2:2(66%) 3:3(10%) 4:4(19%)	Negative 2:2(61%) 4:4(21%)	WT		WT	alive, 2015	1

Number	Hospital	Age (years)	Gender	Tumor location	Histologic Subtype	BRAF		p16 deletion (FISH-9p21//CEP9)	MYB rearrangement	MYBL1 rearrangement	FGFR1 rearrangement	Histones			Follow-up	Survial (years)
						BRAFV600E	FISH-BRAF/KIAA1549//CEP7					H3F3A	H3F3B	HIST1H3I		
LGG54	IPO	8	F	Cerebral Cortex	Ganglioglioma	Positive	Negative 2:2(24%) 4:4(73%)	Negative 2(36%) 3(52%) // 2(41%) 3(19%) 4(35%)	Negative 2:2(36%) 3:3(11%) 4:4(12%) 5:5(31%)	Negative 2:2(35%) 3:3(21%) 4:4(40%)	Negative 2:2(36%) 3:3(14%) 4:4(44%)	WT		WT	alive, 2015	5
LGG55	HSM	15	F	Cerebral Cortex	Ganglioglioma	Negative	Negative 2:2 (73%) // 2 (60%) / 3 (25%) / 1 (10%)	Negative 2:2 (73%) 3:3 (15%)	Negative 2:2 (78%)	Negative 2:2 (84%) 3:3 (11%)	Negative 2:2 (84%)	WT		WT		
LGG56	HPC	10	F	Cerebral Cortex	Ganglioglioma	Negative										
LGG57	HSM	16	F	Cerebral Cortex	Dysembryoplastic neuroepithelial tumor	Negative	Negative 2:2 (69%) /1:1 (15%) // 2 (72%) / 1 (21%)	Negative 2(92%) // 2 (78%) 3(12%)	Negative 2:2(75%) 3:3(9%)	Negative 2:2(63%) 3:3(24%) 4:4(8%)	Negative 2:2(69%) 3:3(18%) 4:4(8%)		WT	WT		
LGG58	HSM	13	M	Cerebral Cortex	Dysembryoplastic neuroepithelial tumor	Negative	Negative 2:2 (74%) /3:3 (15%) // 2 (74%) / 13(14%)	Negative 2(79%) 3 (14%) // 2 (75%) 3(14%)	Negative 2:2(62%) 3:3(24%) 4:4(7%)	Negative 2:2(73%) 3:3(17%) 4:4(7%)	Negative 2:2(66%) 3:3(18%) 4:4(12%)					
LGG59	HSM	10	M	Cerebral Cortex	Papillary glioneuronal tumor	Negative	Negative 5:4 (70%) /2:2 (23%) // 4(70%) / 3 (14%) / 2(14%)	Negative 2(96%) // 2(83%)	Negative 2:2(93%)	Negative 2:2(91%)	Negative 2:2(94%)	WT	WT	WT		
LGG60	HSM	1	M	Cerebral Cortex	Desmoplastic infantile ganglioma	Negative	Negative 2:2 (77%) 4:4 (14%) // 2 (76%) 4 (15%)	Negative 2:2 (78%)	Negative 2:2 (79%) 4:4 (12%)	Negative 2:2 (84%)	Negative 2:2 (64%) / 4:4 (19%)		WT	WT		
LGG61	IPO	0.42	F	Cerebral Cortex	Desmoplastic infantile ganglioma		Negative 2:2(40%) 3:3(14%) 4:4(39%) // 4(43%) 3(27%) 2(21%)	Negative 2(24%) 3(32%) 4(43%) // 2(50%) 3(24%) 4(22%)	Negative 2:2(49%) 3:3(19%) 4:4(31%)	Negative 4:4(40%) 3:3(27%) 2:2(28%)	Negative 2:2(29%) 3:3(26%) 4:4(23%)				alive, 2015	4
LGG62	HSM	10	M	Cerebral Cortex	Gangliocytoma	Negative	Negative 2:2(66%) / 4:4 (28%) // 2(68%) / 4 (30%)	Negative 2(82%) // 2(71%) 3(14%)	Negative 2:2(84%)	Negative 2:2(52%) 3:3(12%) 4:4(33%)	Negative 2:2(68%) 3:3(10%) 4:4(19%)	WT	WT	WT		

Number	Hospital	Age (years)	Gender	Tumor location	Histologic Subtype	BRAF		p16 deletion (FISH-9p21//CEP9)	MYB rearrangement	MYBL1 rearrangement	FGFR1 rearrangement	Histones			Follow-up	Survial (years)
						BRAFV600E	FISH-BRAF/KIAA1549//CEP7					H3F3A	H3F3B	HIST1H3I		
LGG63	HSM	15	F	Cerebral Cortex	Gangliocytoma		Negative 2:2(90%) // 2(86%) / 4 (12%)	Negative 2(81%) 3(8%) // 2(84%) 3(12%)	Negative 2:2(86%)	Negative 2:2(79%)	Negative 2:2(91%)	WT	WT	WT		
LGG64	HSM	10	M	Cerebral Cortex	Subependymal Giant Cell Astrocytoma	Negative	Negative 2:2 (86%) /4:4 (13%) // 2(86%) / 4 (12%)	Positive 2(72%) 1(14%) // 2(80%) 4(10%)	Negative 2:2(81%)	Negative 2:2(79%) 4:4(13%)	Negative 2:2(88%) 4:4(11%)	WT	WT	WT		
LGG65	HDE	5	M	Unknown	Subependymal Giant Cell Astrocytoma	Negative	Negative 2:2(83%) / 4:4 (16%) // 2(78%) / 4 (18%)	Negative 2(77%) 1(13%) // 2(83%)	Negative 2:2(77%) 3:3(7%) 4:4(7%)	Negative 2:2(78%)	Negative 2:2(86%)	WT	WT	WT		
LGG66	IPO	10	M	Unknown	Glioneuronal tumor	Negative	Positive 2:2(76%) / 2:2:1F(13%) // 2 (94%)	Negative 2(79%) 3(16%) // 2(74%) 3(14%) 1(10%)	Negative 2:2(75%) 3:3(17%)	Negative 2:2(71%) 3:3(16%)	Negative 2:2(81%) 3:3(11%)	WT			alive, 2015	1
LGG67	HDE	2	F	Brainstem	Glioneuronal tumor		Negative 2:2(93%) // 2(?%)									
LGG68	IPO	4	F	Hypothalamus/Optic Chiasm	Diffuse Astrocytoma	Positive									alive, 2015	20
LGG69	IPO	9	F	Unknown	Diffuse Astrocytoma		Negative 2:2(51%) 3:3(20%) 3:2(9%) 4:3(7%) // 2(56%) 3(38%)								alive, 2009	4
LGG70	HSM, IPO	4	F	Dienchepalon	Diffuse Astrocytoma		Negative 2:2(97%) // 2(94%)	Negative 2(77%) 3(11%) 1(10%) // 2(68%) 3(11%) 1(13%)	Negative 2:2(50%) 3:3(17%) 1:1(10%)	Negative 2:2(74%)	Negative 2:2(80%)				alive, 2015	6
LGG71	HSM, IPO	3	M	Dienchepalon	Diffuse Astrocytoma	Negative	Positive 2:2 (45%) / 2:2:1 (53%) // 2 (98%)	Negative 2(82%) 3(9%) // 2(68%) 1(25%)	Negative 2:2(68%) 3:3(19%)	Negative 2:2(80%)	Negative 2:2(78%) 1:1(11%)				alive, 2015	8

Number	Hospital	Age (years)	Gender	Tumor location	Histologic Subtype	BRAF		p16 deletion (FISH-9p21//CEP9)	MYB rearrangement	MYBL1 rearrangement	FGFR1 rearrangement	Histones			Follow-up	Survial (years)
						BRAFV600E	FISH-BRAF/KIAA1549//CEP7					H3F3A	H3F3B	HIST1H3I		
LGG72	HSM	4	F	Cerebellum	Diffuse Astrocytoma	Negative	Positive 2:2(49%) 2:2:1F (50%) // 2(92%)	Positive 2(88%) 1(10%) // 2(82%) 1(17%)	Negative 2:2(95%)	Negative 2:2(93%)	Negative 2:2(99%)	WT	WT	WT		
LGG73	HSM	17	F	Cerebellum	Pilomyxoid Astrocytoma	Negative	Positive 2:2(29%) / 4:4:2F(64%) // 2 (24%) / 4 (66%)	Positive 2(81%) 1(16%) // 2(83%) 1(16%)	Negative 2:2(47%) 3:3(49%)	Negative 2:2(51%) 3:3(43%)	Negative 2:2(31%) 3:3(68%)	WT	WT	WT		
LGG74	HDE	1	F	Unknown	Pilomyxoid Astrocytoma	Negative	Positive 2:2(38%) / 2:2:1F(62%) // 2 (98%)	Positive 2(82%) 1(14%) // 2(78%) 1(19%)	Negative 2:2(90%)	Negative 2:2(75%) 1:1(10%)	Negative 2:2(76%) 1:1(9%)	WT				
LGG75	HSM	13	M	Cerebral Cortex	Oligodendroglioma	Negative	Negative 2:2 (73%) / 3:3(13%) 4:4(12%) // 2(58%) /3(20%) / 4 (20%)	Negative 2(82%) 3(7%) 1(9%) // 2(65%) 3(28%)	Negative 2:2(70%) 3:3(17%)	Negative 2:2(80%) 3:3(11%)	Negative 2:2(70%) 3:3(17%) 4:4(11%)	WT	WT	WT		
LGG76	HSM, IPO	5	M	Cerebral Cortex	Oligodendroglioma	Negative	Negative 2:2 (99%) // 2 (88%)	Negative 2(85%) // 2(75%) 3(14%) 1(10%)	Negative 2:2(80%)	Negative 2:2(91%)	Negative 2:2(82%) 3:3(9%)	WT	WT	WT	alive, 2015	8
LGG77	HSM	9	M	Cerebral Cortex	Oligodendroglioma	Negative	Negative 2:2(98%) // 2(92%)	Negative 2(79%) 3(11%) // 2(80%) 3(9%) 1(10%)	Negative 2:2(92%)	Negative 2:2(87%) 3:3(9%)	Negative 2:2(87%) 3:3(8%)	WT	WT	WT	alive, 2015	7
LGG78	HSM, IPO	1,25	M	Cerebral Cortex	Oligodendroglioma	Negative	Negative 2:2(100%) // 2(96%)	Negative 2(88%) // 2(70%) 3(12%) 1(15%)	Negative 2:2(94%)	Negative 2:2(92%)	Negative 2:2(81%)	WT	WT	WT		
LGG79	HDE, IPO	5	M	Cerebral Cortex	Oligodendroglioma		Negative 2:2(97%) // 2(96%)								alive, 2015	2
LGG80	IPO, HSM	6	M	Dienchepalon	Oligodendroglioma	Negative	Negative 2:2 (53%) /4:4 (47%) // 2(48%) / 4 (48%)	Negative 2(64%) 3(10%) 4(20%) // 2(47%) 3(17%) 1(16%)	Negative 2:2(60%) 4:4(27%)	Negative 2:2(70%) 4:4(19%)	Negative 2:2(69%) 4:4(24%)	WT	WT	WT	death, 2009	1
HGG1	HSM, IPO	8	F	Brainstem	Anaplastic Oligoastrocytoma	Negative	Negative 2:2 (46%) /4:4 (48%) // 2(42%) / 4 (44%)	Negative 2(58%) 4(37%) // 2(69%) 3(14%)	Negative 2:2(71%) 4:4(22%)	Negative 2:2(71%) 3:3(28%)	Negative 2:2(48%) 3:3(45%)	K27M	WT	WT	death, 2006	1

Number	Hospital	Age (years)	Gender	Tumor location	Histologic Subtype	BRAF		p16 deletion (FISH-9p21//CEP9)	MYB rearrangement	MYBL1 rearrangement	FGFR1 rearrangement	Histones			Follow-up	Survial (years)
						BRAFV600E	FISH-BRAF/KIAA1549//CEP7					H3F3A	H3F3B	HIST1H3I		
HGG2	HSM	14	M	Unknown	Anaplastic Glioneuronal Tumor	Negative	Negative 2:2(53%) 3:3(26%) 4:4(12%)//2(82%) 3(16%)					WT	WT	WT		
HGG3	HSM, IPO	7	M	Cerebral Cortex	Anaplastic Oligodendroglioma	Negative	Negative 3:3 (90%) // 3 (82%)	Positive 0(100%) // 2(82%) 1(15%)	Negative 2:2(83%)	Negative 2:2(72%) 3:3(14%)	Negative 2:2(82%)	WT	WT	WT	death, 2007	1
HGG4	HSM	7	M	Cerebral Cortex	Anaplastic Oligodendroglioma	Negative	Negative 2:2 (95%) / 2 (92%)	Positive 1(88%) // 1(91%)	Negative 2:2(92%)	Negative 2:2(96%)	Negative 2:2(93%)	WT	WT	WT	alive, 2015	9
HGG5	HSM	0,75	M	Cerebral Cortex	Anaplastic Oligodendroglioma	Negative	Negative 2:2 (75%) /4:4 (21%) // 2(72%) / 4 (20%)	Negative 2(84%) 1(10%) // 2(87%) 1(9%)	Negative 2:2(88%)	Negative 2:2(93%)	Negative 2:2(93%)		WT	WT	alive, 2015	7
HGG6	HSM	7	F	Cerebral Cortex	Anaplastic Oligodendroglioma	Negative	Negative 2:2(95%) // 2(96%)	Negative 2(94%) // 2(85%)	Negative 2:2(87%)	Negative 2:2(91%)	Negative 2:2(91%)	WT	WT	WT	alive, 2015	7
HGG7	HSM, IPO	14	M	Cerebral Cortex	Anaplastic ganglioglioma	Negative	Negative 2:2(64%) 4:4(16%) // 2(54%) 3(12%) 4(29%)	Negative 2(45%) 3(38%) 4(10%) // 2(67%) 3(10%) 4(17%)	Negative 2:2(80%) 1:1(11%)	Negative 2:2(43%) 1:1(46%)	Negative 2:2(50%) 1:1(41%)	WT (linha celular)	WT (linha celular)	WT (linha celular)	death, 2008	1
HGG8	IPO, HSM	11	M	Cerebral Cortex	Anaplastic Astrocytoma	Negative	Negative 3:3 (91%) // 3 (88%)	Negative 2(96%) // 2(84%) 1(10%)	Negative 2:2(86%)	Negative 2:2(90%)	Negative 2:2(95%)	WT	WT	WT	death, 2011	1
HGG9	HSM	16	M	Cerebellum	Anaplastic Astrocytoma	Negative	Negative 2:2 (13%) /4:4 (83%) // 2(10%) / 4 (90%)	Positive 0:4(50%) 0:3(22%) 0:2 (6%) 2:2 (12%)	Negative 2:2(62%) 3:3(15%)	Negative 2:2(38%) 3:3(29%) 4:4(22%)	Negative 2:2(25%) 3:3(21%) 4:4(40%)	WT	WT	WT	death, 2010	1
HGG10	HSM, IPO	10	F	Brainstem	Anaplastic Astrocytoma	Negative	Negative 2:2 (21%) / 6:6(67%) // 2(20%) / 4 (16%) / 5(16%)// 6(36%)	Negative 2(24%) 3(14%) 6(15%) 7(13%) // 2(45%) 3(29%) 4(17%)	Negative 2:2(51%) 3:3(34%)	Negative 2:2(29%) 3:3(32%) 4:4(27%)	Negative 4:4(42%) 5:5(12%) 2:2(21%) 3:3(14%)	K27M	WT	WT	death, 2008	2
HGG11	HDE, IPO	5	M	Brainstem	Anaplastic Astrocytoma	Negative						WT			death, 2013	1
HGG12	HDE, IPO	4	M	Brainstem	Anaplastic Astrocytoma	Negative	Negative 2:2(23%) 4:4(67%)					WT		WT	alive, 2015	1
HGG13	HDE	6	M	Brainstem	Anaplastic Astrocytoma	Positive	Negative 2:2(84%)					WT	WT	WT		

Number	Hospital	Age (years)	Gender	Tumor location	Histologic Subtype	BRAF		p16 deletion (FISH-9p21//CEP9)	MYB rearrangement	MYBL1 rearrangement	FGFR1 rearrangement	Histones			Follow-up	Survial (years)
						BRAFV600E	FISH-BRAF/KIAA1549//CEP7					H3F3A	H3F3B	HIST1H3I		
HGG14	HSM, IPO	14	M	Cerebral Cortex	Xantoastrocytoma	Positive	Negative 2:2 (12%) / 4:4 (83%) // 2 (13%) / 5 (75%)	Negative 2(87%) // 2(81%)	Negative 2:2(99%)	Negative 2:2(13%) 3:3(80%)	Negative 4:4(79%)	WT	WT	WT	alive, 2013	1
HGG15	HSM	11	M	Cerebral Cortex	Astroblastoma	Positive	Negative 2:2 (32%) /4:4 (54%) // 2(36%) / 4 (54%)	Negative 2(88%) // 2(85%)	Negative 2:2(95%)	Negative 2:2(34%) 3:3(26%) 4:4(35%)	Negative 2:2(48%) 3:3(17%) 4:4(33%)	WT	WT	WT	alive, 2015	6
HGG16	IPO	12	M	Cerebral Cortex	Astroblastoma	Negative	Negative 2:2 (75%) 3:3 (17%) // 2 (76%) 3(16%)	Negative 2(92%) // 2(85%) 1(12%)	Negative 2:2(82%) 3:3(12%)	Negative 2:2(74%) 1:1(11%)	Negative 3:3(52%) 4:4(14%)	WT		WT	alive, em 2015	1
HGG17	HSM, IPO	12	M	Cerebral Cortex	Grade IV Oligodendroglioma	Negative	Negative 2:2 (63%) /4:4 (24%) // 2(52%) / 4 (28%)	Negative 2(56%) 3(17%) 4(12%) 1(12%) // 2(47%) 3(24%) 4(21%)	Negative 2:2(51%) 3:3(21%) 4:4(20%)	Negative 2:2(50%) 3:3(18%) 4.4(20%)	Negative 2:2(65%) 3:3(12%) 4:4(17%)	G34R	WT	WT	death, 2006	1
HGG18	HSM	15	M	Cerebral Cortex	Glioblastoma Multiforme	Negative	Negative 2:2(96%) // 2(92%)	Positive 0(98%) 2(2%) // 2(83%) 1(14%)	Negative 2:2(86%)	Negative 2:2(95%)	Negative 2:2(97%)	WT	WT	WT	death, 2012	3
HGG19	HPC	14	F	Cerebral Cortex	Glioblastoma	Negative	Negative 4:4(70%) 2:2(15%) // 4(58%) 3(27%)	Positive 1(67%) 2(29%) // 3(39%) 2(47%)	Negative 3:3(66%) 2:2(17%)	Negative 2:2(91%)	Negative 2:2(88%)	G34R	WT	WT		
HGG20	HPC	13	M	Unknown	Glioblastoma	Negative	Negative 2:2 (91%)	Negative 2(53%) 4(27%) 3(14%) // 4(46%) 3(19%) 2(33%)	Negative 4:4(61%) 3:3(15%) 2:2(18%)	Negative 4:4(60%) 2:2(29%)	Negative 4:4(65%) 2:2(17%)	G34V	WT	WT		
HGG21	HSM	5	M	Brainstem	Glioblastoma	Negative	Negative 2:2(97%) // 2(96%)	Positive 2(83%) 1(10%) // 2(77%) 1(17%)	Negative 2:2(73%) 1:1(11%)	Negative 2:2(59%) 3:3(10%) 1:1(9%)	Negative 2:2(78%) 1:1(11%)	K27M	WT			
HGG22	HDE	7	M	Brainstem	Diffuse Instrinsic Pontine Glioma	Negative						K27M		WT		
NOS1	HDE, IPO	8	F	Unknown	Not otherwise specified glioma	Negative	Negative 2:2(22%) / 4:4 (78%) // 2(33%) / 4 (67%)						WT	WT		
NOS2	IPO	12	F	Cerebral Cortex	Not otherwise specified glioma	Negative	ND ?? //2(46%) 3(51%)	Negative 2(92%) // 2(84%) 1(13%)	Negative 2:2(89%)	Negative 2:2(91%)	Negative 2:2(89%)	WT	WT	WT	alive em 2015	1

Number	Hospital	Age (years)	Gender	Tumor location	Histologic Subtype	BRAF		p16 deletion (FISH-9p21//CEP9)	MYB rearrangement	MYBL1 rearrangement	FGFR1 rearrangement	Histones			Follow-up	Survial (years)
						BRAFV600E	FISH-BRAF/KIAA1549//CEP7					H3F3A	H3F3B	HIST1H3I		
NOS3	HSM	7	M	Cerebral Cortex	Not otherwise specified glioma	Negative	Negative 2:2(99%) // 2(96%)	Negative 2(85%) 3(12%) // 2(75%) 3(14%)	Negative 2:2(73%) 3:3(17%) 4:4(10%)	Negative 2:2(81%) 3:3(12%)	Negative 2:2(77%) 3:3(12%)	WT	WT	WT		
NOS4	HSM, IPO	8	M	Cerebral Cortex	Not otherwise specified glioma	Positive	Negative 2:2(98%) // 2(100%)	Negative 2(84%) 1(9%) // 2(73%) 1(22%)	Negative 2:2(74%) 1:1(11%)	Negative 2:2(79%) 1:1(14%)	Negative 2:2(79%) 1:1(16%)	WT	WT			
NOS5	HSM	9	F	Cerebral Cortex	Not otherwise specified glioma	Positive	Negative 2:2(62%) 3:3(20%) // 2(87%)	Positive (nas duas áreas dos dois blocos)	Positive 1:1(34%) 2:2(21%) 2:1(25%)	Negative 2:2(74%) 3:3(12%)	Negative 2:2(80%) 3:3(11%)	WT	WT		alive, 2015	3
NOS6	IPO	8	F	Unknown	Not otherwise specified glioma	Positive						WT			alive, 2015	4
NOS7	HSM	4	M	Unknown	Not otherwise specified glioma	Negative	Positive 2:2(42%) / 2:2:1F(37%) /2:3(14%) // 2 (79%)	Negative 2(85%)//2(77%) 1(11%) 3(10%)	Negative 2:2(68%) 1:1(20%)	Negative 2:2(87%) 1:1(11%)	Negative 2:2(85%)	WT	WT	WT		